

1991

Development and Applications of High Resolution Kinetic Atmospheric Pressure Ionization Mass Spectrometry in Atmospheric Chemistry

David Michael Myton
Portland State University

Let us know how access to this document benefits you.

Follow this and additional works at: http://pdxscholar.library.pdx.edu/open_access_etds

Recommended Citation

Myton, David Michael, "Development and Applications of High Resolution Kinetic Atmospheric Pressure Ionization Mass Spectrometry in Atmospheric Chemistry" (1991). *Dissertations and Theses*. Paper 1209.

10.15760/etd.1208

This Dissertation is brought to you for free and open access. It has been accepted for inclusion in Dissertations and Theses by an authorized administrator of PDXScholar. For more information, please contact pdxscholar@pdx.edu.

DEVELOPMENT AND APPLICATIONS OF HIGH RESOLUTION KINETIC
ATMOSPHERIC PRESSURE IONIZATION MASS SPECTROMETRY
IN ATMOSPHERIC CHEMISTRY

by

DAVID MICHAEL MYTON

A dissertation submitted in partial fulfillment of the
requirements for the degree of

DOCTOR OF PHILOSOPHY
in
ENVIRONMENTAL SCIENCES AND RESOURCES:
CHEMISTRY

Portland State University
1991

TO THE OFFICE OF GRADUATE STUDIES:

The members of the Committee approve the dissertation of David Michael Myton presented July 3, 1991.

[Redacted Signature]

Robert J. O'Brien

[Redacted Signature]

Horace F. White

[Redacted Signature]

Carl C. Wamser

[Redacted Signature]

Pavel K. Smejtek

[Redacted Signature]

John G. Rueter

[Redacted Signature]

Randy D. Zelick

APPROVED:

[Redacted Signature]

Pavel K. Smejtek, Director, Environmental Sciences and Resources Ph.D. Program

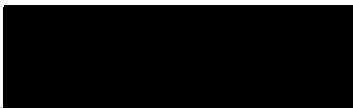
[Redacted Signature]

C. William Savery, Interim Vice Provost for Graduate Studies and Research

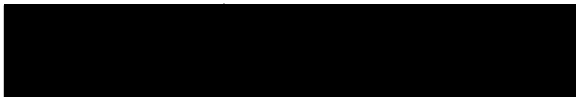
AN ABSTRACT OF THE DISSERTATION OF David Michael Myton for the
Doctor of Philosophy in Environmental Science and Resources: Chemistry
presented July 3, 1991.

Title: Development and Applications of High Resolution Kinetic Atmospheric
Pressure Ionization Mass Spectrometry in Atmospheric Chemistry

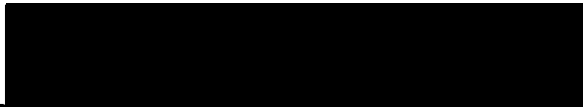
APPROVED BY THE MEMBERS OF THE DISSERTATION COMMITTEE:



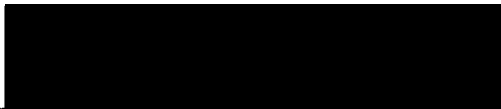
Robert J. O'Brien



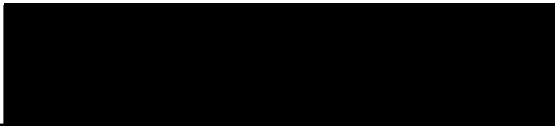
Horace F. White



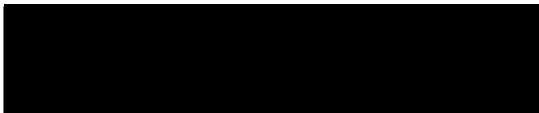
Carl C. Wamser



Pavel K. Smejtek



John G. Rueter



Randy D. Zelick

Much important work has been done to understand reaction pathways and identify products, yields, and reaction rates for atmospheric oxidation processes. Non-methane hydrocarbons (NMHCs) are the most significant of the organic compounds present in the atmosphere from a chemical perspective and are released into the atmosphere from both natural and anthropogenic sources. The oxidation of these hydrocarbons by hydroxyl radical HO generates products that may themselves be toxic, that play a major role in the formation of photochemical smog, and that to a lesser extent contribute to the formation of acid precipitation. NMHCs have chemical reactivities many times that of methane, the most abundant HC in the atmosphere. However, the atmospheric oxidation processes of less than 50% of atmospheric NMHCs are known.

A new experimental technique is needed that can provide insight into atmospheric oxidation products, reaction intermediates, and the relative importance of secondary reaction pathways that follow the initial attack of HO upon a hydrocarbon. The technique should operate at atmospheric pressure to better represent natural reaction processes and conditions, and provide a rapid and direct measure of product identities and yields. In this study we will describe the development and application of a technique that we believe meets these requirements, a technique we call High Resolution Kinetic Atmospheric Pressure Ionization Mass Spectrometry (HRKAPIMS).

We begin with the use of atmospheric pressure ionization mass spectrometry in studies of atmospheric oxidation processes. We first describe a potential pitfall in the use of APIMS for the analysis of smog chamber experiments, a common APIMS application, discussing methods to eliminate

interference reactions that would otherwise make interpretation difficult. A new experimental approach to the use of APIMS for the analysis of oxidation processes is next described and its use demonstrated. The oxidation of toluene by API-source-generated HO produces oxidation products that are protonated and detected by the mass spectrometer. With this approach, we observe all the products found in a variety of previous studies employing a large array of experimental setups and analytical instrumentation. This is significant because our experiments are carried out in a far simpler experimental environment. Toluene is chosen for these experiments because it is an important constituent in polluted urban atmospheres with a complex oxidation mechanism that remains poorly understood.

We describe the development of HRKAPIMS, a powerful new approach that allows the simultaneous detection of stable products along with free radical intermediates. The use of nitric oxide to affect product yields is demonstrated, giving valuable insights into reaction kinetics and mechanisms.

We also address the theoretical aspects of HRKAPIMS, describing semiempirical calculations to estimate gas-phase basicities for a wide variety of compounds and discuss the errors implicit in this approach. The use of gas-phase basicities is discussed in terms of mass spectrometric analysis and analyte response. Kinetic and thermodynamic modeling is used to address the issues of APIMS and HRKAPIMS sensitivity and response and gain insights into the conditions necessary for linear response and quantitative detection of analytes.

ACKNOWLEDGEMENTS

I would like to recognize and thank my graduate advisor and mentor, Dr R.J. O'Brien, for his support, guidance, and help throughout this project. I appreciate the support I have received through the Department of Chemistry and the Environmental Sciences and Resources Program, support both from the staff and faculty, as well as financially. I am certainly grateful for the help and encouragement of Lorne Isabelle of the Oregon Graduate Institute in the daily operation and troubleshooting of the mass spectrometer. Dr. A.H. Grange deserves special mention for sharing with me his interest in APIMS, and the skills and training I needed to complete this project. I have appreciated the support and friendship of my fellow students and colleagues, in particular Dr. Linda George, Dr. Wen Pan, Dr. Tom Hard, Dr. Corny Chan, and Xiong Pan. Special appreciation belong to my family, Mary and Ben, whose love and support and confidence have never wavered. Finally, and most importantly, I acknowledge my Creator, Lord, and Savior, Jesus Christ.

TABLE OF CONTENTS

	PAGE
ACKNOWLEDGEMENTS	iii
LIST OF TABLES	vii
LIST OF FIGURES	ix
LIST OF ABBREVIATIONS AND ACRONYMS	xii
 CHAPTER	
I OVERVIEW OF ATMOSPHERIC OXIDATION PROCESSES	1
Introduction	1
Atmospheric Oxidations	2
Biogenic Emissions	
Anthropogenic Emissions	
Photochemical Smog	
Hydroxyl Radical Chemistry	6
Current Methods in Atmospheric Chemistry	
A New Technique: HRKAPIMS	
Research Goals	
II SUPPRESSION OF SPURIOUS OXIDATION PRODUCTS IN AN ATMOSPHERIC PRESSURE IONIZATION SOURCE	12
Overview	12
Introduction	12
HO Source Reactions	
Experimental	15
Results and Discussion	16

	Mass Spectrometry Kinetic Modeling	
	Conclusions	26
	Other Radical Scavengers New Applications	
III	STUDIES OF ATMOSPHERIC HO OXIDATION MECHANISMS BY IN SITU HIGH RESOLUTION ATMOSPHERIC PRESSURE IONIZATION MASS SPECTROMETRY	29
	Overview	29
	Introduction	30
	Experimental	32
	Results and Discussion	33
	Toluene Products Empirical Formulas Past Toluene Studies API Source Chemistry	
	Conclusions	50
IV	HIGH-RESOLUTION KINETIC ATMOSPHERIC PRESSURE IONIZATION MASS SPECTROMETRY (HRKAPIMS)	52
	Overview	52
	Introduction	53
	HO Chemistry Oxidation Product Measurements HRKAPIMS	
	Results and Discussion	59
	Experimental Free Radical Intermediates Free Radical Intermediate Measurements Chemical Modeling	
	Conclusions	70

V	SEMIEMPIRICAL CALCULATIONS OF GAS-PHASE BASICITIES WITH APPLICATIONS TO MASS SPECTROMETRY	72
	Overview	72
	Introduction	72
	Experimental	75
	Results and Discussion	75
	Conclusions	88
VI	ANALYTE RESPONSE AND QUANTITATION IN ATMOSPHERIC PRESSURE IONIZATION MASS SPECTROMETRY	91
	Overview	91
	Introduction	91
	Quantitation in Mass Spectrometry	93
	Ionization Techniques Quantitation in API	
	Chemical Modeling	99
	Equilibrium Expressions Kinetic Modeling-Rate Constants Kinetic Modeling-Batch Mode	
	Conclusions	125
VII	CONCLUSIONS AND APPLICATIONS	127
	Part I: HRKAPIMS	127
	Oxidation of Small Hydrocarbons	
	Part II: Analyte GB and API Response	134
	Gas-phase Basicities Analyte Response in API	
	Summary	145
	REFERENCES	148

LIST OF TABLES

TABLE		PAGE
I	Atmospheric Reaction Pathways and Selected Gas- Phase Basicities for Methane and Ethane	14
II	Mechanism for Kinetic Modeling of HO and CO Reactions in Hydrocarbon Oxidations	20
III	Toluene Oxidation Products Found Using API Source Reactions .	36
IV	Empirical Formula Combinations for Selected Experimental Masses	42
V	Experimental Masses of Five Free Radical Toluene Oxidation Intermediates	63
VI	Kinetic Modeling Mechanism for HRKAPIMS Source Reactions . .	66
VII	Comparison of the Gas-phase Basicities and Adjusted Heats of Formation for Protonated and Unprotonated Species	76
VIII	Regression Analysis of Calculated Versus Experimental Gas-phase Basicities and Corrected Heats of Formation	82
IX	Heats of Formation for Hydrated Furan and Ethanol	88
X	Comparison of Initial Analyte Response vs. Gas-phase Basicity	103
XI	Mechanism for Kinetic Modeling of Hydronium Hydration	115
XII	Semiempirical Calculations of Heats of Reaction for Hydration $BH^+ + H_2O \leftrightarrow BH^+ \cdot H_2O$	117

XIII	Regression Analysis of Free Energies of Hydration as a Function of Analyte GB for $\text{BH}^+(\text{H}_2\text{O})_{n-1} + \text{H}_2\text{O} \leftrightarrow \text{BH}^+(\text{H}_2\text{O})_n$.	118
XIV	Batch Mode Model of API Response	121
XV	Partial Methane Photooxidation Mechanism	129
XVI	Partial Ethene Photooxidation Mechanism	131
XVII	Partial Propene Photooxidation Mechanism	132
XVIII	Partial Butane Photooxidation Mechanism	135
XIX	Gas-phase Basicities based on Semiempirical Heats of Formation	137
XX	Gas-phase Basicity Calculations for Toluene Free Radical Intermediates and Products	144

LIST OF FIGURES

FIGURE		PAGE
1.	Sources and Structures for Selected Non-methane Hydrocarbons (NMHCs) emitted from Biogenic Sources	4
2.	API Reaction Vessel Analysis of Methyldeuterated Toluene	18
3.	Kinetic Modeling of HO Reactions in the API Source	22
4.	Kinetic Modeling of HO Reactions in an API Source in the Presence of Carbon Monoxide	25
5.	Mass Spectral Sequence Illustrating the Photooxidation of D ₈ Toluene in an Oxygen Carrier Gas	34
6.	Mass Spectra Showing the Course of a Typical HRKAPIMS Experiment	60
7.	Normalized Ion Intensity vs. Scan Number for Methylhexadienedial	62
8.	Partial Toluene Oxidation Mechanism Showing the Production of Several Free Radical Intermediates and Stable Products . .	65
9.	Experimental vs. Modeled Ion Intensities for Toluene Free Radical Intermediates	69
10.	Comparisons of Calculated and Experimental $\Delta H_f(B)$	83
11.	Comparisons of Calculated and Experimental $\Delta H_f(BH^+)$	84
12.	Comparisons of Calculated and Experimental GB	85

13.	Experimental Ion Intensities for Toluene Oxidation Products by Analyte Gas-phase Basicity	99
14.	Analyte Response as a Function of Gas-phase Basicity and Initial Water Concentration in Thermodynamic Equilibrium Case (R10)	102
15.	Sensitivity, Relative to Pyridine, in an API Source as a Function of Analyte GB	106
16.	Analyte Response in Steady State Model (R13) as a Function of GB and $[H_3O^+]_0$	109
17.	Analyte Response in Steady State Model (R13) as a Function of GB and $[H_2O]_0$	110
18.	Analyte Response in Steady State Model (R13) as a Function of GB and k_a	111
19.	Analyte Response in Steady State Model (R13) as a Function of GB and k_f	113
20.	Kinetic Modeling of Hydration Reactions for Water with Hydronium Ions	114
21.	Free Energy for the Hydration Reactions of Protonated Analytes as a Function of GB	116
22.	Forward Rate Constants for Protonation as a Function of Analyte GB	119
23.	Batch-mode Modeling of API Source Reactions at Two Detection Rates	122

24.	Batch-mode Modeling of Analyte Response as a Function of Initial Analyte Concentration	123
25.	Experimental Analyte Response Using TAGA APIMS as a Function of Analyte Concentration	124
26.	Batch-mode Modeling of Analyte Response for Mixtures	125
27.	Low Resolution Mass Spectra From APIMS Analysis of Butane .	141
28.	Partial Toluene Photooxidation Mechanism Showing Formation of Major Ring-opened Products and Free Radical Intermediates	143

LIST OF ABBREVIATIONS AND ACRONYMS

$\Delta G(R1)$	Free energy of Reaction 1
$\Delta H(R1)$	Enthalpy of Reaction 1
$\Delta H_f(B)$	Heat of formation for an unprotonated analyte
$\Delta H_f(BH^+)$	Heat of formation for a protonated analyte
$\Delta S(R1)$	Entropy of Reaction 1
ΔS_{sym}	Entropy from internal/external symmetry values
AM1	Third generation semiempirical parameterization
APCI	Atmospheric pressure chemical ionization
API	Atmospheric pressure ionization
APIMS	Atmospheric pressure ionization mass spectrometry
B, BH ⁺	Generic gas phase bases: unprotonated and protonated
CD	Corona discharge- ionization source for API
CI	Chemical ionization- MS ionization method
CID	Collision induced dissociation
CO	Carbon monoxide
D	Diffusion coefficient
EB	Electrostatic sector/Magnetic sector mass analyzer
EI	Electron impact- standard MS ionization method
FAB	Fast atom bombardment
FTIR	Fourier transform infrared (spectroscopy)

GB	Gas-phase basicity, $GB = -\Delta G_{rxn}(B + H^+ \rightarrow BH^+)$
GC	Gas chromatography
GC/MS	Gas chromatography/mass spectrometry
HC	Hydrocarbon
HCHD	Hydroxycyclohexadienyl radical, HO adduct to benzene
HO	Hydroxyl radical
HPLC	High performance liquid chromatography
HRKAPIMS	High resolution kinetic APIMS
IMMS	Ion mobility mass spectrometry
$K_{eq}(R1)$	Equilibrium constant for Reaction 1
LC	Liquid chromatography
LC/MS	Liquid chromatography/mass spectrometry
MIKES	Mass-analyzed ion kinetic energy spectroscopy
MINDO/3	Second generation semiempirical parameterization
MNDO	First generation semiempirical parameterization
MNDO-PM3	Fourth generation semiempirical parameterization
MO	Molecular orbital (theory)
MOLY	Molecular structure input program
MOPAC	Molecular Orbital PACkage, semiempirical program
MS	Mass spectrometry
MS/MS	Tandem mass spectrometry/mass spectrometry
NAAQS	National Ambient Air Quality Standards
NMHC	Non-methane hydrocarbon
NO	Nitric oxide

NO _x	Sum of NO and NO ₂
PA	Proton affinity, $PA = -\Delta H_{rxn}(B + H^+ \rightarrow BH^+)$
PAN	Peroxy acetyl nitrate
PHPMS	Pulsed high pressure mass spectrometry
QCPE	Quantum chemistry program exchange
RO, RO ₂	Generic Oxy- and Peroxy radical species
RT	Product of the gas constant and temperature
Sciex	Manufacturer of a commercial APIMS system
TAGA	Model name of a commercial APIMS system
VOC	Volatile organic compound

CHAPTER I

OVERVIEW OF ATMOSPHERIC OXIDATION PROCESSES

*"To most people solutions mean finding the answer,
but to chemists solutions are things that
are still all mixed up." (Davis 1969)*

INTRODUCTION

Concerns about the changing state of the atmosphere, and the possible effects such changes could have, is a matter of constant attention in the news media. Mankind has had a dramatic role in producing or facilitating many of these changes through the release of a wide range of substances into the air. In general, public awareness and concern over environmental issues continues to increase, and discussions about greenhouse gases, toxic air pollutants, acid rain, global warming and the ozone hole have become commonplace. While such discussions are not new from a scientific perspective, public attention regarding the delicate balance of chemical, biological and physical processes in the atmosphere has provided an additional impetus for research into these processes.

The following paragraphs will outline the sources of organic compounds in the atmosphere and identify some areas where further work is needed to understand oxidation processes. Current methods used to study atmospheric oxidations are reviewed and their shortcomings are described. Finally, a new approach

to studying atmospheric oxidation processes will be introduced which will be described, and used to address current problems in atmospheric chemistry, in the chapters which follow.

ATMOSPHERIC OXIDATIONS

A wide variety of organic compounds are present in the lower atmosphere. A database of volatile organic compounds (VOCs) present in the atmosphere was recently compiled by the Environmental Protection Agency (Shah and Singh, 1988). This database included a total of 320 VOCs, 261 of which had been measured outdoors and 66 had been measured indoors. These compounds, released from both natural and anthropogenic sources, contribute directly and indirectly to the total chemistry of the troposphere. As examples: photochemical smog is formed when sunlight impinges upon organic compounds in the presence of the oxides of nitrogen, and acid deposition results from the oxidation of hydrocarbons, nitrogen and sulfur oxides. Furthermore, many compounds that are released into the atmosphere are potentially toxic or may form toxic products as a result of atmospheric oxidation processes (Grosjean, 1991; Dumdei et al., 1988).

From the standpoint of atmospheric oxidation processes, the nonmethane hydrocarbons (NMHCs) are among the most important reactive species in the atmosphere. Methane is, of course, an important hydrocarbon due to its ubiquitous presence in the troposphere at relatively high levels. However, methane's chemical reactivity, as a fully hydrogenated compound, is significantly less than that of most NMHCs. Hydrocarbons are released into the atmosphere from the decomposition

of organic matter, from living plants and animals, and from the activities of mankind.

Biogenic Emissions

The first suggestion of the importance of vegetation as a major source of organic compounds in the atmosphere came from Went (1960). Organic compounds are believed to be emitted through natural processes from a wide range of plant species (Zimmerman, 1979), yet emission rates have been measured for less than 100 plant species (Tingey et al., 1979; Lamb, Westberg, and Allwire, 1985). Early estimates of annual worldwide emissions of VOCs from vegetation were in the range of $(200-400) \times 10^{12}$ g/yr (Rasmussen and Went, 1965). Estimates of worldwide emission rates have only increased in more recent studies (Rasmussen, 1972; Zimmerman, 1978; Rasmussen and Khalil, 1988; Zimmerman, Greenberg, and Westberg, 1988). Isoprene and the terpenes lead known biogenic emissions, with estimated global carbon inputs of at least 3.5×10^{14} and 4.8×10^{14} g(C)/yr respectively (Zimmerman et al., 1978). The chemical structures, and examples of the biogenic sources, of several members of the terpene family are shown in Figure 1 (Seinfeld, 1986). The rate of reaction for isoprene, the largest single component of biogenic emissions, with hydroxyl radical (HO) is nearly a factor of 50 greater than that of standard urban hydrocarbon mixtures (Killus and Whitten, 1984). This illustrates isoprene's much greater reactivity in the atmosphere, and is typical of NMHC reaction rates in general. A large HO reaction rate will be reflected in the rapid consumption of the organic compound and the corresponding rapid increase in its atmospheric oxidation products. In spite of the importance of

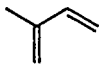


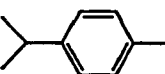
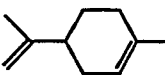
Isoprene (C ₅ H ₈)	Emitted by oak, sycamore, willow, balsam poplar, aspen, spruce and others.
	
α -Pinene (C ₁₀ H ₁₆)	Emitted by numerous pines, firs, spruce, hemlock and cyprus.
	
β -Pinene (C ₁₀ H ₁₆)	Emitted by California black sage, Loblolly pine, spruce and redwood.
	
<i>p</i> -Cymene (C ₁₀ H ₁₆)	Emitted by California black sage and from "disturbed" eucalyptus foilage; found in gum turpentines of Scotch and other pines.
	
<i>d</i> -Limonene (C ₁₀ H ₁₆)	Emitted by Loblolly pine, California black sage, found in the gum turpentine of numerous pines and the essential oils derived from some fruits.
	

Figure 1. Sources and structures for selected non-methane hydrocarbons (NMHCs) emitted from biogenic sources. Emission rates and reactivity are discussed in the text. Source: Seinfeld (1986).

isoprene, and terpenes in general, their atmospheric oxidation processes remain vaguely understood are the subject of continued research (Tuazon and Atkinson, 1990).

In general, biogenic sources of VOCs are in rural settings and, while they comprise a large fraction of the total world emissions, their impact on urban air

pollution has often been considered small. One reason for this is that measurements of ambient concentrations of biogenic NMHCs rarely exceed 5% of the total (Arnts and Meeks, 1981). This is probably a result of the much higher chemical reactivity of isoprene, as has already been mentioned. More recently however the inability of many cities to meet the National Ambient Air Quality Standards (NAAQS) has directed attention to the oxidation of biogenic emissions as sources of ozone in urban settings (Chameides et al., 1988).

Anthropogenic Emissions

Nearly all of the 320 VOCs compiled in the EPA database are emitted as a result of anthropogenic activities (Shah and Singh, 1988). Aromatic hydrocarbons, a subset of the VOCs, are important players in the formation of air pollution. Aromatic hydrocarbons comprise 25-40% of gasoline in the United States and are widely used as solvents (O'Brien and Hightower, 1981). Of the total evaporative (fuel spills and displaced vapors from fuel tanks) and tailpipe emissions, 10-30% are aromatic (Black, High, and Lang, 1980). These compounds, for which toluene is representative, are highly reactive and are often the most abundant of all nonmethane hydrocarbons in polluted urban air. With the Clean Air Amendments of 1990 the number of regulated air pollutants increased from six (CO, nitric dioxide (NO₂), SO₂, particulates, ozone and lead) to a list of 189 hazardous air pollutants, and a large number of these are aromatic compounds.

Photochemical Smog

Photochemical smog forms when sunlight impinges on mixtures of organic compounds and oxides of nitrogen (NO_x). Nitric oxide (NO) is a by-product of

combustion, where high temperatures dissociate molecular oxygen and nitrogen to form NO. NO is converted to nitrogen dioxide (NO₂) through photooxidation reactions; NO_x refers to the total of both NO and NO₂. Photochemical smog occurs in areas where high levels of NO_x and VOCs, organic compounds from natural processes and/or unburnt fuels from automobiles and/or stationary power facilities) are both present in high concentrations. Photochemical smog has been shown to occur in some rural settings, i.e. above the rain forest canopy, and some models suggest that much more stringent anthropogenic emissions standards would be necessary to meet urban air quality standards if biogenic emissions and processes proceed as modeled (Chameides et al., 1988).

The atmospheric fates of many compounds are well understood, particularly those compounds with 4 or less carbon atoms. Unfortunately, most biogenic and anthropogenic sources release larger, more complex compounds. Aromatic compounds, principally from anthropogenic sources, are among the most important reactive compounds in the atmosphere (Seinfeld, 1989). However, known reactions for mechanisms of even the more common of aromatics, toluene for example, can only account for about 50% of the overall reaction byproducts (Tuazon et al., 1984). A better understanding of the reaction mechanisms of both biogenic and anthropogenic VOCs is needed if accurate models of tropospheric chemistry are to be developed (Pierotti et al., 1990).

HYDROXYL RADICAL CHEMISTRY

Most reactive chemical species emitted into the atmosphere, with the exceptions of carbon dioxide and water, are in reduced chemical states. These

include saturated and unsaturated hydrocarbons, hydrogen sulfide, as well as nitric oxide and sulfur dioxide which are oxidized further to nitrates and sulfates). The bulk of atmospheric chemistry involves the subsequent oxidation of these compounds and the removal of the oxidized forms from the atmosphere.

The primary agent of photochemical oxidations is the hydroxyl radical (HO). Hydroxyl radical oxidation processes are termed photochemical since the three primary sources of hydroxyl radicals are the photodissociation of ozone, photodissociation of carbonyl compounds and photodissociation of nitrous acid (Seinfeld, 1989). Atmospheric oxidizers like the hydroxyl radical act as detergents in the air as they transform insoluble pollutant gases into water-soluble compounds which can be eliminated from the atmosphere in precipitation (Graedel and Crutzen, 1989).

Due to the importance of hydroxyl radicals in atmospheric chemistry, much attention and study has been given to their reactions. The products of atmospheric oxidations are also important. Oxidized forms are typically soluble in rainwater, thus increasing the pH of precipitation, and some have been shown to be mutagenic (Dumdei et al., 1988). High levels of hydrocarbons in polluted atmospheres result in the production of ozone, a major component in photochemical smog. In order to better understand atmospheric oxidative processes, atmospheric chemistry in general, and to develop models by which changes in the atmosphere can be predicted and evaluated, an understanding of the rates, intermediates and products of hydroxyl radical oxidations is required.

Current Methods in Atmospheric Chemistry

Hydroxyl radical reactions for organic species present in both natural and polluted atmospheres have been the subject of much study (Atkinson et al., 1979). HO is the major initiator of the photochemical oxidations that ultimately convert organic compounds present in the atmosphere to CO₂ and water. The importance of HO radicals in the production of photochemical air pollution was first speculated upon by Leighton (1961). Since then, studies into HO radical chemistry have focused on three areas: measuring reaction rate constants and activation energies, identifying products of atmospheric oxidation, and elucidating reaction mechanisms. Each area of study has relied on different sets of experimental techniques to address a particular portion of HO radical chemistry, but few techniques address all aspects. Since some techniques (e.g. discharge flow) are normally carried out at very low pressures, the application of a particular experimental finding to atmospheric pressure processes must always be carefully considered.

Rate constants evaluated under traditional laboratory conditions are in generally good agreement with relative measurements obtained under simulated atmospheric conditions and, for most common species, the status of rate constant information for HO/hydrocarbon reactions is quite sound (Atkinson, 1986). The identification and quantitation of atmospheric hydrocarbon oxidation products (which generally contain O and/or N atoms as well as C and H) has been widely addressed, using a great many techniques, yet the complete oxidation schemes and product yields remain unknown for many common compounds. The following is a sampling of the techniques that have been used in the analysis of atmospheric

oxidation processes: gas chromatography (O'Brien et al., 1979; Leone et al., 1985; Shepson et al., 1985; Atkinson et al., 1980), gas chromatography/mass spectrometry (Atkinson et al., 1980; Kenley, Davenport, and Hendry, 1981; Shepson, Edney, and Corse, 1984), high performance liquid chromatography (Fund and Grosjean, 1981; Besemer, 1982), tandem mass spectrometry (O'Brien et al., 1984), long path length Fourier transform infrared spectroscopy (Plum et al., 1983; Tuazon et al., 1986) and differential optical absorption spectroscopy (Tuazon et al., 1984; Bandow, Washida, and Akimoto, 1985).

Many of the aforementioned techniques have been used in studies of toluene oxidation products. Although tentative toluene oxidation mechanisms have been based upon some studies (Leone et al., 1985; Dumdei et al., 1988; Dumdei and O'Brien, 1984; Bandow, Washida, and Akimoto, 1985; Atkinson et al., 1980) elucidation of the reaction mechanisms for toluene and other members of the benzene family remains a major area of uncertainty in atmospheric chemistry (Seinfeld, 1989).

The ability to detect reaction intermediates simultaneously with stable products would be an asset in elucidating the complex mechanisms typical of aromatic compounds. One technique, photoionization-mass spectrometry (Sloane, 1978) has found some success in this area. However, this technique is complex and of limited utility for the study of atmospheric processes since the experiments are conducted at very low pressure. Ionization is generally an energetic process and the parent molecule will fragment unless the excess energy can be lost through some vibration or collision. Ionization at atmospheric pressure reduces the

fragmentation and allows the analysis to more closely mimic actual reactions in the atmosphere (Atkinson, 1986).

A New Technique: HRKAPIMS

Much important work has been done to understand reaction pathways, identify products, yields, and reaction rates for atmospheric oxidation processes. Yet with 50% or less of the of the atmospheric oxidation processes known for many NMHCs (Seinfeld, 1989), there is still a significant need for further work. A new experimental technique is needed that can provide insight into atmospheric oxidation products, reaction intermediates, and the relative importance of secondary reaction pathways which follow the initial attack of HO upon the hydrocarbon. The technique should operate at atmospheric pressure to better represent natural reaction processes and conditions, and provide a rapid and direct measure of product identities and yields. In the following chapters we will describe and demonstrate a technique that we believe meets these requirements, a technique we call High Resolution Kinetic Atmospheric Pressure Ionization Mass Spectrometry (HRKAPIMS).

Research Goals

The chapters which follow examine the application of HRKAPIMS to the study of atmospheric oxidation processes. In the first three chapters we discuss the experimental aspects of HRKAPIMS. We describe a potential pitfall in the use of atmospheric pressure ionization in the analysis of smog chamber experiments, a common APIMS application, discussing methods to eliminate interference reactions which would otherwise make interpretation difficult. A new experimental

approach to the use of APIMS for the analysis of oxidation processes is described, and its use demonstrated. We describe the development of HRKAPIMS, a powerful new approach that allows the simultaneous detection of stable products along with free radical intermediates. The use of nitric oxide to affect product yields is demonstrated, giving valuable insights into reaction kinetics and mechanisms. The final chapters address the theoretical aspects of HRKAPIMS. We describe the use of semiempirical calculations to estimate gas-phase basicities (GBs) for a wide variety of compounds and discuss the errors implicit in this approach. The use of GBs is discussed in mass spectrometric analysis. Kinetic and thermodynamic modeling is used to address the issues of APIMS and HRKAPIMS sensitivity and response and gain insights into the conditions necessary for linear response and quantitative detection of analytes.

It is hoped that the information gained in this study will be useful in unraveling the atmospheric oxidation pathways of the organic compounds present in the troposphere. This information can also be of value in the development of more complete atmospheric oxidation models, used to evaluate and regulate anthropogenic emissions, and provide a basis for improved semiempirical methodology.

CHAPTER II

SUPPRESSION OF SPURIOUS OXIDATION PRODUCTS IN AN ATMOSPHERIC PRESSURE IONIZATION SOURCE

*"After chemists went to all the trouble to learn
how to mix iron and oxygen, they only
came up with rust." (Davis, 1969)*

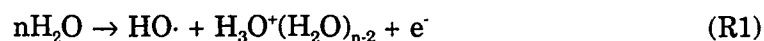
OVERVIEW

The hydroxyl radicals which form in the ionization chamber of an atmospheric pressure ionization source react with analyte molecules present in the sample stream to form oxidation products, partially consuming the analyte and generating interference peaks in the mass spectra. We demonstrate here the effectiveness of about 1% carbon monoxide in inhibiting these reactions, and discuss the use of other radical scavengers.

INTRODUCTION

Atmospheric pressure ionization has grown in importance as an ion source for mass spectrometry (APIMS) in a variety of applications including liquid chromatography/mass spectrometry (LC/MS), analysis of biological samples and the study of atmospheric oxidations (Mitchum and Korfmacher, 1983; Sakairi and Kambara, 1988; Eiceman et al., 1988). Atmospheric pressure ionization is also finding applications in ion mobility spectrometry where it has been used to

determine gas phase proton affinities and gas phase ion/molecule reaction rate constants (Vandiver, Leasure, and Eiceman, 1985; Vandiver, 1987). The series of ion-molecule reactions occurring either in a corona discharge, or as a result of emissions from a radioactive nickel foil, quickly generate hydrated hydronium ions and hydroxyl radicals (HO), as summarized in Reaction 1 (Good, Durden, and Kebarle, 1970a). The electron in this reaction comprises the corona current.



In APIMS, molecules with gas phase basicities (GB) greater than water are generally protonated by these hydronium-water clusters and accelerated into the analyzer region of the mass spectrometer. The production of HO in the ion source through Reaction 1 can be a significant source of interference when using API.

HO Source Reactions

The impact of HO reactions in our ion source became apparent to us as we used API in the analysis of simulated atmospheric oxidations. This interference may impact other applications of API as well. In a typical oxidation experiment, organic compounds contained within a reaction vessel are photo-oxidized in a process simulating atmospheric processes (Atkinson, 1986). Here, as in the atmosphere, hydroxyl radicals are the primary removal agent for these organics (Atkinson et al., 1980). HO, formed in the reaction vessel as a result of irradiation by ultraviolet light, initiates the oxidation of the compounds present. HO reactions with hydrocarbons (HCs) involve either the abstraction of a hydrogen atom from the compound or addition of the hydroxyl radical to an unsaturated carbon-carbon bond. Typical oxidation reactions are listed in Table I for methane and ethene. Mechanisms for larger hydrocarbons may be significantly more complex, yielding

TABLE I
ATMOSPHERIC REACTION PATHWAYS AND SELECTED GAS-PHASE
BASICITIES FOR METHANE AND ETHANE

METHANE	(GB)
$\text{HO}\cdot + \text{CH}_4 \rightarrow \text{CH}_3\cdot + \text{H}_2\text{O}$	126
$\text{CH}_3\cdot + \text{O}_2 \rightarrow \text{CH}_3\text{O}_2\cdot$	123*
$\text{CH}_3\text{O}_2\cdot + \text{NO}\cdot \rightarrow \text{NO}_2\cdot + \text{CH}_3\text{O}\cdot$	151*
$2 \text{CH}_3\text{O}_2\cdot \rightarrow 2 \text{CH}_3\text{O}\cdot + \text{O}_2$	163*
$\text{CH}_3\text{O}_2\cdot + \text{HO}_2\cdot \rightarrow \text{CH}_3\text{OOH} + \text{O}_2$	154*
$\text{CH}_3\text{O}\cdot + \text{O}_2 \rightarrow \text{CH}_2\text{O} + \text{HO}_2\cdot$	164.3
$\text{CH}_2\text{O} + \text{HO}\cdot \rightarrow \text{CHO}\cdot + \text{H}_2\text{O}$	149*
$\text{CHO}\cdot + \text{O}_2 \rightarrow \text{CO} + \text{HO}_2\cdot$	134.4
$\text{HO}_2\cdot + \text{NO}\cdot \rightarrow \text{HO}\cdot + \text{NO}_2\cdot$	~150
$2 \text{HO}_2\cdot \rightarrow \text{H}_2\text{O}_2 + \text{O}_2$	~154
ETHENE	
$\text{HO}\cdot + \text{CH}_2=\text{CH}_2 \rightarrow \text{HOCH}_2\text{CH}_2\cdot$	155.6
$\text{HOCH}_2\text{CH}_2\cdot + \text{O}_2 \rightarrow \text{HOCH}_2\text{CH}_2\text{O}_2\cdot$	171*
$2 \text{HOCH}_2\text{CH}_2\text{O}_2\cdot \rightarrow 2\text{HOCH}_2\text{CH}_2\text{O}\cdot + \text{O}_2$	164*
$\text{HOCH}_2\text{CH}_2\text{O}_2\cdot + \text{NO}\cdot \rightarrow \text{HOCH}_2\text{CH}_2\text{O}\cdot + \text{NO}_2\cdot$	
$\text{HOCH}_2\text{CH}_2\text{O}\cdot + \text{O}_2 \rightarrow \text{HOCH}_2\text{CHO} + \text{HO}_2\cdot$	181*
$\text{HOCH}_2\text{CH}_2\text{O}\cdot \rightarrow \text{H}_2\text{C}=\text{O} + \text{H}_2\text{COH}\cdot$	191*
$\text{H}_2\text{COH}\cdot + \text{O}_2 \rightarrow \text{H}_2\text{C}=\text{O} + \text{HO}_2\cdot$	164.3

Notes: Mechanisms from Atkinson and Lloyd (1984). Gas-phase basicities (kcal/mol) for the italicized species are given in the last column, and may be compared with GB = 159 kcal/mol for water. Values with an asterisk are GBs based on semi-empirical calculations using an approach described in Chapter V, others are from Lias, Liebman, and Levin (1984).

a wide array of oxidation products. Reactions involving the hydroxyl radicals in Reaction 1 within the source can change the composition of the sample, producing oxidation products which consume reagent ions and generally make detection, identification and quantitation confusing and difficult.

In this chapter we describe our efforts to overcome the interferences to API analysis caused from reactions of the source-produced hydroxyl radicals through

the addition of low levels of carbon monoxide. Ideally, a radical scavenger could be used to convert hydroxyl radicals to an unreactive species. However, such an open shell species could possibly affect the neutral or ion reactions in the source in other undesirable ways. We selected carbon monoxide, in spite of its closed-shell electronic structure, because of its availability, its general chemical inertness with species other than HO, its low gas-phase basicity, and consequently, its expected low impact on the ion/molecule chemistry. Added in sufficient quantity to make up for its relatively slow rate of reaction with HO, CO efficiently converts HO to the far less reactive HO₂ in the sequence

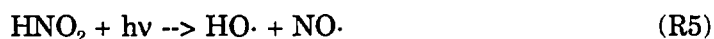


At atmospheric pressure, hydrogen atoms are converted to HO₂ with very high efficiency. The GBs of CO, CO₂, HO₂, and H₂O₂ are all below that of water (159 kcal/mol). Other radical scavengers are considered below.

EXPERIMENTAL

Our API source, developed for use with a high resolution double focusing mass spectrometer, has been characterized (Grange, O'Brien, and Barofsky, 1988b; Grange, O'Brien, and Barofsky, 1988c) and its use demonstrated (Grange, O'Brien, and Barofsky, 1988a). A glass reaction vessel containing synthetic air at 50% relative humidity with 10 ppm toluene and 10 ppm NO_x (90% NO, 10% NO₂) was irradiated with sixteen 40 watt fluorescent black lights (GE F40BL). Nitric oxide was measured with a ThermoElectron Chemiluminescence Analyzer. Hydroxyl

radicals are generated in such reaction vessels by heterogeneous processes such as these involving oxides of nitrogen (Finlayson-Pitts and Pitts, 1986).



Hydroxyl radicals are regenerated homogeneously in reactions controlled by nitric oxide (Table I). In the API source, HO_2/RO_2 reactions (also Table I) may result in radical recombination a larger fraction of the time (Atkinson, 1986), due to a higher RO_2/NO ratio than in the atmosphere. We have observed the production of NO in our corona discharge when run in air, finding in one measurement a concentration of 15 ppm with a 0.2 μA discharge current.

Photo-oxidation products from the reaction vessel were carried out in an airflow of $2.6 \text{ cm}^3 \text{ min}^{-1}$ and then diluted 1:8 into a carrier stream of zero air to reduce relative humidity and improve sensitivity (Grange, 1988). A separate flow system added carbon monoxide to the carrier stream immediately prior to the API source for a CO concentration of 0.8%, the minimum amount possible using pure CO and the flow controllers available to us. A corona discharge was sustained with currents on the order of 0.2 μA .

RESULTS AND DISCUSSION

Mass Spectrometry

Figure 2 shows three mass spectra taken from a reactor containing methyl-deuterated toluene with 0.2 μA corona current. This isotopic form is useful because it predominately forms oxidation products at even masses where the

spectrometer background is lower (Dumdei and O'Brien, 1984; O'Brien et al., 1984). Figure 2a is a mass spectrum acquired after the addition of toluene to the reaction vessel but before irradiation has generated true oxidation products. The predominate peaks are the hydronium-ion water clusters (m/z 37, 55, 73, 91, ...) that are formed in the corona discharge, along with several persistent contaminants and possibly their oxidation products. The peak at m/z 95 is the charge transfer ion (B^+) of toluene. Spurious oxidation products, formed when toluene present in the sample stream reacts with the source produced hydroxyl radicals, appear as (BH^+) and are marked with circles. These products, which were not present before the addition of toluene to the reactor, have been independently identified (Dumdei and O'Brien, 1984; O'Brien et al., 1984). Figure 2b illustrates identical conditions except that CO (0.8% of the total flow) has been added to the carrier gas entering the API source. Note the significant reduction in spurious background peaks as a result of the rapid consumption of HO by CO before HO initiated oxidations could occur. The competition between the hydrocarbon and carbon monoxide for hydroxyl radicals is kinetically modeled below. The final figure, 2c, shows a mass spectrum acquired after 3 hours of reactor illumination. Carbon monoxide is still present in the carrier gas as in Figure 2b. Bona fide oxidation products formed by irradiation in the reaction vessel are now present in the API source and are protonated without interference from source produced HO. Circles in Figure 2c now denote the flask-generated oxidation products of methyl-deuterated toluene whose structures and masses may be found in the next chapter.

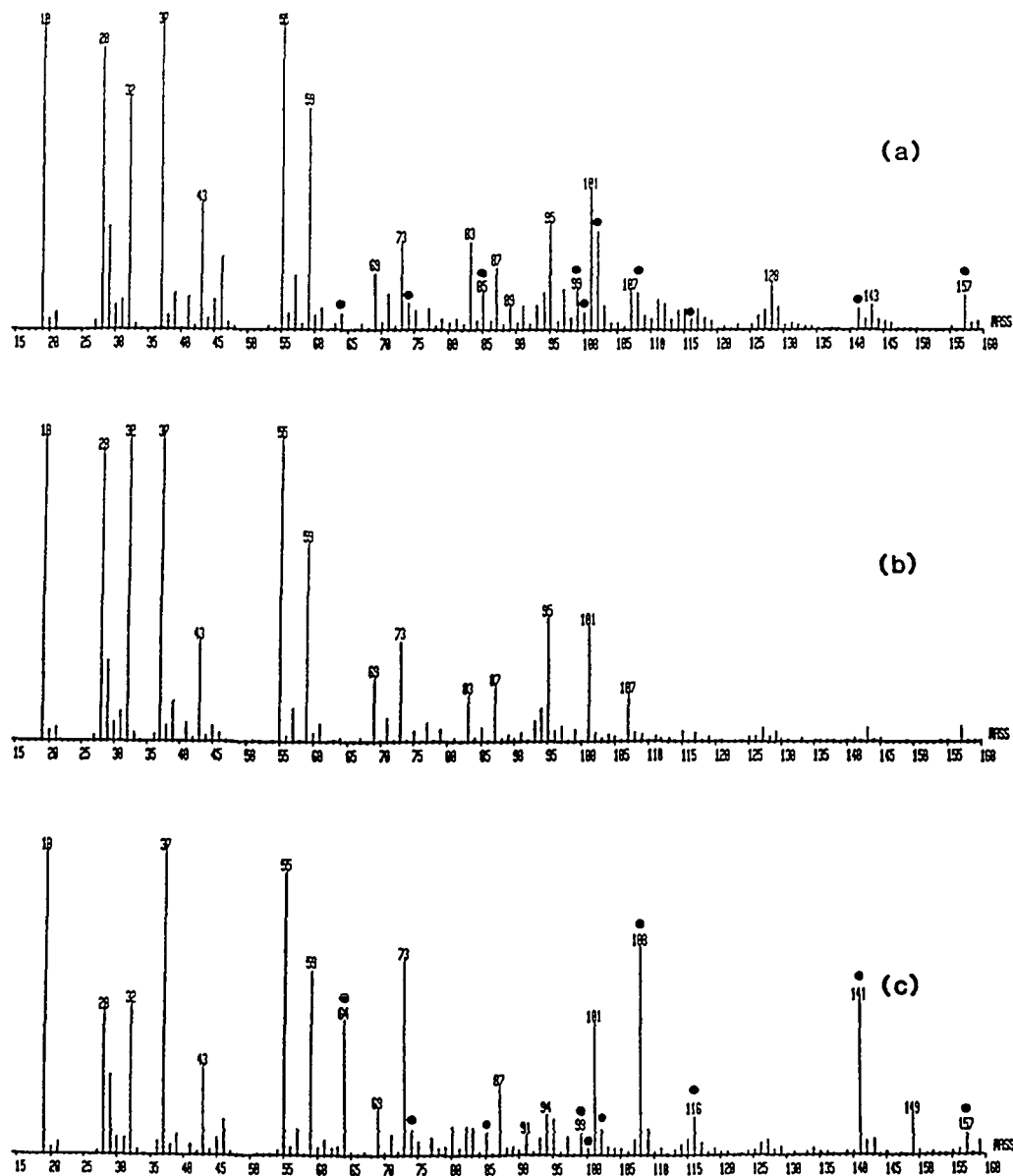


Figure 2. API reaction vessel analysis of methyldeuterated toluene. (a) Spectrum taken after addition of toluene but before any irradiation of the reaction vessel. Circles indicate spurious products not present in the background attributed to HO reactions. (b) With the addition of 0.8% CO to the inlet flow suppressing formation of spurious products. (c) After 3 hours of irradiation the reaction vessel now contains the bona fide toluene oxidation products (circles) which are detected in the presence of CO. Source: Grange (1988).

Kinetic Modeling

Although it is possible that some toluene oxidation is initiated by a process other than HO reaction, for instance quite near the corona needle tip where conditions may be more extreme than in the bulk of the discharge region, the effectiveness of CO in suppressing oxidation products implicates HO as the prime oxidant. Kinetic modeling of the reactions taking place in the source confirms this interpretation. The rate expressions for 30 reactions shown in Table II were numerically integrated, assuming 1 atm and 300K. These modeled reactions include radical/molecule and radical/radical reactions for the species O, H, H₂, HO, HO₂, H₂O₂, O₂ and O₃ as well as the consumption of a generic hydrocarbon (HC) by HO and HO₂ radicals to form generic products. The toluene/HO and toluene/HO₂ rate constants are used here for the hydrocarbon. The initial HO concentration for the modeling was derived from the corona current, 0.2 μA and the inlet flow to the API source of 20 cm³ minute⁻¹ ($[\text{HO}]_0 = [\text{H}_3\text{O}^+]_0 = 0.2 \mu\text{A} * 6.242 \times 10^{18} \text{ ions coulomb}^{-1} / 0.333 \text{ cm}^3 \text{ sec}^{-1} = 3.75 \times 10^{12} \text{ molecules cm}^{-3}$). Figure 3a models changes in concentration as a function of time for the reactions in Table II. After 1 millisecond, 12% of the initial hydrocarbon has been consumed by hydroxyl radicals. Hydroxyl radical concentration falls in the same time by 63% due to its reaction with HC and through other radical loss processes. The residence time in this source is 1.6 seconds based on a cell volume of 0.52 cm³ and the sample flow of 20 cm³ min⁻¹. The modeling may not be quantitative because of uncertainties in the actual volume/time concentration profiles, as well as the source temperature, but are qualitatively correct.

HO Chemistry. The HO concentration in an atmospheric pressure ionization source is directly dependent upon the magnitude of the corona discharge current or emission rate from the radioactive nickel foil. In our source, 0.2 μA is the minimum stable corona discharge current, and it was used to minimize the interferences associated with HO reactions. Interferences are greater at higher currents. One effort (Eiceman et al., 1988) to identify the optimal conditions for APIMS has shown that a 2.0 μA discharge results in a significantly larger analyte ion current and maintains a more stable discharge. Figure 3b models the same species with the same concentrations but at this higher discharge current. The logarithmic scale of the y-axis in Figure 3a was selected to show the concentration

TABLE II

MECHANISM FOR KINETIC MODELING OF HO AND CO
REACTIONS IN HYDROCARBON OXIDATIONS

Reaction				Reaction Rate Constant			
O	O	M	=	O2	M		5.8E-32
H	O2	M	=	HO2	M		1.8E-32
OH	OH		=	H2O	O		1.6E-12
OH	O		=	H	O2		3.8E-11
OH	H		=	H2	O		1.2E-19
OH	H	M	=	H2O	M		6.8E-31
OH	OH	M	=	H2O2	M		6.9E-31
HO2	M		=	H	O2	M	1.7E-42
HO2	H		=	H2	O2		1.3E-11
HO2	H		=	2OH			3.2E-11
HO2	OH		=	H2O	O2		7.0E-11
HO2	HO2		=	H2O2	O2		1.7E-12
H	O2	M	=	HO2	M		5.5E-32
H2O2	H		=	H2	HO2		5.0E-15
O	O2	M	=	O3	M		5.7E-34
OH	O3		=	HO2	O2		6.8E-14
O	HO2		=	OH	O2		5.7E-11
O	O3		=	2O2			8.0E-12
H	HO2		=	H2O	O		3.0E-12

TABLE II
MECHANISM FOR KINETIC MODELING OF HO AND CO
REACTIONS IN HYDROCARBON OXIDATIONS
(continued)

Reaction				Reaction Rate Constant	
O	H2O2	=	OH HO2		2.3E-15
H	O3	=	OH O2		2.9E-11
O	H2O2	=	OH HO2		1.7E-15
OH	H2O2	=	H2O HO2		1.7E-12
HO2	O3	=	OH 2O2		2.0E-15
H2O	H	=	H2 OH		2.2E-25
H2O	O	=	OH OH		4.6E-24
H2O	HO2	=	H2O2 OH		6.1E-35
CO	OH	=	H CO2		3.0E-13
HC	OH	=	PRODUCT1		5.9E-12
HC	HO2	=	PRODUCT2		1.7E-22

INITIAL CONCENTRATIONS

O2	OH	CO	HC	M
5.00E+18	3.74E+12	0.00E00	2.45E13	2.45E+19

Note: Rate constants at T=300K in units of $\text{cm}^3 \text{molecules}^{-1} \text{sec}^{-1}$ or $\text{cm}^6 \text{molecules}^{-2} \text{sec}^{-1}$ as appropriate, where e represents the base ten exponent. Initial concentrations for HO and CO were adjusted to provide different inputs for Figures 2 and 3. A 0.2 μA discharge current corresponds to a 3.74×10^{12} molecules cm^{-3} HO concentration; 0.8% CO corresponds to 1.96×10^{17} molecules cm^{-3} .

changes of all species, but it compresses the scale for the hydrocarbon's consumption. At the larger HO concentration in Figure 3b, the decrease in HC concentration due to HO reaction is very apparent, and the oxidation products are also more abundant in agreement with experimental results. The source sampling rate influences modeled radical concentrations in a similar fashion, with higher flow rates resulting in proportionately lower initial radical concentrations.

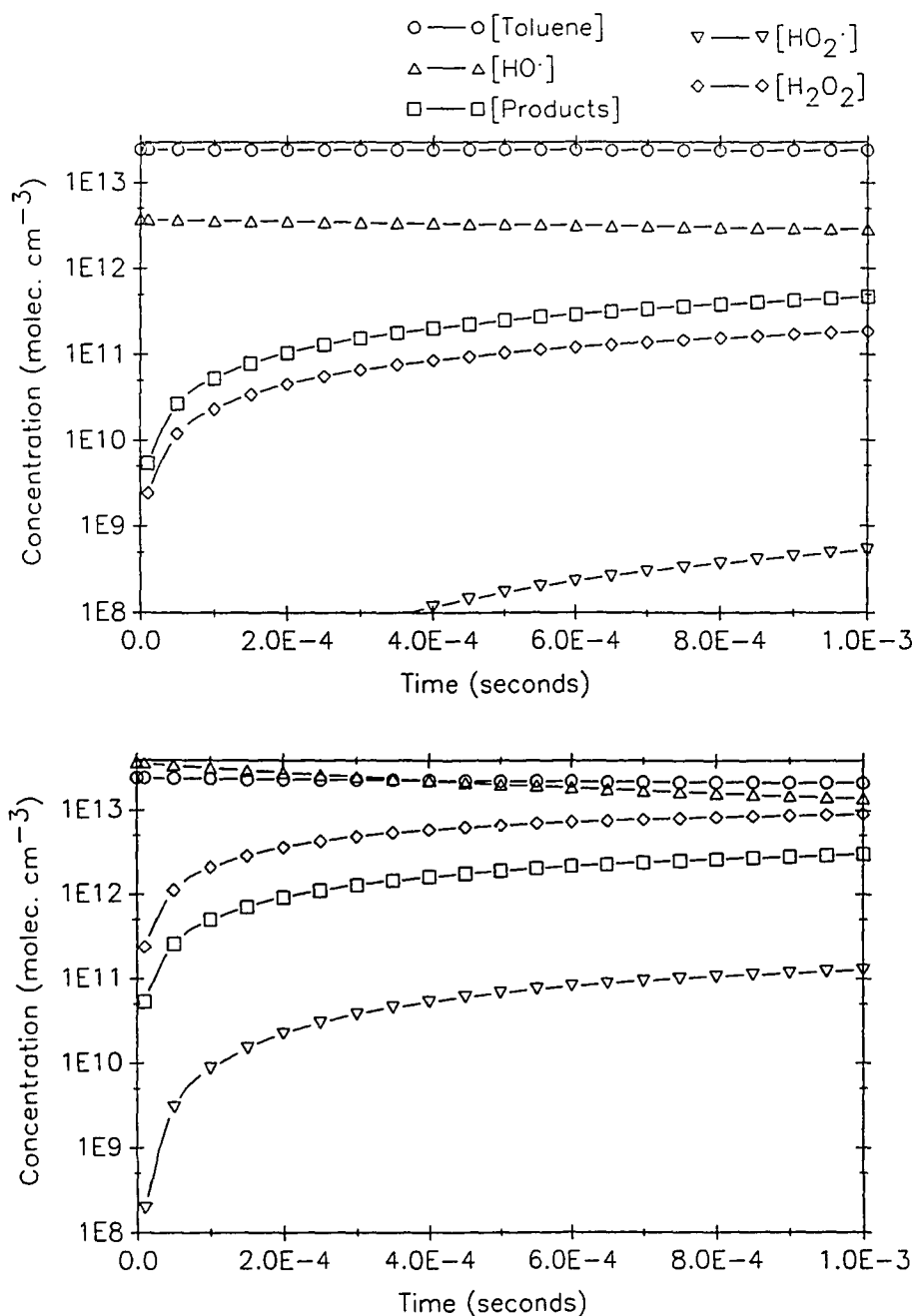


Figure 3. Kinetic modeling of HO reactions in the API source. (a) Hydronium ion concentration equivalent to a 0.2 μA discharge. After 1 millisecond, 12% of the initial compound is converted by HO to product. (b) Modeling of a 2.0 μA discharge. A substantial decrease in the HC concentration and increase in product formation is evident. HC consumption is non-linearly related to the initial HC concentration because of HO self reactions at higher concentrations.

It should be noted that a significant APIMS signal from spurious oxidation products will be obtained even with only a slight oxidation of the parent hydrocarbon. In our source, toluene appears as a charge transfer ion proportionately less intense than its oxidation products. For hydrocarbons which appear as BH^+ ions, the much higher gas-phase basicities of the oxygen-containing oxidation products relative to their parent hydrocarbons result in even greater (relative to toluene) sensitivity for the oxidation products. For analytes below $GB \approx 200$, a 9 kcal/mole difference in basicity was shown in one study (Sunner, Nicol, and Kebarle, 1988) to result in about a ten-fold reduction in relative API sensitivity. The response differences based on the relative sensitivities of the oxidation products will be most pronounced for saturated hydrocarbons, which have much lower GBs than alkenes or aromatics. For instance, the GB of propane is 142 kcal/mole while the basicity of one oxidation product, acetone, is more than 190 kcal/mole. Table I lists the GB values of a range of simple alkane and alkene oxidation products arising from the atmospheric oxidation of methane and ethene.

CO Chemistry. To demonstrate the effects of carbon monoxide on API source chemistry, the reactions in Table II were reintegrated using a CO concentration of 0.8% (1.96×10^{17} molecules cm^{-3}). This concentration is somewhat more than necessary to suppress the source reactions of HO with toluene. The relative rates of the HO reactions with CO and with toluene indicate that 0.8% provides a four fold excess of CO beyond the level needed to assure that 99% of the hydroxyl radicals will be consumed with CO. Figures 4a and 4b show the immediate decrease in the HO concentration due to reaction of hydroxyl radicals with carbon monoxide, while the initial hydrocarbon concentration is unchanged.

Figure 4a is modeled with a 0.2 μA current whereas Figure 4b models the higher 2.0 μA discharge level. In each case where CO is present, the rapid conversion of HO to HO₂ preserves the analyte for subsequent detection by the mass spectrometer and eliminates spurious signals at other masses corresponding to analyte or contaminant oxidation products. Of course, alkanes and alkenes would not be likely analytes for APIMS, but aromatics have been routinely measured with the Sciex TAGA system. Heteroatom containing organic analytes (likely candidates for APIMS analysis) will also react with HO, usually with higher rates than the hydrocarbons from which they are derived. Since these analytes have appreciable GBs, their oxidation products may not have the high relative API sensitivity typical of the oxidation products of pure hydrocarbons.

HO₂ Chemistry. Many compounds have rate constant ratios for reactions with HO₂ vs. HO that are larger than in the case of toluene, and it is possible that conversion of HO to HO₂ by CO might still allow some conversion of an analyte to oxidation products by HO₂ reactions. Compared to HO, HO₂ abstracts aldehydic hydrogen atoms and adds to non-aromatic double bonds proportionately much faster than it reacts with toluene (e.g. by 8 and 5 orders of magnitude, respectively, for formaldehyde and ethene). API source reactions of ethene and formaldehyde with HO and HO₂ were each modeled at 0.2 μA corona current using available rate constants (Atkinson and Lloyd, 1984). Without CO, approximately 3% of both compounds were consumed; after the addition of 0.8% CO, these losses were reduced to 0.08% for formaldehyde and 0.04% for ethene. This suggests that while HO₂ reactions of many species are faster than toluene's, analyte concentrations will still not be significantly perturbed by CO conversion of HO to HO₂.

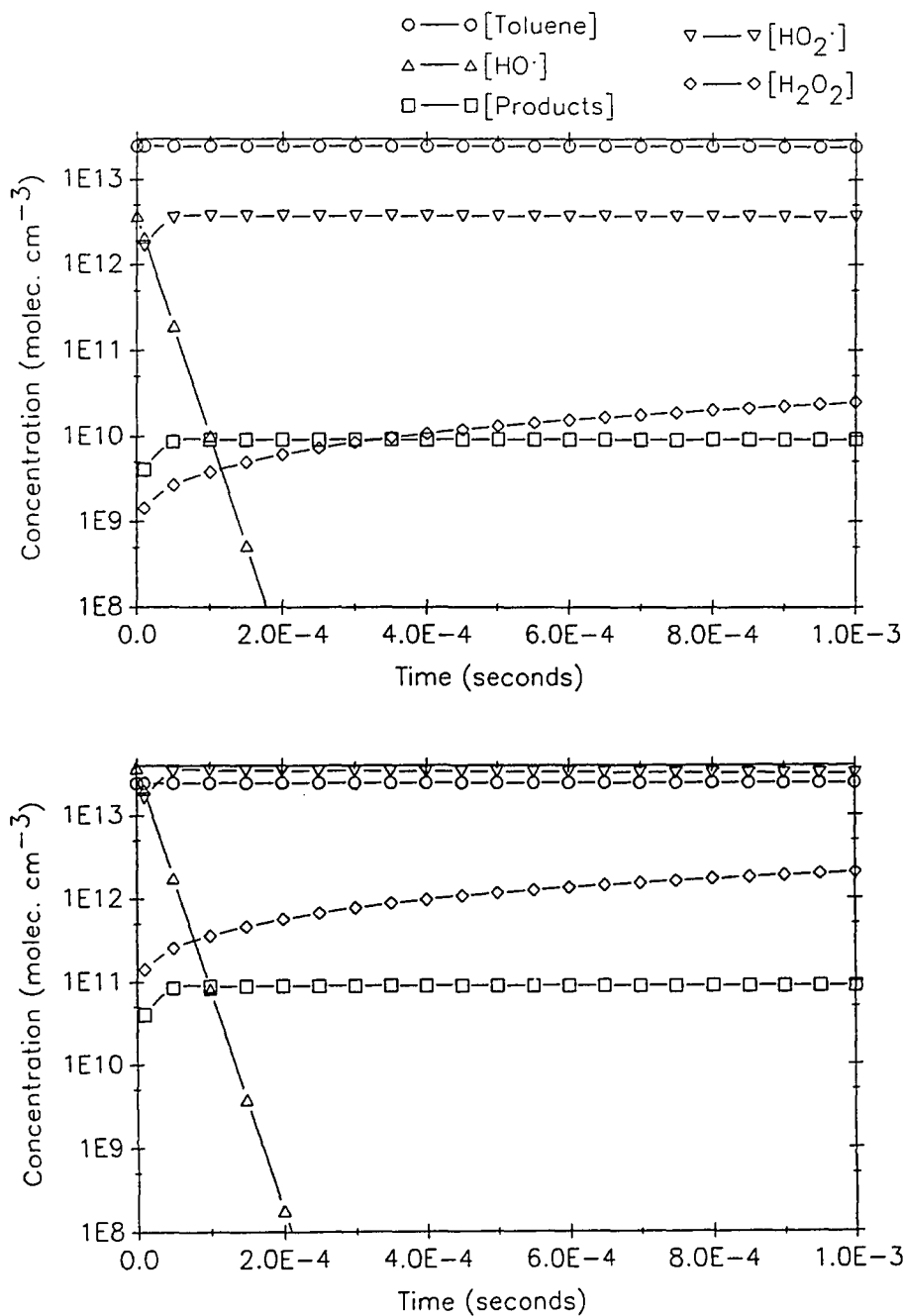


Figure 4. Kinetic modeling of HO reactions in an API source in the presence of carbon monoxide. Figures 4a and 4b correspond to the same plots in Figure 3: (a) 0.2 μA current without CO; (b) 2.0 μA current plus 0.8% CO. HO is now prevented from initiating the oxidation of the hydrocarbons. Modeling based on the mechanism in Table II.

CONCLUSIONS

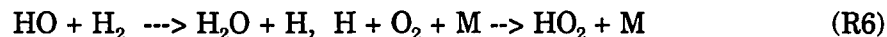
The potential influence of source-produced hydroxyl radicals should be considered in any application involving atmospheric pressure ionization. We are aware of only one previous discussion of source-related chemistry in APIMS (Mahle, Cooks, and Korzeniowski, 1988), viz. the observation of several hydrocarbon/oxygen adducts from an API source at elevated temperature, sampling an unspecified concentration of benzene, toluene, or other aromatic hydrocarbon. Although the authors suggested these products resulted from "probably ionic intermediates" in the source, we believe that HO-initiated reactions are a more likely cause, and that CO would be effective in alleviating their concern that "The extent to which oxygenated products can occur under normal API conditions indicates that caution should be exercised when interpreting these spectra" (Mahle, Cooks, and Korzeniowski, 1988).

We believe APIMS to have great potential for the analysis of oxidation products in atmospheric chemistry or combustion research but studies of oxidation products can be greatly complicated if significant HO radical reactions occur in the source. Carbon monoxide is a useful reagent for eliminating HO reactions, although its low reactivity with HO requires that fairly high concentrations be added. In our source, the small sampling rate facilitates the use of sufficiently high CO concentrations. In sources with larger sampling rates (requiring higher scavenger flow rates) or when analytes are more reactive and/or present at higher concentrations than in this study, a more reactive HO scavenger may be desirable to reduce the total amount of scavenger needed.

The relationship between the minimum amount of CO necessary to avoid source reactions and the hydrocarbon reaction rate can be illustrated. The upper limit to analyte/HO rate constants is given by the gas phase collision rate, about $5 \times 10^{10} \text{ cm}^{-3} \text{ sec}^{-1}$. In order to assure that 99% of the available HO will react with CO and not with a highly reactive hydrocarbon present at 1 ppm, one must add at least 0.165% CO. However, few analytes would react as quickly as the collision rate. Extensive tabulations of HO reaction rate constants with a variety of organic compounds (Atkinson, 1986) will allow the assessment of HO reactions with many potential analytes and most compound families.

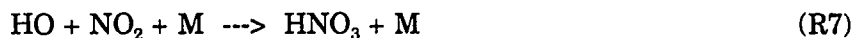
Other Radical Scavengers

HO scavengers other than CO could be considered. H_2 cleanly converts HO to HO_2 , but at 300K reacts 34 times slower than CO, requiring correspondingly higher concentrations.



Before this reagent is tried, the possibility of explosion should be considered.

NO_2 reacts with hydroxyl radicals under atmospheric conditions 40 times faster than CO (R7). NO_2 is available in permeation tubes, although these tubes may not have high enough permeation rates to be useful.



Any of the lighter hydrocarbons could be used, with the caveat that its oxidation products may appear in the mass spectrum, consuming reagent ions in the process. Thus it is desirable to use a reactive hydrocarbon (a gas might be most convenient for delivery) that generates oxidation products with low gas-phase

basicity. Ethene (Table I) reacts with HO 30 times faster than CO and has few products with GB greater than the value of 159 kcal/mole for water. Higher hydrocarbons, although they may react faster with HO, have the disadvantage of producing a larger number of products, many with significant GBs.

New Applications

Although reactions of analytes with HO in an API source may be a nuisance in some applications, it should be possible to use the source-produced hydroxyl radicals for efficient study of atmospheric oxidation mechanisms and kinetics in a complete elimination of the reaction vessel. Such an approach would be useful for atmospheric chemistry or combustion research and will be discussed in detail in the following chapter.

CHAPTER III

STUDIES OF ATMOSPHERIC HO OXIDATION MECHANISMS BY IN SITU HIGH RESOLUTION ATMOSPHERIC PRESSURE IONIZATION MASS SPECTROMETRY

*"Some oxygen molecules help fires to burn while others
choose to help make water, so sometimes it is
brother against brother." (Davis, 1969)*

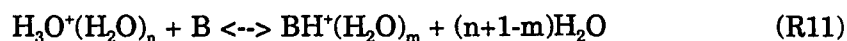
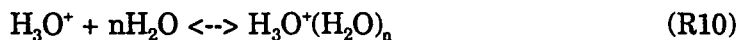
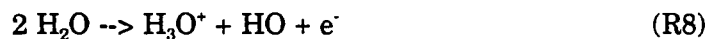
OVERVIEW

In this chapter we describe a new approach to studying atmospheric oxidation mechanisms that uses the hydroxyl radicals created along with hydronium ions in a mass spectrometers' atmospheric pressure ionization source. Hydroxyl radicals formed in the source quickly react with organic compounds added to the sample line to initiate the formation of oxidation products from those compounds. These products are then efficiently protonated by the reagent hydronium ions and mass analyzed. APIMS source reactions are used to analyze toluene's oxidation products, which are shown by their high resolution masses to be identical to those found in previous experiments using a wide variety of other experimental approaches. The use of empirical formulas derived from accurate mass assignment using APIMS can reduce dependence on calibration standards, few of which are available for environmental analysis.

INTRODUCTION

Atmospheric pressure ionization (API) has grown in importance as an ionization source in mass spectrometric analysis since its introduction by Horning et al. (1973). This technique offers significant advantages in mass spectrometry, including high ionization efficiencies (sensitivities in the ppt to ppb range), a dynamic range of up to 3 decades (Reid et al., 1978) and high selectivity for most compounds having proton affinities greater than water (Mitchum and Korfmacker, 1983). There are a variety of spectrometric applications for API, including the direct sampling of gases at ambient pressures from real or simulated atmospheres. Ambient pressure sampling is useful in the analysis of degradation pathways of trace organic compounds in atmospheric chemistry (Grange, O'Brien, and Barofsky, 1988a; Dumdei et al., 1988), an area of particular interest to us.

In positive ion API, the series of ion-molecule reactions occurring within the API source quickly leads to the generation of protonated analyte molecules, (BH⁺), as illustrated by the simplified reaction mechanism shown below (Good, Durden, and Kebarle, 1970a; Proctor and Todd, 1983).



The electron formed in Reaction 8 (R8) is removed at the corona needle, while the hydronium ion participates in proton transfer reactions with an analyte (B).

Declustering of hydrated hydroniums and analytes, which are formed in Reactions

10 and 11, occurs as the ions pass through a dry curtain gas (Reid et al., 1979) or a collision-induced dissociation (CID) region within the ion source (Kambara and Kanomata, 1977), depending on the design of the API source. Declustering concentrates the analyte signal at the single mass of BH^+ without the spectral complication of hydrating water molecules. An important feature of this reaction sequence is the production of the hydroxyl radical (HO) along with the first hydronium ion-water cluster in R8. Hydroxyl radicals are the primary oxidizing agent for trace organics found in the atmosphere (Atkinson et al., 1979), and in combustion processes (Atkinson, Bull, and Shuff, 1980).

The following paragraphs describe the development and applications of a novel application of API in studying atmospheric oxidation processes. Hydroxyl radicals produced in R8 initiate the oxidation of reactant molecules carried in the inlet sample stream. The oxidation products formed within the source mimic those formed by natural processes in the atmosphere. This technique provides significant advantages in the analysis of atmospheric oxidation processes, which we apply here to the chemical degradation of toluene. Toluene is of environmental significance because of its widespread use in fuels and its worldwide presence in the troposphere, measured at levels up 0.1 ppm (Singh et al., 1985). Although much study has been made into toluene's oxidation mechanism, this mechanism has not yet been fully characterized, in part due to the large number of products, their structural complexity (Atkinson et al., 1980; Dumdei and O'Brien, 1984; Leone et al., 1985), and their propensity to adsorb on reaction vessel walls and plumbing (O'Brien et al., 1983). Because of the importance of aromatic compounds

in the troposphere, unraveling their oxidation pathways remains one of the greatest needs in atmospheric chemistry research (Seinfeld, 1989).

EXPERIMENTAL

All mass spectrometry was performed on a VG 7070E-HF double-focusing high resolution mass spectrometer using an API source described elsewhere (Grange, O'Brien, and Barofsky, 1988b; Grange, O'Brien, and Barofsky, 1988c). Coupled with this high resolution mass spectrometer, the API source has provided resolutions of 2800 or more which is both necessary and sufficient to distinguish between oxidation products near 100 Daltons, differing in mass by as little as 0.036 Dalton ($M/\Delta M = 100/0.036 \approx 2800$) (Grange, O'Brien, and Barofsky, 1988a). This resolution corresponds to the mass difference between a carbonyl $R_2C=O$ and an ethyl group $R-CH_2-CH_2-R$, moieties which are unresolvable with quadrupole mass filters or lower resolution magnetic sector instruments. Two isotopically labeled forms of toluene, methyldeuterated ($C_6H_5CD_3 \equiv D_3$) and perdeuterated ($C_6D_5CD_3 \equiv D_8$), were used in addition to unlabeled toluene ($C_6H_5CH_3 \equiv H_8$) as a means to verify the product identifications and the reproducibility of the technique.

Toluene was delivered to the API source at a level of 2 ppm in a $25 \text{ cm}^3 \text{ min}^{-1}$ oxygen carrier gas. Corona discharge currents were varied from 0.2 to 10 μA . The inlet flow rate to the ion source was generally $26 \text{ cm}^3 \text{ min}^{-1}$. With a cell volume of 0.52 cm^3 , the neutral residence time in the source was on the order of 1.2 seconds.

RESULTS AND DISCUSSION

Toluene Products

Mass spectra representative of API source reactions are shown in Figure 5. These were taken using toluene D₈ in an oxygen carrier gas with a 2.0 μ A discharge current. Figure 5a is a background spectrum acquired prior to the addition of toluene to the API source. Ion signals at 37, 55, 73, 91, etc. represent hydrated hydronium ions which are incompletely declustered in the CID region; most other peaks arise from persistent background contaminants. Figure 5b is a spectrum acquired after toluene had been added to the carrier gas for a 2 ppm concentration in the API source. The resulting oxidation products are now evident, particularly the m/z 113 peak arising from protonated benzaldehyde, and the ring opened products at m/z 89, 105 and 133. The role of hydroxyl radicals in initiating toluene's oxidation was confirmed by experiments in which 0.8% CO was added to the airstream. Carbon monoxide is a stable species, whose only significant atmospheric loss process is by HO-oxidation to CO₂. The CO experiments (described in the previous chapter) were effective in the suppression of the observed toluene oxidation products.

Table III summarizes the toluene oxidation products identified using API source reactions. Although more than one isomeric form is possible at a given experimental mass, usually only one representative structure is named, based on a rational elemental composition containing carbon, hydrogen, oxygen and nitrogen. In most cases these isomeric forms would have functional groups (e.g. the methyl group) located at different positions in the molecule. However, three of the 30

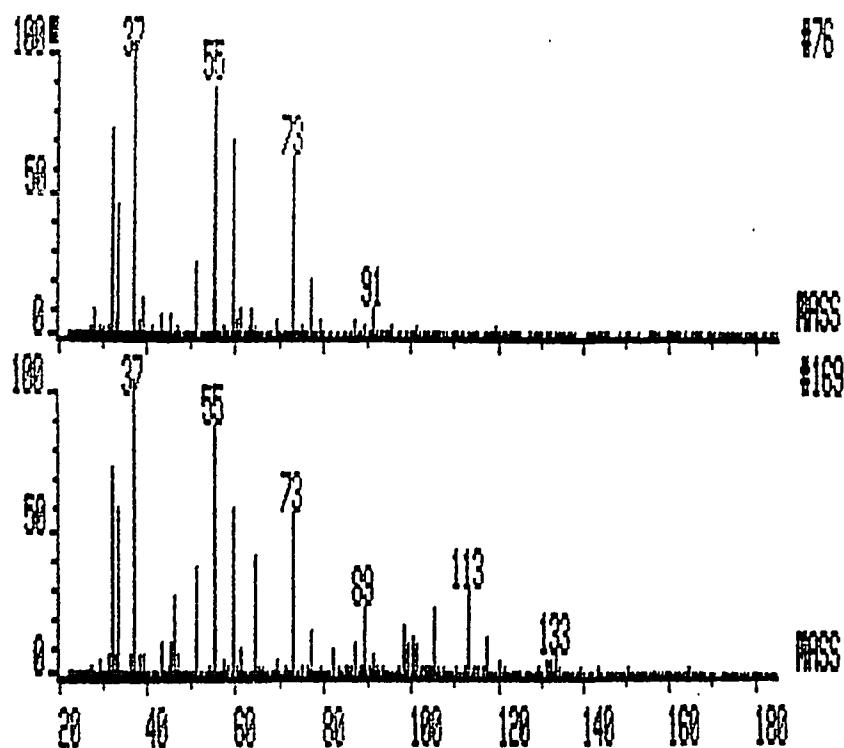


Figure 5. Mass spectral sequence illustrating the photooxidation of D_8 toluene in an oxygen carrier gas. (a) Background spectrum: dominant peaks include hydrated hydronium ions (m/z 37, 55, 73, and several persistent background compounds); (b) After the addition of 2 ppm toluene to the carrier gas, source produced HO radicals initiate toluene's oxidation. Prominent products include signals at m/z 64, 89, 105, 113 and 133 (see Table III).

identified products which are isomeric in the perhydrogenated form are separated in the methyl- or perdeuterated forms. These compounds occur in toluene- H_8 at 99.044, 123.048 and 125.058 Daltons. In these three cases, the deuterated forms of toluene further resolve the identities of these products using empirical formula information. Products whose H_8 masses are similar to dominant background peaks can also be resolved by employing a deuterated form. Elemental analysis is discussed in detail below.

For each compound, and for each of the three experiments, the experimental mass assignments are based on the protonated form of that compound (BH^+), except for toluene and phenol which were detected as charge transfer ions (B^+). The product masses are replaced with an asterisk when the peak was not detected or identified, usually because of a large background peak at the same nominal mass as the product. In such cases the smaller product peak may not be distinguishable on the shoulder of the background peak by the data processing unit of the mass spectrometer. The uncertainty in mass assignment which follows each product mass is the standard deviation in experimental masses based on a series of scans (generally 3-6). The differences between the experimental masses and calculated masses for each product are given in parentheses following each set of product mass and uncertainty. At the foot of the column for each isotopic form of toluene, the average of the differences, Δm , between the calculated and experimental masses is shown, along with the corresponding standard deviation in those differences.

The mass assignments summarized in Table III for each isotopic form confirm the empirical formulas for toluene's primary oxidation products. An alternative description of instrument resolution can be derived from the average uncertainty in the mass assignments. This uncertainty, expressed as the standard deviation of the average mass differences (calcd-exptl), ranges from 0.004 to 0.008 Daltons, Table III. Using this alternative resolution definition, the uncertainty in mass assignment for a product at mass 100 yields an effective resolution ($M/\Delta M$) of $(100/0.006) \approx 17,000$. This indicates the high degree of certainty which may be attributed to the mass assignments in these experiments. Although some of the

TABLE III

TOLUENE OXIDATION PRODUCTS FOUND USING API SOURCE REACTIONS

Product	[Isomers]	$.C_6H_5CH_3$	$.C_6H_5CD_3$	$.C_6D_5CD_3$
Glyoxal		*	*	61.023 \pm .005 (-.003)
(Dumdei et al., 1988; Bandow, Washida, and Akimoto, 1985; Shepson, Edney, and Corse, 1984; Gery et al., 1985)				
Acetic acid	[9]	61.023 \pm .014 (-.006)	64.046 \pm .007 (-.002)	64.042 \pm .006 (-.006)
(Dumdei et al., 1988; Dumdei and O'Brien, 1984)				
Furan	[13]	69.034 \pm .009 (0.000)	69.042 \pm .014 (+.008)	*
(Shepson, Edney, and Corse, 1984)				
Methyl vinyl ketone	[14]	71.048 \pm .007 (-.002)	74.068 \pm .006 (-.001)	77.075 \pm .012 (-.012)
(Dumdei et al., 1988; Dumdei and O'Brien, 1984; Shepson, Edney, and Corse, 1984)				
Methyl glyoxal		*	76.053 \pm .008 (+.005)	*
(Dumdei et al., 1988; Dumdei and O'Brien, 1984; Bandow, Washida, and Akimoto, 1985; Gery et al., 1985)				
Methyl furan	[16]	83.053 \pm .003 (+.003)	86.067 \pm .012 (-.002)	89.083 \pm .004 (-.004)
(Dumdei et al., 1988; Shepson, Edney, and Corse, 1984)				
Butenedial	[17]	85.029 \pm .005 (0.000)	85.033 \pm .001 (+.004)	89.052 \pm .006 (-.002)
(Dumdei et al., 1988; Dumdei and O'Brien, 1984; Shepson, Edney, and Corse, 1984)				
Hydroxyoxobutene	[18]	87.056 \pm .001 (+.010)	90.062 \pm .006 (-.001)	92.080 \pm .009 (+.004)
(Dumdei et al., 1988; Dumdei and O'Brien, 1984)				

TABLE III
TOLUENE OXIDATION PRODUCTS FOUND USING API SOURCE REACTIONS
(continued)

Toluene	[17]	92.064 ±.005 (+.001)	95.084 ±.004 (+.003)	100.121 ±.006 (+.008)
Phenol	[19]	94.045 ±.008 (+.003)	94.064 ±.010 (+.022)	99.064 ±.007 (-.009) (Dumdei and O'Brien, 1984)
Furfural	[20]	97.029 ±.029 (0.000) (Grange, O'Brien, and Barofsky, 1988a; Shepson, Edney, and Corse, 1984)	98.057 ±.004 (+.022)	*.
Oxohexadiene	[20]	97.065 ±.007 (0.000) (Grange, O'Brien, and Barofsky, 1988a; Dumdei et al., 1988; Dumdei and O'Brien, 1984)	100.085 ±.004 (0.000)	105.112 ±.023 (-.004)
Methylbutendial	[22]	99.044 ±.010 (-.001) (Grange, O'Brien, and Barofsky, 1988, Dumdei et al., 1988; Dumdei and O'Brien, 1984)	102.066 ±.005 (+.003)	105.088 ±.008 (+.005)
Hydroxypentadienal	[22]	99.044 ±.010 (-.001)	99.045 ±.008 (0.000) (Grange, O'Brien, and Barofsky, 1988a)	104.084 ±.011 (+.008)
Hydroxybutendial		*.	*. (Dumdei et al., 1988; Dumdei and O'Brien, 1984)	104.046 ±.010 (+.003)
Hydroxyoxobutanal	[22]	103.042 ±.011 (+.002)	106.063 ±.003 (+.005) (Dumdei et al., 1988; Dumdei and O'Brien, 1984)	108.070 ±.008 (-.001)
Oxohexadiene	[20]	97.065 ±.007 (0.000) (Grange, O'Brien, and Barofsky, 1988a; Dumdei et al., 1988; Dumdei and O'Brien, 1984)	100.085 ±.004 (0.000)	105.112 ±.023 (-.004)

TABLE III
TOLUENE OXIDATION PRODUCTS FOUND USING API SOURCE REACTIONS
(continued)

Benzaldehyde	[24]	107.050 \pm .012 (0.000)	108.051 \pm .003 (-.005)	113.086 \pm .014 (-.001)
Dumdei et al., 1988; Dumdei and O'Brien, 1984; O'Brien et al., 1979; Atkinson et al., 1989; Gery et al., 1985)				
Cresol	[24]	109.071 \pm .000 (+.006)	112.083 \pm .005 (-.001)	116.110 \pm .012 (+.001)
(Dumdei and O'Brien, 1984; O'Brien et al., 1979; Gery et al., 1985; Atkinson et al., 1989)				
Oxyhydroxyhexadiene	[25]	113.056 \pm .007 (-.005)	116.080 \pm .003 (+.001)	120.104 \pm .010 (.000)
(Dumdei et al., 1988; Dumdei and O'Brien, 1984)				
Hydroxymethylbutendial	[26]	115.039 \pm .008 (-.001)	118.058 \pm .009 (0.000)	120.070 \pm .007 (-.001)
(Dumdei et al., 1988; Dumdei and O'Brien, 1984)				
Hydroxybenzaldehyde	[27]	123.048 \pm .024 (+.003)	124.063 \pm .005 (+.012)	128.062 \pm .008 (-.014)
(Dumdei and O'Brien, 1984)				
Benzoic Acid	[27]	123.048 \pm .024 (+.003)	123.049 \pm .003 (+.005)	128.062 \pm .008 (-.014)
(Dumdei and O'Brien, 1984)				
Dioxyheptadiene	[28]	125.058 \pm .026 (-.002)	128.077 \pm .014 (-.002)	133.105 \pm .014 (-.005)
(Dumdei et al., 1988; Dumdei and O'Brien, 1984)				
Hydroxycresol	[28]	125.058 \pm .026 (-.002)	128.077 \pm .014 (-.002)	131.094 \pm .014 (-.004)
(Dumdei and O'Brien, 1984)				
Trioxyhexene	[27]	127.030 \pm .007 (-.010)	130.062 \pm .019 (+.004)	133.076 \pm .007 (-.001)

TABLE III
TOLUENE OXIDATION PRODUCTS FOUND USING API SOURCE REACTIONS
(continued)

		(Dumdei et al., 1988; Dumdei and O'Brien, 1984)		
Nitrotoluene	[30]	138.057 ±.007 (+.001) (Dumdei and O'Brien, 1984; O'Brien et al., 1979; Gery et al., 1985; Atkinson et al., 1989)	141.076 ±.010 (+.002)	145.086 ±.014 (-.013)
Nitrophenol	[32]	140.042 ±.008 (+.007)	*. (Dumdei and O'Brien, 1984; Gery et al., 1985)	144.057 ±.011 (-.003)
Dioxyhydroxyheptadiene	[32]	141.057 ±.007 (+.002)	144.078 ±.012 (+.004) (Dumdei et al., 1988; Dumdei and O'Brien, 1984)	148.081 ±.013 (-.018)
Nitrocresol		*.	* (Dumdei and O'Brien, 1984; Gery et al., 1985)	160.072 ±.007 (-.016)
Benzylnitrate		* (Dumdei and O'Brien, 1984; O'Brien et al., 1979; Gery et al., 1985; Atkinson, et al., 1989)	*.	161.107 ±.007 (+.013)
$\Delta m \pm \sigma$ (Dalton)		+0.0005 ±.0041	+0.0034 ±.0067	-0.0015 ±.0083

Notes: Columns give the mass for the protonated form of each analyte (BH+) except for toluene and phenol which occur as charge transfer ions (B⁺). Square brackets enclose the number of CHON compounds falling within ±0.036 Dalton of the assigned structure. Experimental mass uncertainties are 1σ based upon averages of 3-6 replicate scans. The values in parentheses are differences between actual and experimental masses (actual-experimental). The average mass differences and standard deviations of mass differences are given at the foot of the column for each isotopic form. References indicate independent experiments which identified the same oxidation product.

product peaks reported here were observed at very low ion intensities (Fig. 5), it is significant that accurate mass assignments for these products were still obtained. It is possible that additional products were formed yet not identified due to their low ion intensities; further work in this area is still needed.

Empirical Formulas

The assignment of empirical formulas based on accurate masses acquired using APIMS may deserve further discussion. While the resolution provided by our instrument is lower than that in a typical high-resolution EI analysis, the double focusing electrostatic/magnetic sector (EB) configuration of the mass analyzer provides resolutions that are high relative to any other API technique known to us. For any single mass there are a number of possible combinations of atoms which lie within any arbitrary mass window around each compound in Table III. Our previously reported resolution ≥ 2800 for this instrument (Grange, O'Brien, Barofsky, 1988a) corresponds to a mass window of 0.036 Daltons for a nominal mass of 100 Daltons. This window is \geq four times the standard deviation (4.5σ) of assigned masses achieved in Table III, which range from 0.004-0.008 Dalton. Table III includes in square brackets the number of combinations of carbon, hydrogen, oxygen and nitrogen atoms which lie within this ± 0.036 Dalton window for the H_3 experiments. Two examples of these combinations are shown in Table IV. They are based on the experimental masses of two oxidation products: m/z 125.058 (dioxyheptadiene or hydroxycresol) and 138.057 (nitrotoluene). For our purposes here, we have allowed as maximums: 10 carbons, 20 hydrogens, 10 oxygens and 5 nitrogen atoms. Each row in Table IV represents a unique

empirical formula where the number of each atom type is in its respective column, the calculated mass for that empirical formula is given next, followed by the mass difference between the experimental value and the respective calculated value (calcd-exptl).

The product peak at 125.058 Daltons has 28 possible empirical formula solutions using the parameters described above. Most of these are nonrational, based on rules of chemical bonding. Rational structures that can be hypothesized: $C_2H_7O_5N$, a pentahydroxy amino ethane and $C_6H_7O_2N$, a dihydroxy amino benzene. These structures have masses 0.026 and 0.010 below the assigned structure, respectively, but they do not include an additional hydrogen from proton transfer reactions with the reagent ions. If the ion signal arose from these compounds they would be expected as charge transfer species. Three other structures ($C_2H_9O_4N_2$, a tetrahydroxy diamino ethane (-0.002); $C_3H_9O_5$ hexahydroxy propane (-0.013) and $C_6H_9ON_2$ diamino hydroxy benzene (+0.013)) are reasonable in their bonding and include an additional proton to account for protonation by hydroniums. However, the formation of reduced-nitrogen oxidation products in 4 of these species and of a multiply hydroxylated species in the fifth is inconsistent with the oxidizing nature of the corona discharge. The only viable formula from this list is $C_7H_9O_2$, corresponding to either heptadiendial or hydroxycresol (+0.002). The deuterated toluene oxidation experiments confirm the formation of both these individual products, as shown in Table III. Mechanisms for the oxidation of toluene to these products have been hypothesized (Dumdei and O'Brien, 1984; Dumdei et al., 1988), and heptadiendial is a major product under API source conditions. The second example given in Table IV is attributed to nitrotoluene, m/z 138.057.

TABLE IV

EMPIRICAL FORMULA COMBINATIONS FOR SELECTED
EXPERIMENTAL MASSES

Experimental Mass	C	H	O	D	N	Calculated Mass	Δ Mass (calcd-exptl)
	0	5	4	0	4	125.031	-.027
	0	7	3	0	5	125.055	-.003*
	0	13	7	0	0	125.066	.008*
	0	15	6	0	1	125.090	.032
	1	7	4	0	3	125.044	-.014
	1	9	3	0	4	125.068	.009
	1	11	2	0	5	125.091	.033
	2	7	5	0	1	125.032	-.026
	2	9	4	0	2	125.056	-.002*
	2	11	3	0	3	125.080	.022
	3	3	1	0	5	125.034	-.024
	3	9	5	0	0	125.045	-.013
	3	11	4	0	1	125.069	.011
	3	13	3	0	2	125.093	.035
	4	3	2	0	3	125.023	-.035
	4	5	1	0	4	125.046	-.012
	4	7	0	0	5	125.070	.012
	4	13	4	0	0	125.081	.023
	5	5	2	0	2	125.035	-.023
	5	7	1	0	3	125.059	.001*
	5	9	0	0	4	125.083	.025
	6	5	3	0	0	125.024	-.034
	6	7	2	0	1	125.048	-.010
	6	9	1	0	2	125.072	.013
125.058	7	9	2	0	0	125.060	.002*
	7	11	1	0	1	125.084	.026
	9	3	0	0	1	125.027	-.031
	10	5	0	0	0	125.039	-.019

No. of solutions = 28

	0	4	4	0	5	138.026	-.031
	0	10	8	0	0	138.038	-.019
	0	12	7	0	1	138.061	.004*
	0	14	6	0	2	138.085	.028
	1	6	4	0	4	138.039	-.018
	1	8	3	0	5	138.063	.006*
	1	14	7	0	0	138.074	.017
	2	6	5	0	2	138.028	-.029

TABLE IV
EMPIRICAL FORMULA COMBINATIONS FOR SELECTED
EXPERIMENTAL MASSES
(continued)

Experimental Mass	C	H	O	D	N	Calculated Mass	Δ Mass (calcd-exptl)
	2	8	4	0	3	138.052	-.006*
	2	10	3	0	4	138.075	.018
	3	8	5	0	1	138.040	-.017
	3	10	4	0	2	138.064	.007*
	3	12	3	0	3	138.088	.031
	4	4	1	0	5	138.042	-.015
	4	10	5	0	0	138.053	-.004*
	4	12	4	0	1	138.077	.020
	5	4	2	0	3	138.030	-.027
	5	6	1	0	4	138.054	-.003*
	5	8	0	0	5	138.078	.021
	5	14	4	0	0	138.089	.032
	6	6	2	0	2	138.043	-.014
	6	8	1	0	3	138.067	.010
	6	10	0	0	4	138.091	.034
	7	6	3	0	0	138.032	-.025
138.057	7	8	2	0	1	138.056	-.002*
	7	10	1	0	2	138.079	.022
	8	10	2	0	0	138.068	.011
	8	12	1	0	1	138.092	.035
	9	2	0	0	2	138.022	-.035
	10	4	0	0	1	138.034	-.023

No. of solutions = 30

Notes: Empirical formulas based on the following maximum numbers of atoms: Carbon-10, Hydrogen-20, Oxygen-10, Nitrogen-5. The absolute value of the mass difference between the experimental and calculated values was less than or equal to 0.036 Daltons, corresponding to an effective resolution of 2700. Masses indicated with asterisks lie within the 1σ resolution of 0.008 Daltons.

Among the thirty possible empirical formulas listed, only ten give rise to viable structures for charge transfer or proton transfer reactions. While charge transfer reactions do predominate for toluene and phenol, proton transfer is the

predominant pathway for all other known products. Possible empirical formulas, correct in their bonding but without a protonating hydrogen, include: $C_3H_{10}O_4N_2$ diaminotetrahydroxypropane (+0.007); $C_4H_{10}O_5$ pentahydroxybutane (-0.004); $C_6H_6O_2N_2$ dicyanoxyhydroxybutane (-0.014); $C_7H_6O_3$ hydroxybenzoic acid (-0.025) and $C_8H_{12}O$ dioxyoctatriene (+0.035). All these compounds would be expected to appear as a protonated (BH^+) ion, and the latter two are well outside the 1σ error bounds. The nitrogen containing compounds may be further discounted for including reduced amine species in an oxidizing environment. The pentahydroxy compound is a very unlikely oxidation product, as is dioxyoctatriene, which contains one more carbon atom than toluene. Hydroxybenzoic acid is a conceivable toluene oxidation product, but its mass difference lies 6σ from the experimental value and it would be expected to occur as an BH^+ ion rather than as the observed B^+ mass. Several empirical formulas do allow for proton transfer: $C_3H_8O_5N$ aminotetrahydroxyoxypropane (-0.017); $C_4H_{12}O_4N$ aminotetrahydroxybutane (+0.020); $C_7H_{10}ON_2$ diaminobenzyl alcohol ((+0.022) and $C_8H_{12}ON$ cyanoxyheptatriene (+0.035). As before, amines and cyano functionalities are not typical of the oxidizing nature of the source region nor of atmospheric oxidations in general. The remaining empirical formula is $C_7H_8O_2N$, nitrotoluene, whose empirical formula is confirmed in the D_3 and D_8 experiments.

Past Toluene Studies

Each of the oxidation products listed in Table III has been found in at least one other investigation of toluene's atmospheric degradation, examples are given for each compound in Table III. These previous inquiries used techniques which

were very different from the approach used here but they yielded similar results. The techniques included GC or GC/MS (O'Brien et al., 1979; Shepson, Edney, and Corse, 1984), direct FTIR analysis of smog chambers (Bandow, Washida, and Akimoto, 1985), direct-probe-injection methane CI MS/MS analysis of wall washings (Dumdei and O'Brien, 1984), APIMS (Grange, O'Brien, and Barofsky, 1988a), APIMS/MS (Dumdei et al., 1988; O'Brien et al., 1984), and multimode analysis of irradiated Teflon chambers (Gery et al., 1985; Atkinson et al., 1989).

Of particular interest is confirmation of ring fragmentation products. Fragmentation products found in this gas phase technique are identical to compounds found in extracts taken by washing the walls of 22-liter reaction vessels (Dumdei and O'Brien, 1984), the most thorough prior characterization of the toluene oxidation process. Although that study (Dumdei and O'Brien, 1984) was questioned by some as suffering from possible heterogeneous effects, the confirmation of nearly every oxidation product found by Dumdei and O'Brien in the present study suggests that heterogeneous effects did not alter product identities from those characteristic of gas-phase reactions. The presence of most toluene oxidation products on the reaction vessel walls emphasizes the importance of wall adsorption of gas-phase oxidation products in simulated atmospheric reaction chambers as discussed by O'Brien et al. (1983). It also serves to highlight the simplicity of in situ APIMS in minimizing the effects of heterogeneous processes.

Although the volume of our API reaction chamber is small compared to that of a typical reaction vessel, the residence time for oxidation products within the API source is smaller still. Using a protonation rate constant of $3 \times 10^{-9} \text{ cm}^3 \text{ molecules}^{-1} \text{ sec}^{-1}$ (Horning et al., 1973) and a corona current of 2 μA (yielding

$[H_3O^+]_0 = 2.0 \mu A * 6.242 \times 10^{18} \text{ ions coulomb}^{-1} / 0.433 \text{ cm}^3 \text{ sec}^{-1} = 2.88 \times 10^{13} \text{ molecules cm}^{-3}$, the time until product protonation is on the order of 1×10^{-5} seconds. Once protonated, the oxidation product ions are accelerated by the 3 kV electric field into the analyzer sector of the mass spectrometer after a residence time of 0.46 $\text{cm} / 2 \times 10^4 \text{ cm sec}^{-1} = 2.3 \times 10^{-5} \text{ sec}$. In contrast, neutrals diffuse to the API source walls much more slowly, on the order of $4.2 \times 10^{-2} \text{ sec}$ (0.46 cm needle to wall distance / 11.0 cm sec^{-1} based on a root mean square diffusion distance $x = (2Dt)^{1/2}$ using a typical D of $60 \text{ cm}^2/\text{sec}$).

Previous studies of toluene's atmospheric oxidation have identified additional compounds which were not found in this study. These products include: acetylene and acetaldehyde (O'Brien et al., 1979); pyruvic acid, acetal, propenal, hexadienedial, hydroxydioxohexenal, hydroxyoxyhexenal (Dumdei et al., 1988); dinitrotoluene and nitrobenzaldehyde (Dumdei and O'Brien, 1984; Gery et al., 1985); maleic acid (Bandow, Washida, and Akimoto, 1985); formaldehyde and formic acid (O'Brien et al., 1979; Bandow, Washida, and Akimoto, 1985); PAN (Dumdei et al., 1988; Gery et al., 1985; Shepson, Edney and Corse, 1984; Bandow, Washida, and Akimoto, 1985 and many older studies); formaldehyde, methyl nitrite and methyl-p-benzoquinone (Gery et al., 1985); CO (Gery et al., 1985; O'Brien et al., 1983; Shepson, Edney, and Corse, 1984), and $C_6H_4O_2$ (Shepson, Edney, and Corse, 1984). Many of these products are believed to result from secondary reactions of the primary oxidation products formed in the reaction vessel. As examples, the C_6 tricarbonyls have been attributed to secondary reactions of cresol (Dumdei et al., 1988), and PAN is attributed to reactions of methylglyoxal (Bandow, Washida, and Akimoto, 1985). One would not expect to find extensive

secondary products when directly employing source reactions, due to the short residence time of products before protonation and extraction to the analyzer region. Assuming equal initial H_3O^+ and HO concentrations, the net rate for protonation is about 10-100 times faster than that of HO reaction, based on $k(\text{proton transfer})=3 \times 10^9 \text{ cm}^3 \text{ s}^{-1}$ (Bohme, Mackay, and Tanner, 1979), $k(\text{HO} + \text{toluene})=5.9 \times 10^{-12}$ (Atkinson and Lloyd, 1984), and the fact that most toluene oxidation products protonate 2-50 times faster than toluene itself. Thus it is expected that products should be protonated, and the resultant BH^+ ions extracted, before either can react extensively with HO.

Although the compounds thought to be secondary toluene oxidation products in one study (Dumdei et al., 1988) indeed may have resulted from their reaction with HO in the remote smog chamber, it is also possible that some may have resulted from the action of source-produced HO on primary oxidation products produced in the reaction vessel. A radical scavenger (e.g. carbon monoxide) can be employed to eliminate such a permutation of smog chamber oxidation products or ambient trace organics. This was the approach described in Chapter II.

Although this study is primarily qualitative, an analysis of relative response factors among analytes in APIMS by Sunner, Nicol, and Kebarle (1988) may be pertinent to the relative sensitivity for the hydrocarbon oxidation products detected here. In that study, API sensitivities were found to roughly correlate with the gas-phase basicity (GB) of an analyte when analyte GB is below a threshold of about 200 kcal/mole, and to be uniformly high above this GB threshold. While the experimental data showed considerable scatter, relative sensitivities decreased by over an order of magnitude for each 10 kcal/mole decrease in GB below the 200

kcal breakpoint. The reduced relative sensitivities for very low GB compounds such as carbon monoxide and formaldehyde will account for our not detecting them in this study, even if they were formed in the API source. However, the toluene oxidation products which we do detect here have GBs which range from less than 160 to 230 kcal/mole. Many of these compounds have GBs which fall well below the 200 kcal/mole breakpoint found for the Sciex TAGA system (Sunner, Nicol, and Kebarle, 1988). This suggests that the falloff region may occur at lower GB in our instrument. Moreover, the TAGA system has been used (Dumdei et al., 1988) to determine products with GBs below 165, suggesting analyte sensitivity may depend heavily on instrumental and experimental parameters. Further study is necessary.

API Source Chemistry

We know of only one previous observation of reactivity within an API source, the observation by Mahle, Cooks, and Korzeniowski (1983) of reaction products of benzene, toluene, and other aromatic hydrocarbons. These experiments were carried out with a heated API source on an MS/MS instrument and also using a mass-analyzed ion kinetic spectroscopy (MIKES) source. We here discuss the API work. Benzene was observed to generate strong oxygen-adduct ion signals at $m/z=94$ and 95 corresponding to $(B+16)^+$ and $(B+17)^+$. The authors used $H_2^{18}O$ with benzene to determine that the oxygen did not come from water, and they employed declustering to show that the oxygen adduct was not weakly bound. Spectra from toluene and *o*-xylene were shown and were similar to benzene but contained a larger array of products. Several other aromatic hydrocarbons were stated to give

similar results, all of which were considered to be "suggestive of cationic intermediates".

The high temperature (150 or 200°C) of the reported (Mahle, Cooks, and Korzeniowski, 1983) API experiments places the chemical reactivity into a different kinetic regime than reactions in our unheated source, a regime even less understood mechanistically than the low temperature kinetics (see for instance, Atkinson, 1986). However, we may speculate on the possible mechanistic pathways which might explain the observations of Mahle, Cooks, and Korzeniowski. HO is believed to add to aromatic hydrocarbons, which are then partially converted to phenolic products at lower temperatures. However, the inverse Arrhenius behavior observed at higher temperatures (Perry, Atkinson, and Pitts, 1977; Tully et al., 1981) indicates that the HO adduct dissociates, and with benzene the more likely reaction is abstraction of a ring hydrogen atom. The failure of Mahle, Cooks, and Korzeniowski to find ^{18}O incorporation with benzene is consistent with this interpretation. If a ring H atom is abstracted, it then could be replaced with oxygen to form a dioxygen adduct which could be protonated to yield the minor product near m/z 110 apparent in Figure 1 of Mahle, Cooks, and Korzeniowski. Alternatively, the O_2 adduct could lose an oxygen atom to source-produced NO, or two O_2 adduct radicals could eliminate O_2 , forming an O adduct which would be protonated to form the ^{16}O phenol at 94 Daltons.

Figure 1 of Mahle, Cooks, and Korzeniowski also shows a strong signal due to phenol- H^+ at 95 Daltons, and Figure 2 in the same paper gives similar peaks attributable to cresol $^+$ and cresol- H^+ when using toluene. These products are less easily explained mechanistically, but the protonated ions are consistent with our

observation of cresol-H⁺ from toluene in our low temperature source. Figure 2 of Mahle, Cooks, and Korzeniowski (1983) presents a toluene spectrum different from that obtained in our low temperature source (Figure 5b), but the major peaks in both the toluene and o-xylene spectra can be attributed to reaction mechanisms analogous to those of benzene described above. There are similarities to our spectra as well, for instance the peak at m/z 107 may be protonated benzaldehyde and m/z=125 may be the ring-opened compound, both of which we found as major products (see Table III). All of these mechanistic comments are speculative however, pending further API source studies conducted at varying temperatures.

CONCLUSIONS

Although the detailed nature of the reactions occurring within an API source remains to be explored, the similarity of the oxidation products we observe to those found in a wide array of other techniques (Table III) indicates an API source can be used to generate both the hydroxyl radicals necessary to initiate oxidation processes, and the hydroniums needed to protonate the resulting oxidation products. High resolution mass assignments for toluene's oxidation products, resulting from the coupling of our API source with a high resolution mass spectrometer, facilitates assignment of empirical formulas for these products. Deuterium labeling on the reactant hydrocarbon assists greatly in the interpretation of oxidation product spectra, but considerable inferences may be drawn simply from the high-resolution masses of the perhydrogenated oxidation products. The use of in situ API source reactions thus offers significant

advantages over techniques which require the synthesis of authentic reference compounds to verify the identities of the oxidation products.

The use of API source reactions to generate in situ oxidation products also offers several unique advantages over traditional reactor experiments. These advantages include: simplification of the experimental procedures, elimination of the time consuming set-up and irradiation of a simulated atmosphere, minimizing the persistent questions of wall adsorption by polar compounds of low vapor pressure (O'Brien et al., 1983; O'Brien et al., 1984) and eliminating the necessity for chromatographic separation of a complex array of reaction products.

The API source utilized in this study (Grange, O'Brien, and Barofsky, 1988b; Grange, O'Brien, and Barofsky, 1988c) was designed for sampling atmospheric oxidation products from the open atmosphere, rather than for in situ kinetic studies. It seems likely that improvements in source design will produce an apparatus with even greater suitability for the study of atmospheric HO kinetics.

CHAPTER IV

HIGH-RESOLUTION KINETIC ATMOSPHERIC PRESSURE IONIZATION MASS SPECTROMETRY (HRKAPIMS)

*"A scientific fact was only a theory
as a child."* (Davis, 1969)

OVERVIEW

Reactions of hydroxyl radical (HO) with organic compounds are of fundamental importance in air chemistry because they dominate the low temperature oxidations which maintain the cleanliness of the global atmosphere. At the same time, these reactions contribute to undesirable phenomena, such as photochemical smog and acid precipitation. We have developed a new technique, High-Resolution Kinetic Atmospheric Pressure Ionization Mass Spectrometry (HRKAPIMS), for the direct study of these atmospheric oxidations. This technique allows the identification of both stable reaction products and free radical reaction intermediates by empirical mass assignments. Furthermore, studies of reaction kinetics are possible by observing the effect of added reagents on product yields. This versatile technique offers significant advantages for the chemical analysis of atmospheric oxidations, as we demonstrate here for toluene (methylbenzene), a widespread constituent of the lower atmosphere, whose origin is almost entirely through the use of fuels and solvents.

INTRODUCTION

HO Chemistry

HO is known to be an important catalyst in combustion (Atkinson, Bull, and Shuff, 1980), and the importance of HO radicals in the production of secondary air pollution (e.g photochemical smog) was first speculated upon by Leighton in 1961 (Leighton, 1961). The role of HO in maintaining a low, stable, trace-gas composition for the global atmosphere was first alluded to by Weinstock (Weinstock, 1969), who pointed out its role in oxidizing CO to CO₂. HO is also responsible for the removal of most atmospheric organic compounds of natural or industrial origin. Studies of HO reactivity with organic compounds have focused on three areas: measuring rate constants for HO/organic reactions, identifying the products of atmospheric oxidation processes, and elucidating oxidation reaction mechanisms.

HO/organic reactions have been studied in laboratory systems ranging from very low pressure mass spectrometers to simulated atmosphere containment vessels called smog chambers. Experimental determinations of reaction rate constants is an area of broad interest and the HO reaction rates are generally well understood for many organic compounds (Atkinson, 1986; Atkinson, in press). These rate constants, measured under rigorous laboratory conditions, are in good agreement with relative rate measurements made under simulated atmospheric conditions (Atkinson, 1986), corroborating HO's presumed control of organic reactivity in the open atmosphere.

Atmospheric oxidation, initiated by HO, results in intermediate oxidation products which incorporate O and/or N atoms into the organic, yielding stable products such as aldehydes, nitrates, and many others. The identification and quantitation of these oxidation products has been widely addressed, yet the complete oxidation schemes and product yields remain unknown for many common compounds (Atkinson et al., 1989). Gery et al. (1985) have concluded that HO-alkylbenzene chemistry has remained elusive due to the high reactivity of HO radicals and their low concentrations, thus making the HO chemistry difficult and expensive to simulate and monitor.

Oxidation Product Measurements

A summary of the experimentation required in several recent studies may give some insights into the difficulties and expense generally associated with studies of atmospheric oxidation. Atkinson et al. (1989) used a 6400 L Teflon irradiated chamber to generate toluene oxidation products. Gas chromatography with flame ionization detection was used to analyze products which had been collected onto a Tenax solid absorption columns. The system was first calibrated using authentic samples. Gas chromatography-mass spectrometry was used to analyze gaseous samples. Chemiluminescence analysis was used to measure NO and the sum of initial NO, NO₂ and CH₃ONO concentrations. Gery et al. (1985) also used a Teflon reaction vessel, in their case a 200 L chamber surrounded by 34 UV fluorescent lamps. Nitrous acid was generated using liquid phase reactions of sodium nitrite with sulfuric acid. Toluene was measured using a GC with flame-ionization detector and a heated trap. GC with electron capture detection was

used to monitor PAN, methylglyoxal and organic nitrates trapped on a Carbowax column. Glyoxal and methylglyoxal were collected with a bubbler containing an absorbing reagent, 2,4-dinitrophenylhydrazine, and the derivatives analyzed using high performance liquid chromatography (HPLC). Qualitative analysis of some products was conducted using GC/MS and others using GC with flame-ionization and/or thermionic-specific detectors. A chemiluminescent NO_x analyzer was used in the NO-only mode for the oxides of nitrogen, and ozone was monitored using a different chemiluminescent analyzer. Carbon monoxide was monitored using GC and formaldehyde analyzed using a colorimetric analyzer. Not all of these species are directly monitored by HRKAPIMS; chemiluminescent detectors are needed to measure nitrogen oxides, and other methods (i.e. GC) would be necessary to measure compounds with low gas-phase basicities such as carbon monoxide, carbon dioxide and PAN.

Additional examples of the experimental techniques and studies used in the analysis of toluene oxidation include: gas chromatography (O'Brien et al., 1979; Shepson et al., 1985; Atkinson et al., 1980; Leone et al., 1985; Atkinson, Carter, and Winer, 1983; Dumdei et al., 1988), gas chromatography/mass spectrometry (Atkinson et al., 1980; Shepson, Edney, and Corse, 1984; Kenley, Davenport, and Hendry, 1981), tandem mass spectrometry (Dumdei et al., 1988; Dumdei and O'Brien, 1984; O'Brien, et al., 1984), long path length Fourier transform infrared spectroscopy (Bandow, Washida, and Akimoto, 1985; Plum et al., 1983; Tuazon et al., 1986; Tuazon et al., 1984), high performance liquid chromatography (Fund and Grosjean, 1981; Besemer, 1982) and differential optical absorption spectroscopy (Tuazon et al., 1984; Tuazon et al., 1986; Bandow, Washida, and Akimoto, 1985).

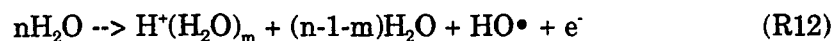
These techniques and others have identified a wide array of toluene oxidation products, but although tentative oxidation mechanisms have been based upon some studies (Atkinson et al., 1989; Gery et al., 1985; Atkinson et al., 1980; Leone et al., 1985; Dumdei et al., 1988; Dumdei and O'Brien, 1984; Bandow, Washida, and Akimoto, 1985; Atkinson and Lloyd, 1984), elucidation of the reaction mechanisms of toluene and other members of the benzene family remains a major area of uncertainty in atmospheric chemistry (Seinfeld, 1989). The ability to detect reaction intermediates simultaneously with stable products would be an asset in elucidating such mechanisms. Zellner, Fritz, and Preidel (1985) have detected the hydroxy-cyclohexadienyl radicals formed from the HO addition reaction with benzene using ultraviolet (UV) laser absorption. However experiments that measured the rates of reaction with NO and NO₂ were conducted at near 20 Torr and may not reflect the processes occurring in the atmosphere (Atkinson et al., 1989). Photoionization mass spectrometry (Sloane, 1978) has found some success in this area yet this technique is very complex and of limited utility for the study of atmospheric processes (Atkinson, 1986). Experiments such as this, which are conducted at low pressures, may not simulate well the actual reaction pathways which occur at atmospheric pressure. Collisions with neutral molecules at higher pressures can deactivate excited molecules, reducing the chances of dissociation.

In a recent review article Niki concludes "... further quantification of reaction products by means of various complementary analytical tools is urgently needed to establish the reaction pathways occurring in the HO-initiated oxidation of aromatic hydrocarbons under atmospheric conditions." (Niki and Maker, 1990) Such an analytical tool should provide insights into the formation of atmospheric

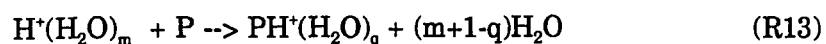
oxidation products, reaction intermediates, and the relative importance of the secondary reaction pathways that follow the initial attack of HO upon the organic. The technique should operate at atmospheric pressure to better represent natural reaction processes and conditions, and provide a rapid and direct measure of product identities and yields. We believe HRKAPIMS can be such a technique.

HRKAPIMS

We have previously developed and characterized an atmospheric pressure ionization (API) source for a high resolution, double-focusing mass spectrometer (Grange, O'Brien, and Barofsky, 1988b; Grange, O'Brien, and Barofsky, 1988c). The API source uses a positive corona discharge at a high-voltage needle tip to generate hydrated proton clusters in the effective net reaction (Good, Durden, and Kebarle, 1970a)



Although hydrocarbons (compounds of carbon and hydrogen only) such as toluene generally have low proton affinities and are detected with low sensitivity, their nitrogen- or oxygen-atom containing oxidation products (P) have much higher proton affinities and can be detected at the ppb to ppt range (Mitchum and Korfmacher, 1983) as an ion current of PH^+ in the mass spectrometer. This is accomplished through protonation (R13) and subsequent dehydration (R14), both occurring in the API source of the mass spectrometer.



This configuration has successfully identified atmospheric oxidation products formed in simulated atmospheres (Grange, O'Brien, and Barofsky, 1988a). When sampling real or simulated atmospheres, HO formed in the API source by R12 can greatly complicate mass spectral interpretation by reacting with atmospheric constituents to form oxidation products not present in the sample. As discussed in Chapter II the HO-initiated API source reactions can be suppressed by the addition of ca. 1% carbon monoxide to scavenge HO. The suppression of oxidation products by CO provides strong evidence that the oxidations are initiated by source-produced HO, rather than by other processes in the immediate vicinity of the corona needle.

Alternatively, we have demonstrated in the previous chapter the potential for producing and evaluating atmospheric oxidation products directly within the API ion source. These experiments form the basis for the technique we here call HRKAPIMS, in which the hydroxyl radicals produced in R12 initiate the oxidation of a hydrocarbon introduced into the sample stream, and the proton clusters are used to detect the resultant oxidation products. In an analysis of toluene oxidation, discussed in Chapter III using three isotopically different forms of toluene, we identified 29 distinct oxidation products formed within the ion source. All of these products had been identified in one or more previous studies using other techniques, although only one previous study (Dumdei and O'Brien, 1984) was able to identify such a large array of products. The standard deviation between the observed and actual masses for the stable toluene oxidation products was ≤ 0.008 atomic mass units, which allows assignment of empirical formulas in most cases without the necessity of reference compounds. A single HRKAPIMS

experiment provides the information in Chapter III, as well as information in this chapter on detection and identification of reaction free radical intermediates and the effects of changing reagent concentrations on product ratios.

RESULTS AND DISCUSSION

Experimental

The experiments described below and the experimental conditions associated with this discussion are the same as Chapter III. They are in fact the same experiments. Toluene concentrations on the order of 2 ppm were employed and a corona current of 0.2 μA produces an initial HO concentration of 3.7×10^{12} molecules cm^{-3} .

Mass Spectra. Mass spectra representative of API source reactions are shown in Figure 6 where perdeuterated toluene ($\text{C}_7\text{D}_8 = 100.113$ Dalton) was delivered to the API source in a zero air carrier gas. Figure 6a is a background spectrum in which ion signals at m/z 37, 55, 73 and 91 ... arise from hydrated hydronium ions which were incompletely declustered in the CID region; other peaks constitute a persistent background. Figure 6b illustrates conditions where toluene has been added to the carrier gas entering the API source. Prominent evident toluene oxidation products are the ring-opened dialdehydes at 105.088 and 133.105 Daltons shown in Figure 6b. Toluenes' stable oxidation products were discussed in the previous chapter. The effect of NO on source reactions is evident in Figure 1c. Here, upon addition of 10 ppm NO to the inlet air stream, the product ratios have shifted to favor the 133.105 Daltons product in preference to the 105.088 Daltons product and the yield of nitrotoluene (145.086 Daltons) has

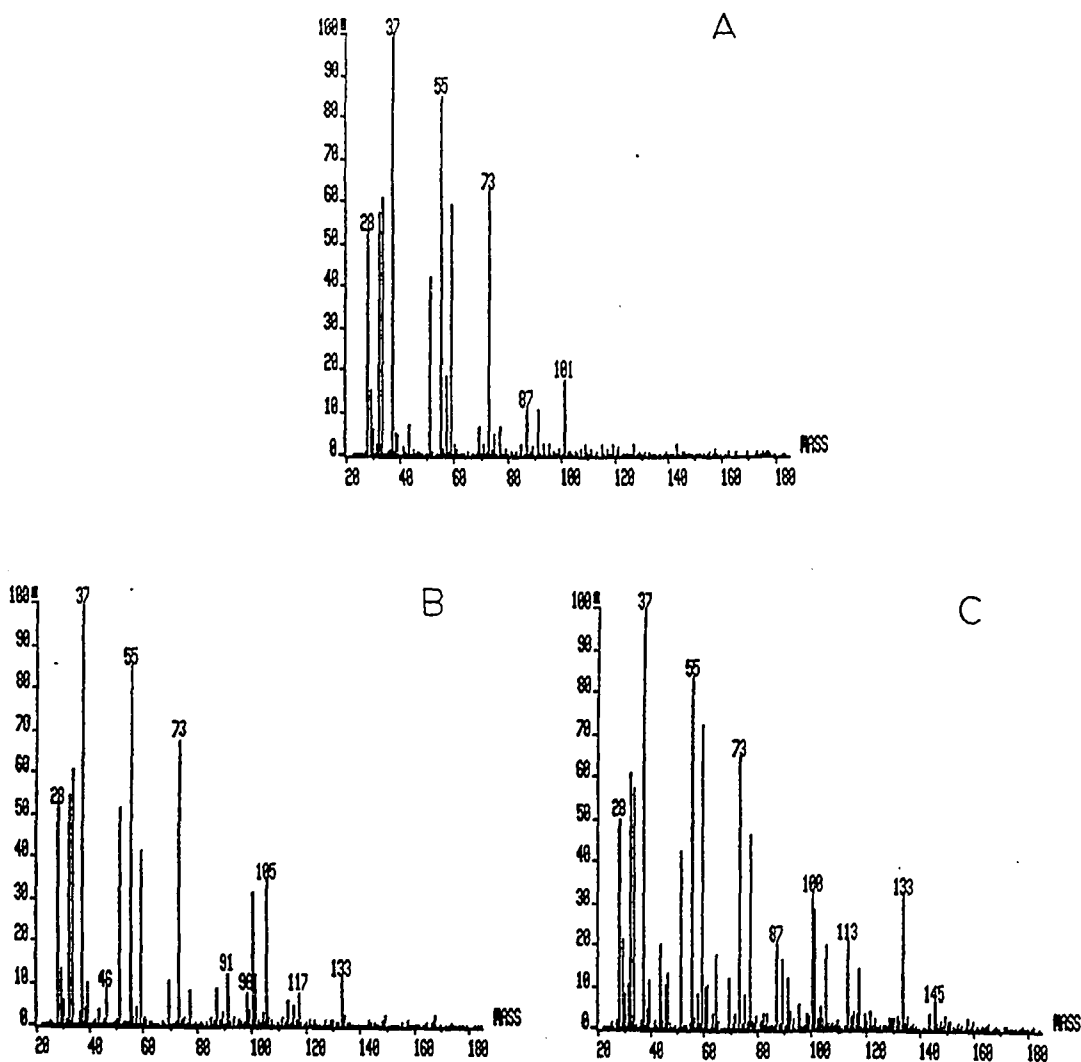


Figure 6. Mass spectra showing the course of a typical HRKAPIMS experiment. (a) Background spectrum in which predominant peaks include water clusters (m/z 19, 37, 55, 73, ...) and persistent background peaks. (b) With 2 ppm perdeuterated toluene in air present in the ion source the major oxidation products are evident at m/z 105 and 133. (c) After the addition of 10 ppm NO the product ion intensities shift to the formation of the ring fragmentation product methylheptadienedial at m/z 133 and nitrotoluene m/z 145.

also increased. The semi-quantitative analysis of the effect of NO concentration on the free radical intermediates of toluene oxidation is addressed in a later section.

Product Ion Currents. The consistent ability of API source reactions to reproduce photo-oxidation processes is illustrated in Figure 7, which compares three plots of normalized ion intensity versus scan number for methylhexadienedial (C7 in Figure 8) formed under API source reactions. The three separate plots correspond to the three isotopic forms of toluene used in these experiments, which were conducted on different days, using oxygen as the carrier gas. The experimental masses of this product are 125.058, 128.077 and 133.105 Daltons in the H₈, D₃ and D₈ forms of toluene respectively. The horizontal axis is not identical in each of the three experiments, but each numbered region (1-6) represents the same changes in experimental conditions, described below. The differences in the horizontal axes are based solely on the sequence and number of scans taken under each condition. Ion intensities are normalized to show the maximum peak in each scan at 100%. Regions 1-3 chart ion intensity before the addition of toluene to the inlet flow and represent the background levels, while regions 4-6 are after the addition of toluene. Regions 1 and 4 indicate scans where the corona current was increased in increments from 0.2 to 10 μ A, generally to include 0.2, 0.5, 1.0, 2.0, 5.0 and 10 μ A. Regions 2 and 5 record the addition of nitric oxide (NO) at levels of 0, 2, 5, 10 and 38 ppm at a constant current of 0.2 μ A, and scans in regions 3 and 6 were acquired while the current was again varied from 0.2 to 10 μ A at a constant NO level of 10 ppm. The 1.2 second residence time within the API source allows the experimental conditions to be quickly and easily adjusted. Regions 4 and 6 in Figure 7 show marked increases in ion intensity resulting from the higher discharge current. Increasing the corona discharge current increases the concentrations of both

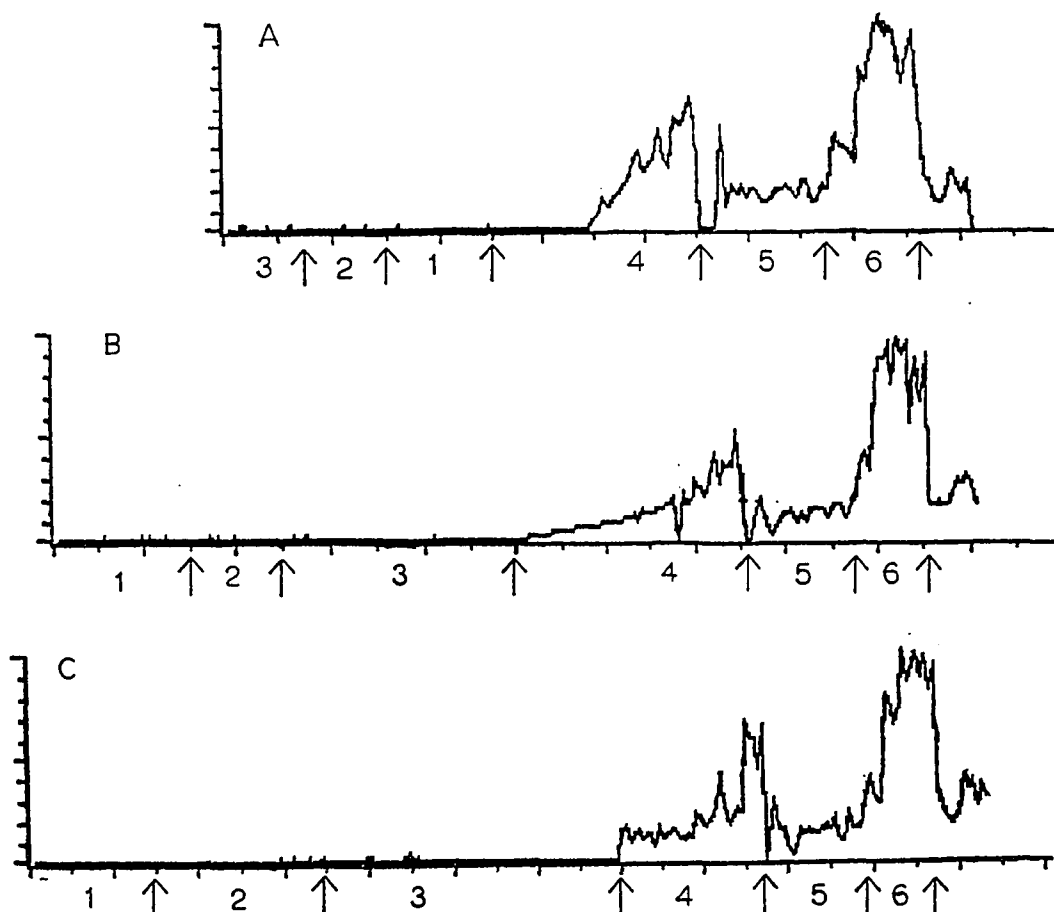


Figure 7. Normalized ion intensity vs. scan number for methylhexadienedial. In the three isotopic forms of toluene: (a) hydrogenated, (b) methyldeuterated, and (c) perdeuterated, the product appears at $m/z=125.058$, 128.077 , and 133.105 respectively. Each region, described in the text, represents differing experimental conditions affecting product yields and distributions.

hydroxyl radical and hydronium, increasing the extent of HO initiated oxidation and the availability of hydroniums to protonate the products.

Free Radical Intermediates

In analyzing the stable toluene oxidation products produced in the API source, we found that the concurrent presence of HO and H_3O^+ water clusters, and

the relatively short time scale for their reactions, allows free radical reaction intermediates to be protonated and measured simultaneously with the stable products. Five such reaction intermediates, detected in our experiments with toluene, are listed in Table V. The experimental data represent three separate experiments using toluene $\text{CH}_3\text{C}_6\text{H}_5$, methyldeuterated toluene $\text{CD}_3\text{C}_6\text{H}_5$, and perdeuterated toluene $\text{CD}_3\text{C}_6\text{D}_5$; the intermediates are therefore measured at different masses in each of the three experiments. The experimentally determined accurate mass is given along with the standard deviation of 3 to 6 replicate measurements. The mass differences (shown in parentheses) between the proposed structures and the observed masses compare favorably with those obtained for the stable products discussed in Chapter III.

TABLE V
EXPERIMENTAL MASSES OF FIVE FREE RADICAL TOLUENE
OXIDATION INTERMEDIATES

	$.\text{C}_6\text{H}_5\text{CH}_3$	$.\text{C}_6\text{H}_5\text{CD}_3$	$.\text{C}_6\text{D}_5\text{CD}_3$
b1	110.086 \pm .023 (+.013)	113.091 \pm .012 (-.006)	118.126 \pm .029 (+.003)
d1	142.066 \pm .023 (+.003)	145.092 * (+.010)	150.096 \pm .022 (-.017)
d2	126.064 \pm .009 (-.004)	129.080 \pm .016 (-.007)	134.105 \pm .023 (-.013)
e2	174.037 * (-.016)	177.054 * (-.018)	182.082 \pm .012 (-.021)
e3	158.084 \pm .020 (+.026)	161.097 * (+.020)	166.044 * (-.064)

Notes: Masses in each isotopically labeled form are given for the protonated radical (PH+), whose structure is given in Figure 8. 1σ uncertainties are based upon 3-6 multiple determinations. Values in parentheses are differences between observed and actual molecular weights. *-insufficient data to assign uncertainty

Free Radical Intermediate Measurements

Zellner, Fritz, and Preidel (1985) have measured reaction rates for NO, NO₂ and O₂ with the hydroxycyclohexadienyl (HCHD) radical. These experiments found

that the reaction of HCHD with NO was independent of the O₂ concentration. This apparently conflicts with earlier descriptions of toluene photooxidation including Atkinson and Lloyd (1984) and may agree with the recent findings of Atkinson et al. (1989) who found that the production of nitrotoluene did not extrapolate to zero in the absence of NO₂. However since the rates of Zellner were measured at low pressures conclusions drawn from this experiment cannot be immediately applied directly to processes at atmospheric pressure. This uncertainty lead to the observation (Atkinson 1990) that "... at the present time the actual reactions of the hydroxycyclohexadienyl radicals formed from the OH radical reactions with the aromatic hydrocarbons are not known."

One persistent obstacle to the measurement of aromatic hydrocarbon oxidation products is the difficulty associated with finding them. While a particular study may report finding 55-75% of the reacted carbon (Gery et al., 1985) this generally requires using very high concentrations of NO and NO₂ which force the oxidation toward those products more easily detected. Experiments that use lower levels of nitric oxides typical of the real atmosphere form different products which are more difficult to detect experimentally. As a result the product yields which can be accounted for in more realistic studies are significantly lower.

Chemical Modeling

The NO concentration plays an important role at branch points in most atmospheric oxidation sequences. Figure 8 presents a simplified reaction mechanism for toluene oxidation that reflects the potential influence of NO on the formation of various toluene oxidation products. This mechanism and its rate

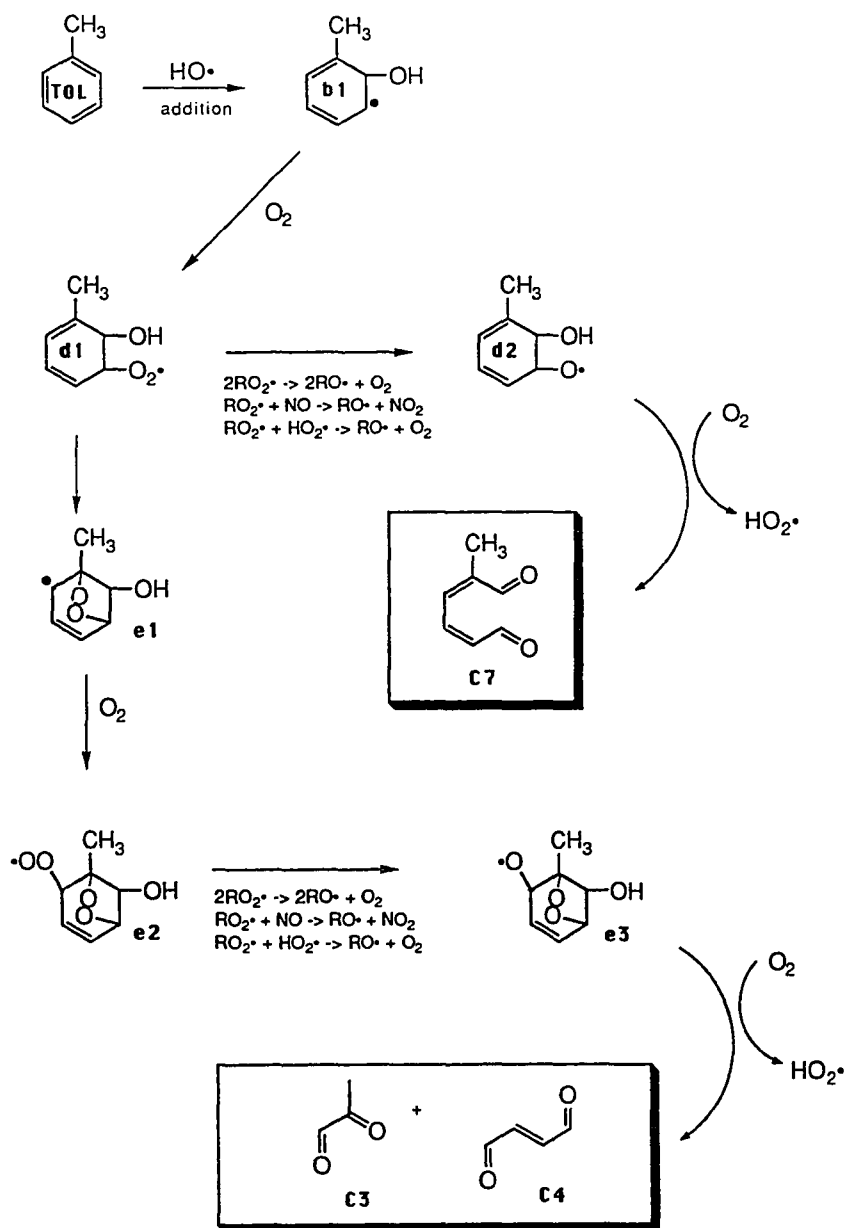


Figure 8. Partial toluene oxidation mechanism showing the production of several free radical intermediates and stable products. Experimental accurate mass assignments for the stable products are in Chapter III, masses for the free radical intermediates in Table V.

constants are given in Table VI and are taken largely from Atkinson and Lloyd (1984). It should be emphasized that many of the rate constants may be

TABLE VI
KINETIC MODELING MECHANISM FOR HRKAPIMS
SOURCE REACTIONS

Reaction				Rate Constant
TOL	OH	=	B1	5.9E-12
B1	O2	=	D1	3.3E-15
D1	NO	=	D2 NO2	7.0E-12 (7E-11)
D1	D1	=	D2 O2	4.3E-15
D1	HO2	=	D2 OH O2	8.5E-12
D2	O2	=	C7 HO2	7.0E-15
D1		=	E1	8.0E4
E1	O2	=	E2	1.0E-12
E2	NO	=	E3 NO2	7.0E-12 (7E-11)
E2	E2	=	E3 O2	4.3E-16
E2	HO2	=	E3 OH O2	8.5E-12
E2	A2	=	E3 A3 O3	4.3E-16
E2	D1	=	E3 D2 O2	4.3E-16
E3	O2	=	C4 C3 HO2	7.0E-15
B1	H3O	=	B1H H2O	3.0E-9
D1	H3O	=	D1H H2O	3.0E-9
D2	H3O	=	D2H H2O	3.0E-9
E1	H3O	=	E1H H2O	3.0E-9
E2	H3O	=	E2H H2O	3.0E-9
E3	H3O	=	E3H H2O	3.0E-9
C7	H3O	=	C7H H2O	3.0E-9
C4	H3O	=	C4H H2O	3.0E-9
C3	H3O	=	C3H H2O	3.0E-9
O	O	M	O2 M	5.8E-32
H	O2	M	HO2 M	1.8E-32
OH	OH		H2O O	1.6E-12
OH	O		H O2	3.8E-11
OH	H		H2 O	1.2E-19
OH	H	M	H2O M	6.8E-31
OH	OH	M	H2O2 M	6.9E-31
HO2	M		H O2 M	1.7E-42
HO2	H		H2 O2	1.3E-11
HO2	H		2OH	3.2E-11
HO2	OH		H2O O2	7.0E-11
HO2	HO2		H2O2 O2	1.7E-12
H2O2	H		H2 HO2	5.0E-15
H	O2	M	HO2 M	5.5E-32
O	O2	M	O3 M	5.7E-34
OH	O3		HO2 O2	6.8E-14
O	HO2		OH O2	5.7E-11

TABLE VI
KINETIC MODELING MECHANISM FOR HRKAPIMS
SOURCE REACTIONS
(continued)

Reaction				Rate Constant
O	O3	=	2O2	8.0E-12
H	HO2	=	H2O O	3.0E-12
O	H2O2	=	OH HO2	2.3E-15
H	O3	=	OH O2	2.9E-11
O	H2O2	=	OH HO2	1.7E-15
OH	H2O2	=	H2O HO2	1.7E-12
HO2	O3	=	OH 2O2	2.0E-15
H2O	H	=	H2 OH	2.2E-25
H2O	O	=	OH OH	4.6E-24
H2O	HO2	=	H2O2 OH	6.1E-35
 \$INITIAL CONDITIONS				
TEMP	NO	O2	OH	
H3O	TOL	H2O	M	
2.98E+02	1.225E+16	5.0E+18	3.740E+13	
3.740E+13	2.450E+13	1.0E+16	2.5E+19	

Notes: Toluene oxidation products are identified in Figure 8 and modeling results presented in Figure 9. Reaction rate constants are from Atkinson and Lloyd (1984) where available (see discussion in text). $\text{RO}_2^\bullet + \text{NO}$ reactions were modeled at the faster 7×10^{11} rate. Rate constants at $T=300\text{K}$ in units of $\text{cm}^3 \text{molecules}^{-1} \text{sec}^{-1}$ or $\text{cm}^6 \text{molecules}^{-2} \text{sec}^{-1}$ as appropriate, e indicates power of ten.

considered as provisional values, since no experimental measurements of their values are reliable. A new comprehensive kinetic model has been compiled by Carter (1990) to describe atmospheric oxidation processes. However in this model "no attempt to speculate on the nature and detailed reactions of the uncharacterized aromatic products" is made, and the rates of Atkinson and Lloyd (1984) appear to be the best available.

Using the provisional rate constants (Atkinson and Lloyd, 1984), we found that NO was predicted to have a smaller effect on the intermediate concentrations than we observed experimentally. However, if we increased the rate constants for the reactions of NO with intermediates d1 and e2 by a factor of ten, we were able to reproduce the general trends in the experimental data. This is illustrated in Figure 9 which compares experimental ion intensities for five of the free radical intermediates listed in Table I, and identified in Figure 1, with the calculated results from the kinetic model in Table II. The measured protonated ion intensities ($b1H^+$, $d1H^+$, etc.), based on an experiment using perdeuterated toluene, are shown as filled points in Figure 9 with error bars representing the experimental uncertainty. The open points (with curves) are the modeled concentrations calculated from the integration of Table VI. The experimental data (measured ion currents) were all multiplied by a single constant to bring them to the same scale as the calculated concentrations. The mechanism in Table VI contains a complete sequence of HO/ HO_2 radical reactions, the toluene oxidation mechanism from Figure 8, and protonation steps for all reaction intermediates and stable products. In this simplified treatment, H_3O^+ is the only source of protons, and all protonation reactions have the same rate constant (Bohme, Mackay, and Tanner, 1979). In fact, H_3O^+ water clusters also serve as proton sources, and the protonation rate constants vary somewhat, resulting in somewhat different sensitivities for various products P. For oxidation products with low gas-phase basicities, transfer of protons back to water should be included as well. Full treatment of the processes in the source is complex, and beyond the scope of the presentation here. The intermediate concentrations are calculated by integrating

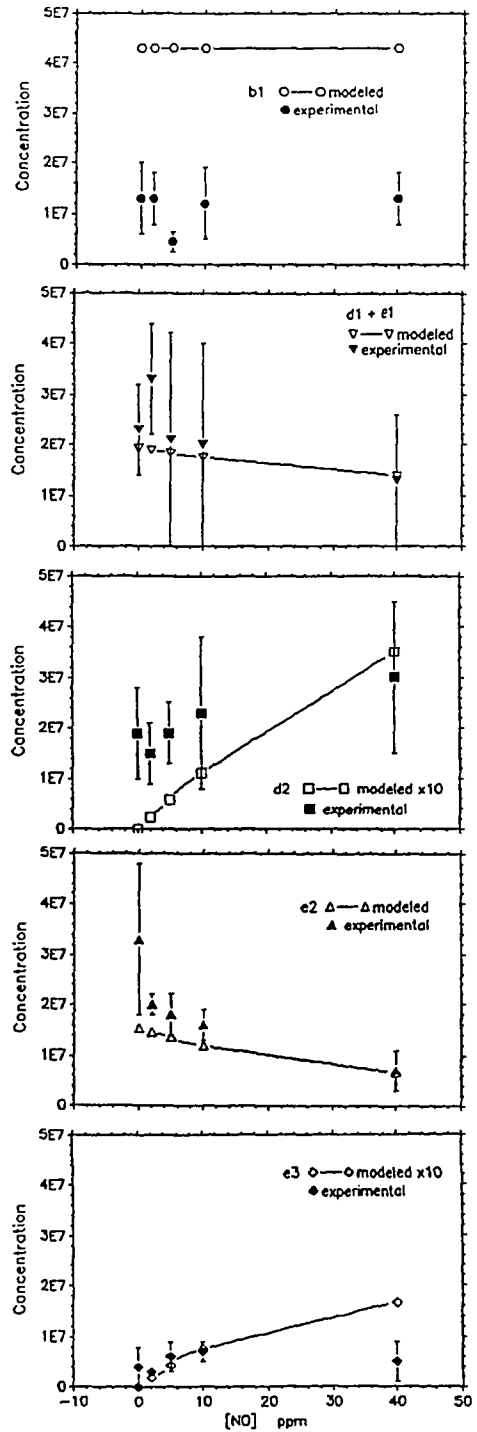


Figure 9. Experimental vs. Modeled ion intensities for toluene free radical intermediates. Modeled data from the mechanism in Table VI. Experimental values uniformly scaled to the modeling data.

the mechanism until steady-state ion concentrations are achieved, requiring about 25 milliseconds reaction time with an initial HO=H₃O⁺ concentration of 1.5 ppm. The residence time for neutrals in the source is about 1.6 seconds based on a flow of 20 cm³ min⁻¹.

CONCLUSIONS

At this point in the development of HRKAPIMS, there remain uncertainties about the processes occurring within the API source and further study using compounds having understood chemistry will be required before full confidence in kinetic modeling can be developed. Since these data were obtained with an API source designed for atmospheric sampling rather than kinetic analysis, it seems likely that improvements in source design will also improve the quantitative abilities of HRKAPIMS. Nevertheless, the successful semi-quantitative modeling of NO effects suggests that reliable quantitative data can be obtained using this technique.

Although considerable knowledge regarding atmospheric oxidation mechanisms has been accumulated over the last several decades, especially for smaller hydrocarbons, a great deal of information remains to be unraveled, especially for single ring and polycyclic aromatic hydrocarbons. The ability of HRKAPIMS analysis to detect 29 stable products, as well as the 5 free radical intermediates, simultaneously under conditions similar to the ambient atmosphere places this technique in a unique class. Our detection here of the hydroxycyclohexadienyl radical suggests that under atmospheric conditions O₂ addition to the aromatic ring is an important pathway, affirming the earlier

proposed mechanisms. We believe that HRKAPIMS can be an important tool in the study of these compounds and will provide valuable insights into the details of aromatic hydrocarbon oxidation processes in the atmosphere.

CHAPTER V

SEMIEMPIRICAL CALCULATIONS OF GAS-PHASE BASICITIES WITH APPLICATIONS TO MASS SPECTROMETRY

*"We say the cause of perfume disappearing is evaporation.
Evaporation gets blamed for many things people forget
to put the top on." (Davis 1969)*

OVERVIEW

The gas-phase basicity of a compound is important in a variety of chemical systems involving proton transfer reactions; these include the ionization steps in chemical ionization, fast atom bombardment, atmospheric pressure ionization mass spectrometry (APIMS) and ion mobility spectrometry. Gas phase basicities (GBs) for 127 organic compounds containing carbon, hydrogen, nitrogen and oxygen are calculated. Linear regression analysis of semi-empirical calculated heats of formation give GBs with an overall uncertainty of 3.1 kcal/mol for a subset of 99 compounds with GBs near 200. The remaining 28 compounds are separated into 5 classes and their characteristic errors are discussed individually.

INTRODUCTION

The decreasing cost of computational power and the increasing availability of computational software have made semiempirical molecular orbital (MO) calculations available to an ever widening circle of chemists. The ability of

semiempirical calculations to deal with large and complex molecules which would be prohibitive to study with ab initio methods encourages the use of MO theory in a variety of applications. In the field of mass spectrometry (MS) for instance, the relative sensitivity of analytes in atmospheric pressure ionization (API) and fast atom bombardment (FAB) is a function of a compound's gas-phase basicity (GB) (Lacey and Keough, 1989; Sunner, Kulatunga, and Kebarle, 1986; Sunner, Nicol, and Kebarle, 1988; Sunner, Ikonomou, and Kebarle, 1988a; Sunner, Ikonomou, and Kebarle, 1988b). Response factors in ion mobility mass spectrometry (IMMS) are also dependent on a compound's basicity, when using an atmospheric pressure ionization source (Vandiver, Leasure, and Eiceman, 1985). Recent MO calculations compared the effectiveness of MINDO/3, MNDO and AM1 in the prediction of proton affinities (Voets et al., 1989) and hydrocarbon acidities (Kass 1990) and found AM1 superior. The heats of formation for protonated organics (BH^+) are of particular interest, but less theoretical work has been done in this area than for species resulting from charge transfer (B^+) or other processes. MINDO/3 and MNDO calculations have been performed on a variety of cations (B^+) giving errors of -7 and +9 kcal/mol respectively by parameterization when compared to experimental values (Halim et al., 1986). The present work expands the number and variety of compounds examined with the AM1 parameterization by calculating heats of formation for 127 species in neutral and protonated forms. These compounds were selected as representative of several general classes of compounds in which analytical and environmental chemists might be interested. Furthermore, many of these compounds and their chemical classes are important in atmospheric chemistry and we are particularly interested in their detection using atmospheric

pressure ionization mass spectrometry. Atmospheric oxidation processes result, for example, in the formation of ketones, aldehydes, alcohols, acids, nitro and nitrate compounds, etc. The calculated heats of formation are then used to derive gas-phase basicities for the compounds. A newly developed optimization, MNDO-PM3 (Stewart 1989), which includes parameters for 12 elements, offers only slight improvement for the neutral C, H, N and O compounds evaluated here. MNDO-PM3 was not utilized in this study.

Gas-phase basicities are important in mass spectrometry where the fundamental reaction is proton transfer from a reagent ion (for example: water, methane or ammonia) to the analyte. GB is defined as the negative of the free energy change for Reaction 15 (R15) (Lias, Liebman, and Levin, 1984) and is related to the equilibrium constant for proton transfer from water by Equation 1 (E1). Our own interest in calculating GB of CHNO compounds comes from a desire to quantify our APIMS studies of atmospheric hydrocarbon oxidations: Chapters II-IV, and Grange, O'Brien, and Barofsky (1988a). We express K_{eq} in terms of protonation from a hydronium ion (R9). E1 would be similarly written for transfer from hydronium ion/water clusters, ammonia, methane or other reagents.



$$K_{eq}(R9) = [BH^+][H_2O]/[H_3O^+][B] = \exp((GB(B)-GB(H_2O))/RT) \quad (E1)$$

Although extensive experimental values for the free energy of reaction ($\Delta G(R15) = -GB$) have been tabulated (Lias, Liebman, and Levin, 1984), experimental gas-phase basicities are unavailable for many compounds of environmental significance, in particular many atmospheric oxidation products.

Toluene, for example, has over 30 identified primary photo-oxidation products (Dumdei and O'Brien, 1984; Shepson, Edney, and Corse, 1984; Dumdei et al., 1988; Grange, O'Brien, and Barofsky, 1988a; among others) but the GBs of only a few have been measured (Lias, Liebman, and Levin, 1984). In this study we calculated most of the compounds from Lias, Liebman, and Levin (1984) which might relate to atmospheric oxidation processes.

EXPERIMENTAL

All semiempirical calculations were carried out using the AM1 Hamiltonian (Dewar et al., 1985) in the program MOPAC 4.0 available from QCPE (Quantum Chemistry Program Exchange, Department of Chemistry, University of Indiana, Joliet IN 44444.). This parameterized form improves on the MNDO model with no increase in computational time. Parameters are available in this release for carbon, hydrogen, nitrogen and oxygen. All computer modeling was done on an Apollo DN10000 workstation with molecular structures input using MOLY-86. MOLY-86 (also available from QCPE) is an interactive molecular modeling system developed by Rohm and Haas, Inc., allowing entry, manipulation and preliminary optimization of molecular structures. Some modification of MOLY was required so that it would accept protonated species. MOPAC calculated the enthalpy of formation, bond lengths, bond orders and other parameters for any given structure.

RESULTS AND DISCUSSION

Table VII summarizes our results for 127 compounds, tabulating the derived heats of formation $\Delta H_f(B)$ for the unprotonated analyte B, $\Delta H_f(BH^+)$, for the

TABLE VII

COMPARISON OF THE GAS-PHASE BASICITIES AND ADJUSTED
HEATS OF FORMATION FOR PROTONATED AND
UNPROTONATED SPECIES

	$\Delta H_f(B)$		$\Delta H_f(BH^+)$		GB	
	value	error	value	error	value	error
nitric oxide	0.3	-21.2	231.2	-28.8	120.2	1.2
carbon dioxide	-78.2	15.8	142.1	1.1	133.9	9.5
N ₂ O (NNO)	27.2	7.2	246.5	-2.5	136.3	4.9
hydrogen peroxide	-34.8	-2.3	175.6	4.6	142.9	-11.1
ethene	52.9	-1.1	263.5	-3.4	144.2	-1.9
phenol	-22.2	0.8	168.5	22.5	149.6	-25.4
water	-58.2	-0.4	137.9	-3.1	159.0	0.0
cyclopropane	16.8	3.8	206.2	7.7	166.0	-6.0
methanol	-56.0	-8.0	132.0	-3.5	167.7	-6.4
formaldehyde	-31.2	-5.2	156.5	-11.5	168.7	4.4
2-butene	-3.7	-0.7	180.8	-2.2	171.5	-0.1
hydrogen cyanide	29.7	-2.3	213.7	-12.3	172.3	8.5
propene	6.3	-6.7	189.8	-8.7	172.6	0.6
nitrobenzene	24.2	8.2	208.0	19.5	172.9	-12.7
dimethyl ether	-52.3	-8.3	131.3	1.3	173.2	-11.1
cyclobutene	44.1	6.6	225.9	13.9	174.4	-8.6
benzene	20.9	0.9	204.3	0.3	175.0	-0.6
cyclohexene	-10.2	-9.2	170.5	-4.5	175.6	-5.9
ethanol	-61.5	-5.5	118.7	-2.3	175.8	-4.4
nitroethane	-16.9	7.1	162.4	5.9	177.2	0.2
<i>n</i> -propyl alcohol	-68.2	-7.2	111.0	-3.0	177.8	-5.2
nitromethane	-19.9	-1.9	159.0	-9.5	178.3	6.6
cyclopentene	2.4	-6.6	181.9	-9.1	180.0	1.8
acetaldehyde	-41.0	-1.0	135.6	-3.4	180.3	1.7
methylbenzene (toluene)	13.5	1.5	190.4	2.4	180.4	-1.6
1,3-butadiene	28.6	2.6	204.6	5.6	181.3	-3.6
methyl cyanide (acetonitrile)	18.3	0.3	193.7	-1.3	181.5	0.9
isopropyl alcohol	-66.6	-1.6	108.6	-0.4	181.5	-1.9
ethylbenzene	9.2	2.2	184.1	3.1	182.4	-1.4
methyl ethyl ether	-57.7	-5.7	117.9	-0.1	182.5	-6.1
ethyl cyanide (propionitrile)	12.1	0.1	185.4	0.4	183.4	-0.7
isobutanal	-51.8	0.2	122.0	1.0	183.5	-1.3
<i>n</i> -butanal	-54.2	-4.2	119.3	-4.7	183.9	0.2
propanal	-47.6	-2.6	125.7	-5.3	184.3	2.4
isobutene	-1.6	2.4	170.8	4.8	184.6	-2.7
dimethyl glyoxal	-70.2	7.8	101.5	8.5	185.2	-1.0

TABLE VII

COMPARISON OF THE GAS-PHASE BASICITIES AND ADJUSTED
HEATS OF FORMATION FOR PROTONATED AND
UNPROTONATED SPECIES
(continued)

	$\Delta H_f(B)$		$\Delta H_f(BH^+)$		GB	
	value	error	value	error	value	error
pentanal	-60.7	-5.7	111.6	-6.4	185.2	0.4
PhCN (benzonitrile)	51.4	-0.6	223.7	1.7	185.6	-2.5
acetic acid	-100.8	2.2	69.9	-2.1	185.7	4.0
di-1-propenyl ether	-13.5	-6.5	157.8	-0.2	186.1	-6.5
diethyl ether	-63.5	-3.5	107.9	2.4	186.3	-6.1
methacrolein	-23.5	1.5	147.3	2.3	186.5	-0.9
propenal	-14.9	3.1	155.4	2.4	186.7	0.6
NH ₂	36.3	-7.7	206.6	-16.4	187.6	8.6
<i>t</i> -butyl alcohol	-70.3	4.7	99.9	2.9	187.7	1.8
1,2-dimethylcyclobutene	26.0	9.0	196.2	14.2	188.9	-5.1
propanoic acid	-106.7	0.3	62.0	-5.0	189.4	5.4
methoxybenzene (anisole)	-15.8	0.2	151.9	2.9	190.0	-2.5
1,2 dimethoxyethane	-97.2	-16.2	69.2	-10.3	190.1	-5.7
furan	2.4	10.4	170.3	5.3	190.2	5.2
di- <i>n</i> -butyl ether	-89.8	-10.3	77.5	-4.5	190.3	-5.6
styrene	36.9	1.9	204.5	5.5	190.8	-3.4
acetone	-48.0	4.0	118.6	1.6	191.6	2.7
CH ₃ CHCO (methyl ketene)	-13.9	11.1	152.5	11.5	191.6	0.0
1,3-pentadiene	19.1	1.1	185.6	3.6	191.7	-2.2
cyclopentanone	-54.4	-8.4	112.3	-8.7	192.2	0.7
methyl ethyl ketone	-54.2	2.8	111.3	2.3	193.0	1.0
benzaldehyde	-9.2	-0.2	156.3	-0.7	193.4	1.0
dicyclopropyl ketone	8.9	-30.1	173.6	-20.4	193.7	-9.2
tetrahydrofuran	-54.1	-10.1	110.9	-12.1	193.9	2.5
methyl cyclopropyl ketone	-19.9	8.1	144.6	11.6	194.4	-2.9
<i>t</i> -butyl-ONO (<i>t</i> -butyl nitrite)	-44.9	-3.9	118.7	-0.3	194.9	-3.0
methyl vinyl ketone	-23.9	5.1	139.2	3.2	194.9	2.5
2-butenal	-26.2	-4.2	137.3	-6.7	195.0	3.1
dimethyl carbonate	-133.7	-2.2	29.9	-4.1	195.0	2.6
2,5-dimethyl furan	-11.1	18.9	152.6	25.6	195.3	-6.0
methyl isopropyl ketone	-58.1	4.9	105.6	3.6	195.3	2.0
di- <i>n</i> -pentyl ether	-103.2	-13.2	60.7	-10.3	195.7	-2.2
diethyl ketone	-60.0	2.0	102.1	0.1	196.2	2.7
cyclohexanone	-62.1	-8.1	100.1	-9.9	196.6	2.6
di-isopropyl ether	-70.4	5.6	90.5	6.5	196.8	-0.2

TABLE VII

COMPARISON OF THE GAS-PHASE BASICITIES AND ADJUSTED
HEATS OF FORMATION FOR PROTONATED AND
UNPROTONATED SPECIES
(continued)

	$\Delta H_f(B)$		$\Delta H_f(BH^+)$		GB	
	value	error	value	error	value	error
methyl <i>t</i> -butyl ketone	-58.8	10.2	102.2	8.2	197.4	2.9
4-methylbenzaldehyde	-16.9	1.1	143.3	-0.7	198.3	2.8
2-methylfuran	-4.4	14.6	155.2	14.2	199.3	1.5
di-isopropyl ketone	-67.5	6.5	92.2	5.2	199.3	2.3
pyrrole	38.3	12.3	198.3	14.3	199.4	-0.9
benzoic acid	-66.7	3.3	91.5	-5.5	199.5	9.9
methyl vinyl ether	-25.4	-1.4	133.7	-0.3	199.7	0.1
formamide	-44.1	-0.1	114.7	-8.3	199.9	9.3
pyrimidine	42.2	-3.8	201.4	0.4	200.5	-3.0
methyl ethyl carbonate	-139.5	1.5	18.4	-3.1	200.7	5.8
methyl phenyl ketone	-15.0	6.0	143.6	3.6	201.0	3.6
2,5,8-trioxanonane	-142.2	-23.2	9.8	-17.2	202.8	-4.6
diphenyl ketone (benzophenone)	19.5	7.5	175.0	8.0	204.0	0.9
ethyl vinyl ether	-30.9	3.1	124.4	0.4	204.7	4.3
aminobenzene (aniline)	19.3	-1.7	172.9	-4.1	206.0	4.1
ammonia	-7.6	3.4	145.1	-5.9	206.6	11.0
dimethylformamide	-36.1	9.9	116.9	8.9	206.7	2.8
2,5-hexanedione	-90.9	-1.9	57.6	-5.9	207.3	5.8
methylamine	-7.7	-2.7	143.1	-2.9	207.7	2.0
dimethylamine	-6.0	-1.5	143.6	3.6	209.8	-3.0
pyridine	30.7	-2.3	181.0	3.0	209.8	-3.3
trimethylamine	-2.2	3.8	146.6	11.6	211.8	-5.5
ethylamine	-13.6	-2.6	132.5	-4.5	212.8	4.3
<i>n</i> -propylamine	-20.3	-3.3	125.0	-6.0	215.3	5.2
<i>i</i> -propylamine	-19.2	0.8	124.3	-2.7	217.2	6.2
2-oxy-3-penten-4-ol	-74.8	17.2	65.0	-1.0	220.5	21.2
<i>t</i> -butylamine	-21.3	7.7	118.4	2.4	221.5	8.5
triethylamine	-18.2	3.8	120.9	9.9	221.6	-2.9
formic acid	-88.1	2.4	87.0	-9.0	181.1	10.7
methyl formate	-89.1	-4.1	79.6	-12.4	189.3	8.3
ethyl formate	-94.1	-2.1	73.5	-6.5	189.8	4.5
<i>n</i> -propyl formate	-100.6	9.4	65.6	4.6	191.4	5.0
<i>n</i> -butyl formate	-107.8	-4.8	57.8	-10.2	192.6	5.7

TABLE VII
 COMPARISON OF THE GAS-PHASE BASICITIES AND ADJUSTED
 HEATS OF FORMATION FOR PROTONATED AND
 UNPROTONATED SPECIES
 (continued)

	$\Delta H_f(B)$		$\Delta H_f(BH^+)$		GB	
	value	error	value	error	value	error
ethyl acetate	-100.0	6.0	57.3	-1.7	201.9	9.0
methyl benzoate	-53.5	15.5	102.6	9.6	202.8	7.3
carbon monoxide	-6.1	20.4	185.3	-11.7	164.3	29.9
diatomic nitrogen	10.4	10.4	234.1	-13.4	129.2	18.2
diatomic oxygen (triplet)	-27.2	-27.2	241.1	-23.9	81.6	-13.4
ethane	-16.3	3.7	216.0	14.0	119.0	-16.8
propane	-24.1	0.9	207.0	16.0	120.5	-21.5
isobutane	-29.1	2.9	199.8	29.8	122.4	-33.1
cyclohexane	-38.0	-9.0	177.5	10.5	136.6	-24.4
1,4-butanediol	-118.9	-16.9	56.6	4.6	175.4	-22.6
1,4-dimethoxybutane	-111.2	-13.2	59.6	13.6	181.7	-27.3
1,2-cyclohexanedione	-79.1	-9.1	92.7	1.7	186.5	-10.9
1,3-cyclohexanedione	-84.3	-5.3	83.8	8.8	190.7	-13.8
oxirane	-9.2	3.8	177.6	12.6	170.1	-10.5
2-methyloxirane	-15.8	7.2	134.1	-13.9	210.1	23.2
cyclopropene	72.3	6.3	225.9	-8.1	206.2	16.2
1-methylcyclopropene	62.5	4.5	235.4	17.4	184.8	-13.2
propyne	41.8	-3.2	252.6	24.6	141.8	-32.2
2-butyne	36.0	1.0	244.8	31.8	144.1	-34.9
methylnitrite	-31.5	-15.5	149.4	-7.6	175.6	-9.1
ethylnitrite	-37.2	-12.2	158.1	14.1	160.5	-29.0
<i>i</i> -propylnitrite	-42.0	-10.0	160.2	28.2	152.6	-41.5

Note: All enthalpies and gas-phase basicities in kcal/mol. The first column in each case gives the derived thermodynamic value corrected for systematic offsets using the best fit line given in Table VIII. Compounds are listed in order of increasing derived GB. Following each column of derived values is the difference between that value and the experimental value (Lias, Liebman, and Levin, 1984), (calcd - exptl). Compounds below the second line were excluded from the linear regression analysis of Table VIII.

protonated analyte BH^+ , and the GB for each compound. Semiempirical

calculations for each analyte provided the heats of formation for each form, B and

BH⁺. The calculated values were then compared to the published experimental values and linear regression analysis provided the best fit lines for each data set. The corrected values for enthalpy of formation given in Table VII are the MOPAC calculated values after adjustment using the regression analysis results which are summarized in Table VIII.

$$\Delta H_f(B)_{\text{corr.}} = \{\Delta H_f(B)_{\text{MOPAC}} - \text{Intercept}/\text{Slope}\} \quad (\text{E2})$$

The GB of each analyte was computed from the corrected heats of formation of the unprotonated and protonated analytes as described below, where $\Delta G(\text{R15})$, $\Delta H(\text{R15})$ and $\Delta S(\text{R15})$ refer respectively to the free energy change, enthalpy of reaction and entropy change for Reaction 15. GB values themselves were also corrected for systematic offsets in the same manner as for $\Delta H(B)_{\text{corr.}}$ in (E3).

$$\text{GB}(B) = -\Delta G(\text{R15}) = -[\Delta H(\text{R15}) - T\Delta S(\text{R15})] \quad (\text{E3})$$

$$\Delta H(\text{R15}) = (\Delta H(\text{BH}^+) - [\Delta H(B) + \Delta H(\text{H}^+)]) \quad (\text{E4})$$

$$\Delta S(\text{R15}) = \Delta S(\text{H}^+) + \Delta S(B \rightarrow \text{BH}^+) \quad (\text{E5})$$

$$\text{GB}(B) = -\Delta H(\text{BH}^+) + \Delta H(B) + \Delta H(\text{H}^+) + T\Delta S(\text{R15}) \quad (\text{E6})$$

In all cases the proton heat of formation 356.7 kcal/mol was used (Lias, Liebman, and Levin, 1984), as was the entropy term for proton transfer $T\Delta S(\text{H}^+) = -7.8$ kcal/mol (Chase et al., 1982). The contribution to the entropy change for the half reaction ($B \rightarrow \text{BH}^+$) can be approximated by the rotational entropy change ΔS_{on} (Moylan and Brauman, 1983). This "trivial" entropy contribution can be found by comparing the symmetry numbers of reactant and products (Bailey and Monahan, 1978). These values, taken from Lias, Liebman, and Levin (1984), typically gave $T\Delta S_{\text{on}} < 1$ kcal/mol. Proton affinities are readily derived from the heats of formation (Voets et al., 1989) and are not tabulated here. A sample calculation

provided near the end of the chapter demonstrates these calculations and discusses their application to compounds not measured experimentally. A more complete discussion of proton affinities, heats of formation for protonated and unprotonated forms, structures and in a few cases the dissociations of protonated forms, as well as the errors associated with functional group classes, is beyond the scope of this study but preliminary findings are discussed in the summary, Chapter VII. The signed differences between the experimentally measured (Lias, Liebman, and Levin, 1984) and theoretically derived values are shown after each column of calculated values (derived - measured) in Table VII.

Table VIII presents several statistical measures of agreement between the experimental and theoretical values for each graph. For the purposes of this analysis, 99 compounds were used to determine the best fit line based on the corrected heats of formation and experimental values. The remaining 28 compounds, separated in Table VII by a solid line, are discussed in the following paragraph. Figures 10 and 11 graphically compare the corrected heats of formation for B and BH^+ , listed in Table VII, with the experimental values. Superimposed on each graph is a line of unit slope and zero intercept. Figure 13 compares the corrected GB values with the experimental values. Again the solid line is for a perfect correlation between experimental and derived values. Three values are given in Table VIII for each data set which compare the errors implicit in the semiempirical calculations. The standard deviations of the signed differences from Table VII give errors of 7.77, 8.41 and 5.80 kcal/mol respectively for the heats of formation of B, BH^+ and GB. Table VIII also gives the standard

TABLE VIII
REGRESSION ANALYSIS OF CALCULATED VERSUS EXPERIMENTAL
GAS-PHASE BASICITIES AND CORRECTED HEATS
OF FORMATION

	$\Delta H_f(B)$	$\Delta H_f(BH^+)$	GB(B)
n:	99	99	99
Slope:	1.0267	0.9362	0.9056
Intercept (kcal):	0.5293	14.747	17.760
R:	0.9835	0.9847	0.9471
<u>Error based on signed differences</u>			
Standard deviation:	7.767	8.4075	5.796
<u>Error based on absolute value of differences</u>			
Average Difference:	5.596	6.173	4.178
Standard Deviation:	5.386	5.708	4.017

Notes: Linear regression analysis for MOPAC calculated values compared to experimental values. This information is then used to derive the corrected theoretical heats of formation and gas-phase basicities given in Table VII. All errors are based on the difference between the derived value and the experimental value (Lias, Liebman, and Levin, 1984) ($AM1_{\text{derived}} - \text{exptl}$).

deviation of the absolute values of the errors which are 5.39, 5.71 and 4.02 kcal/mol for the heats of formation of B, BH^+ and GB respectively.

The AM1 parameterization has several known deficiencies (Dewar et al., 1985) in its ability to evaluate heats of formation. However, a large error in the heat of formation for a compound need not produce a large error in the resulting GB. If AM1 has difficulty evaluating a given structure in the unprotonated form, that error may also appear in the protonated form and would then cancel in the calculation of the gas-phase basicity. This is borne out in Table VIII where the errors in GB are slightly lower than those for either heat of formation. The 28

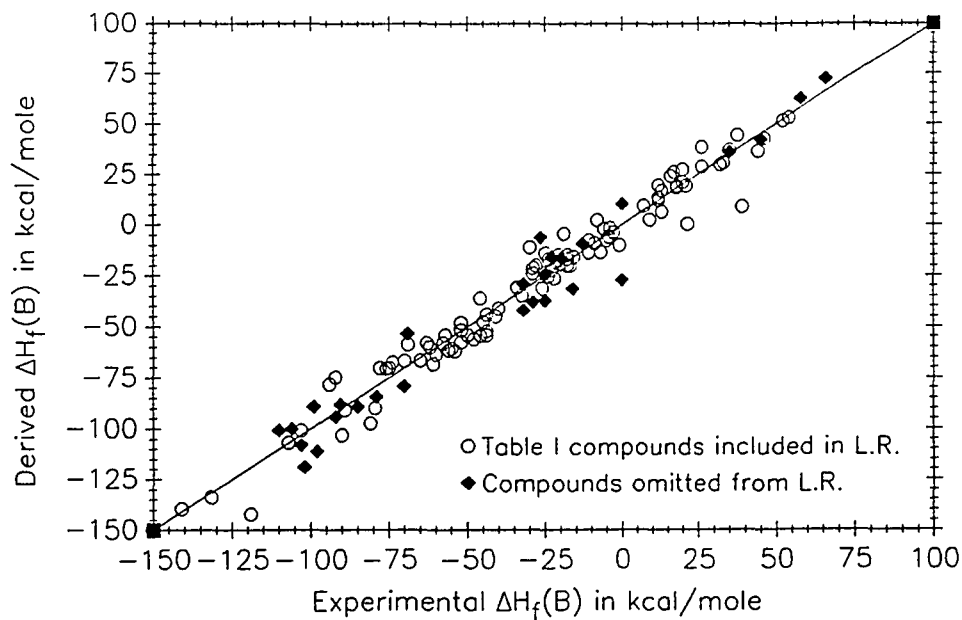


Figure 10. Comparisons of calculated and experimental $\Delta H_f(B)$. Experimental values taken from Lias, Liebman, and Levin (1984). Theoretical values taken from Table VII are based on MOPAC calculations adjusted with the linear regression analysis in Table VIII ($\Delta H_f(B)_{\text{corrected}} = [\Delta H_f(B)_{\text{AM1 calculated}} - 0.53]/1.03$). The solid line represents a perfect correlation, slope=1 and intercept=0.

compounds not included in the 3 regression analyses were excluded based on characteristic deficiencies. Categories of neutral compounds identified previously as being poorly modeled with AM1 include diatomics, geometrically crowded molecules and compounds with both nitrogen and oxygen functionalities (Dewar et al., 1985). In most cases, these compounds also had large errors in their GBs. Large errors have also been reported with AM1 for nitro compounds (Stewart 1989), but nitro compounds evaluated here were within the uncertainty of other groups, perhaps because protonation did not affect the source of the error. Organic nitrates were also modeled adequately, but nitrites had large and unpredictable

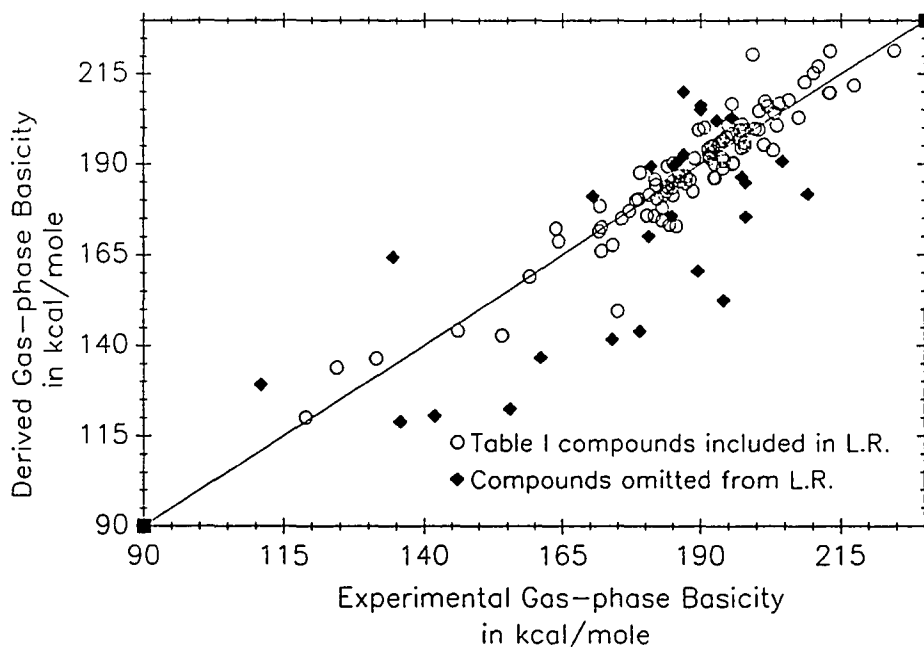


Figure 11. Comparisons of calculated and experimental $\Delta H_f(\text{BH}^+)$. Experimental values taken from Lias, Liebman, and Levin (1984). Theoretical values taken from Table VII are based on MOPAC calculations adjusted with the linear regression analysis in Table VIII ($\Delta H_f(\text{BH}^+)_{\text{corrected}} = [\Delta H_f(\text{BH}^+)_{\text{AM1 calculated}} - 14.75]/0.94$). The solid line represents a perfect correlation, slope = 1 and intercept = 0.

errors. Four strained ring compounds, oxiranes and cyclopropenes, resulted in larger errors than for other small rings such as cyclopropane or cyclobutene.

The diatomic molecules oxygen, nitrogen and carbon monoxide had, as expected, large errors in GB, +14.9, +18.2 and +29.9 kcal/mol respectively. Some of the largest errors seem to be associated with alkanes and alkynes. Unprotonated alkanes have been shown to have an incremental error in the heat of formation of the unprotonated species. This error increases with increasing chain length at -1.9 kcal/mol per methylene group (Dewar et al., 1985). Including this correction has a small effect in the overall accuracy since most of the error in GB for alkanes

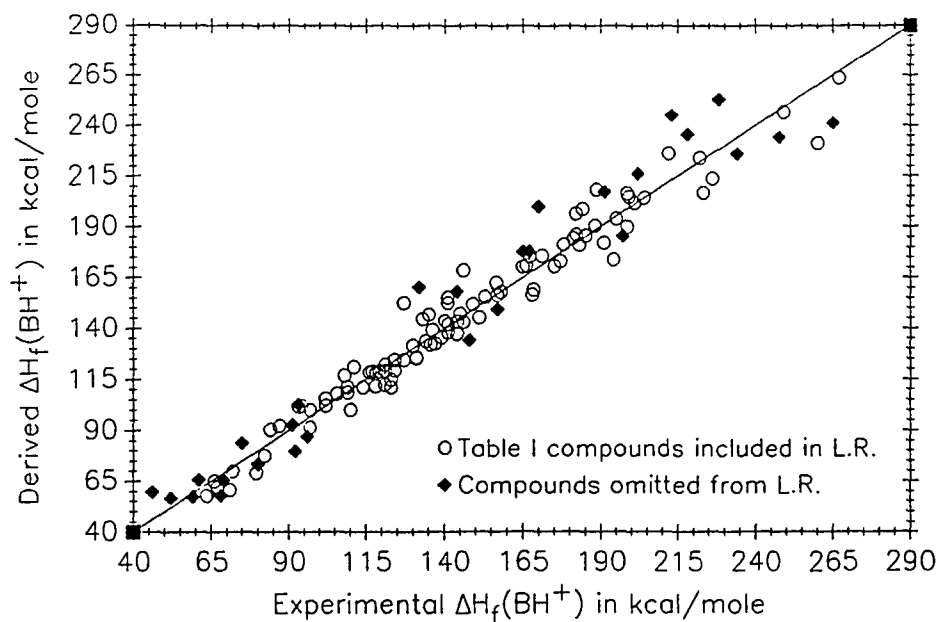


Figure 12. Comparisons of calculated and experimental GB. Experimental values taken from Lias, Liebman, and Levin (1984). Theoretical values taken from Table VII are based on MOPAC calculations adjusted with the linear regression analysis in Table VIII ($GB_{\text{corrected}} = [GB_{\text{AM1 calculated}} - 17.8]/0.91$). The solid line represents a perfect correlation, slope = 1 and intercept = 0.

arises from the protonated species. The exclusion of alkanes for the purpose of GB calculations is not a serious limitation for APIMS. The relative basicities of alkanes are generally below the reagent hydronium's basicity and they are not typically detected as protonated species. Similarly, the energies of the protonated alkynes are not well estimated using this parameterization of AM1. One additional group not included in the regression analysis and not previously identified as poorly estimated with semiempirical methods are the esters. The errors in ester family compounds excluded from the linear regression show systematic positive offsets in GB ranging from +5.0 to +15.0 kcal/mol.

Uncertainties in the relative gas-phase basicities based on equilibrium measurements are small, 0.5 kcal/mol (Keese and Castleman, 1986). In practice it is the relative basicity of a compound compared to the proton transfer reagent which is important in determining API sensitivity. In assigning an absolute basicity scale the smaller error associated with assigning relative uncertainties must be combined with the larger uncertainties in fixing the placement of reference compounds. This latter uncertainty is at least 2 kcal/mol and much more for compounds at high or low values of GB (Lias, Liebman, and Levin, 1984). For the basicities calculated here, a routine propagation of random errors indicates that the actual error in the derived absolute basicities ($[(4.0)^2 - (2.5)^2]^{0.5} = 3.1$ kcal) is only slightly greater than the cumulative experimental uncertainty. This is impressive since neither M^+ nor MH^+ ions were included in the AM1 parameterization data base.

The experimental sensitivity of analytes in APIMS has been studied as a function of the compounds' GB (Sunner, Nicol, and Kebarle, 1988; Sunner, Ikononou, and Kebarle, 1988a). For compounds below about 195 kcal/mol, sensitivity was found to be logarithmically proportional to GB, increasing about 1 decade for a 9 kcal/mol increase in GB. Above the breakpoint GB value near 195 kcal/mol, APIMS response was similar for all compounds. Thus, a 3.1 kcal/mol uncertainty in assigning the basicity of a compound will not have any effect on its anticipated API response if its GB is above 200 kcal/mol. However, for a compound below this breakpoint, the uncertainty in assigning the GB using either experimental or semiempirical methods may have a large effect on the predicted API sensitivity. Since the experimental measures of API sensitivity themselves

show wide scatter (Sunner, Nicol, and Kebarle, 1988) the magnitude of the uncertainty may be difficult to assess.

The effect of hydration on the sensitivity of certain compounds when detected using APIMS has also been investigated (Sunner, Nicol, and Kebarle, 1988; Nicol, Sunner, and Kebarle, 1988). The unusually low sensitivities for some compounds was shown to result from the unfavorable energies of hydration associated with carbon and sulfur bases. Protonation of furan at the α -carbon is favored over protonation on the oxygen (Houriet, Schwarz, and Schleyer, 1981), and AM1 reproduces this carbon base behavior. However, this carbon protonated species has a low ability to form hydrogen bonds in hydration. Experimental measurements of hydration enthalpies were made with furan using Pulsed High Pressure Mass Spectrometry (PHPMS) (Nicol, Sunner, and Kebarle, 1988) and a value of $\Delta H = -10.4$ kcal/mol was reported for the first hydration reaction. Experimental measurements of the higher order hydration reactions were not reported. Uncorrected MOPAC calculations of the hydration energies for furan and ethanol are summarized in Table IX and show excellent agreement with the respective experimental measurements. Proton transfer reactions generally occur from hydrated hydronium clusters when the water levels are high, as commonly found in APIMS. Compounds which are able to accept the proton along with some portion of the hydration molecules are thus more likely to be protonated. It is clear in Table IX that hydration of ethanol, typical of the compounds whose sensitivity was proportional to GB, is much more favorable than for furan whose experimentally measured sensitivity was many orders of magnitude less. The

TABLE IX

HEATS OF FORMATION FOR HYDRATED FURAN AND ETHANOL

Species	ΔH_f (Calcd)	ΔH_f (Exptl)
Furan	3.3	-8
Furan (oxygen protonated)	206.1	
Furan (α carbon protonated)	174.8	165
Protonated furan monohydrated	106.3	
Protonated furan dihydrated	38.2	
Protonated furan trihydrated	-26.2	
Ethanol	-62.6	-56
Protonated EtOH	125.8	121
Protonated EtOH monohydrate	46.8	
Protonated EtOH dihydrated	-25.6	
Protonated EtOH trihydrated	-95.6	

n-1,n	Furan Hydration		Ethanol Hydration	
	calcd	exptl	calcd	exptl
	$\Delta H_{n-1,n}$	$\Delta H_{n-1,n}$	$\Delta H_{n-1,n}$	$\Delta H_{n-1,n}$
0,1	-10.7	-10.4	-21.2	-27.6
1,2	-10.3		-14.6	-19.8
2,3	-6.6		-12.2	-14.1

Notes: All enthalpies in units of kcal/mol. Enthalpies of hydration reactions are for $BH^+ \cdot (H_2O)_{n-1} + H_2O = BH^+ \cdot (H_2O)_n$. Experimental measurements of furan hydration from Nicol, Sunner, and Kebarle (1988), ethanol hydration from Hiraoka, Heinrich, and Morise (1986).

ability of AM1 to evaluate these hydration energies is also of direct applicability to APIMS when the reagent ions occur as hydrates.

CONCLUSIONS

The procedure whereby AMI-derived heats of formation may be used to derive the 'best-fit' value of gas-phase basicity can be illustrated. As an example, we choose hydrogen peroxide, a compound included in Table VII. The heats of

formation for H_2O_2 in the unprotonated ($\Delta H_f(\text{B}) = -35.2$ kcal/mol) and protonated ($\Delta H_f(\text{BH}^+) = 179.1$ kcal/mol) forms are first obtained from the semiempirical calculations with MOPAC. (By way of comparison, Lias, Liebman, and Levin (1984) report $\Delta H_f(\text{B}) = -32.5$ and $\Delta H_f(\text{BH}^+) = 171.0$ kcal/mol.) Using the slopes and intercepts from Table VIII in Equation 2, the AM1 values are corrected for systematic offsets. $\Delta H_f(\text{B})_{\text{corr.}} = \{\Delta H_f(\text{B})_{\text{MOPAC}} - \text{Intercept}\} / \text{Slope} = \{-35.2 - 0.5293\}$ kcal/mol / 1.0267 = -34.8 kcal/mol. Similarly, $\Delta H_f(\text{BH}^+)_{\text{corr.}}$ is corrected to 175.6 kcal/mol. The gas-phase basicity is first calculated from the adjusted heats of formation for the unprotonated and protonated species using equation 6. $\text{GB}(\text{B}) = -\Delta H_f(\text{BH}^+)_{\text{corr.}} + \Delta H_f(\text{B})_{\text{corr.}} + \Delta H_f(\text{H}^+) + T\Delta S(1) = -(175.55) + (-34.8) + (365.7) + [(-7.8 + -0.4)] = 147.14$ kcal/mol. The final term combines the entropy for the proton (-7.8 kcal/mol), and a second term (-0.4 kcal/mol) for the "trivial" entropy loss. When evaluating the GB for a compound not in Lias, Liebman, and Levin (1984), the magnitude of the "trivial" entropy loss can be estimated from the symmetry changes for the molecule (Bailey and Monahan, 1978; Moylan and Brauman, 1983). In the direct count method (Bishop and Laidler, 1965) the symmetry change for hydrogen peroxide protonation is approximated by $RT\ln(1/2) = -0.4$, where the fraction 1/2 is based on there being two paths to protonate the molecule but four paths for deprotonation. The final step is to correct the GB for systematic offsets, as was done for the enthalpies. $\text{GB}(\text{B})_{\text{corr.}} = \{147.14 - 17.76\}$ kcal/mol / 0.9056 = 142.9 kcal/mol.

Gas-phase basicities are important in many chemical applications. These include studies of gas-phase proton transfer reactions, evaluation of solvation and hydration effects and APIMS. Experimentally determined GBs are not available

for many compounds of interest in environmental or atmospheric chemistry. The ability of semiempirical calculations to predict GB theoretically to within a few kilocalories of experimental uncertainty should have important implications for analytical chemists in a variety of applications. Chapter VII demonstrates the calculations of GB for a range of compounds for which experimental values were not available. These compounds include nitrites, nitrates and nitro compounds as well as a variety of multifunctional compounds typical of atmospheric oxidation processes. We also demonstrate the use of semiempirical calculations to evaluate whether HRKAPIMS could be effectively used to study the oxidation products of several organic compounds.

CHAPTER VI

ANALYTE RESPONSE AND QUANTITATION IN ATMOSPHERIC PRESSURE IONIZATION MASS SPECTROMETRY

"One way to tell for sure if a sweater is made of wool is to hold it over a flame. If it burnt slowly it was wool." (Davis, 1969)

OVERVIEW

In this chapter we address the quantitative capabilities of atmospheric pressure ionization mass spectrometry. The general nature of quantitative analysis for mass spectrometry is first discussed in terms of the different ionization processes commonly used. Past measurements of API response are reviewed and compared with the results of chemical modeling. Three distinct and complementary approaches are used to model the nature of API response. Solving the thermodynamic equilibrium expressions for proton transfer reactions is the simplest and most direct approach. A steady state model can be used which assumes equilibrium is reached where the sources and sinks for a species sum to zero. Finally, the kinetic modeling approach integrates the simultaneous chemical rate expressions that determine API response to provide a more complete analysis.

INTRODUCTION

High resolution atmospheric pressure ionization mass spectrometry (HRKAPIMS) offers many advantages for the analysis of environmental and

biological samples. Among these advantages are: the capability to directly measure from the gas phase without sample concentration or derivatization; the capability of generating oxidation products directly within the source; a high instrumental sensitivity and selectivity for organics that contain a heteroatom; and the ability to determine empirical formulas through accurate mass assignments. In addition, the ability to detect free radical reaction intermediates and study the effects of NO on product yields is beneficial when evaluating reaction mechanisms. These capabilities have been discussed in previous chapters. The direct analysis of mixtures by this soft ionization technique gives a parent ion spectrum free of fragmentation patterns (Grange, 1988) which would otherwise make interpretation complex.

Several areas of uncertainty remain to be explored, in particular the viability of obtaining quantitative measurements of analyte concentrations when using API. The following observations may help form a basis for further discussions. Carrol et al. (1981) have commented that "API spectra normally show relative concentrations of ions under conditions of chemical and thermal equilibrium, while EI and CI spectra reflect relative rates of ionization reactions." Eiceman et al. (1988) have noted that "the CD [corona discharge] is likely not in thermodynamic equilibrium". Kebarle (Sunner, Ikonou, and Kebarle, 1988b) has concluded that "it is not clear what chemical and thermal equilibrium means in terms of ion intensities in the API source." In this chapter we will examine analyte sensitivity using API in an effort to address these uncertainties and better understand the processes occurring in an API source. The conclusions derived here may also have applications to the related ionization processes used in ion mobility

spectrometry, fast atom bombardment and chemical ionization as well as to processes beyond mass spectrometry. As a result we hope to increase the now somewhat limited applications of API as an ionization technique.

QUANTITATION IN MASS SPECTROMETRY

Ionization Techniques

We begin by reviewing the aspects of quantitative analysis which are relevant to all mass spectrometric techniques. Washburn and coworkers (Washburn, Wiley, and Rock, 1943; Washburn, Wiley, and Rock, 1945) are credited with having worked out the fundamental methods and calculations for quantitative analysis in mass spectrometry. There are several assumptions based upon their work which must be considered in any approach to quantitative mass spectrometry (Roboz, 1968). The wide variety of ionization techniques currently in use requires that these assumptions be applied appropriately, based on the particular conditions. These assumptions are as follows.

1. Each chemical compound will have its own characteristic mass spectrum and fragmentation pattern. API spectra are predominately parent ion spectra, free of fragmentation, as a result of the low energy proton transfer reactions and the thermalization of the ions due to the high collision rate at atmospheric pressure.

2. The response for any one compound is independent of the presence of any other compound present in the ion source. This is of particular importance in the analysis of mixtures where the signal intensities of the components must be linearly additive. Not all ionization processes used in mass spectrometry can meet this requirement under all experimental conditions, as we discuss below. A viable

alternative would be to know how the relative response of any one analyte varies as a function of some intrinsic property (i.e. GB).

3. Finally, the measured signal intensity for an ion must be proportional to its concentration or its partial pressure in the ion source. As with the previous requirement, this is not always the case. Competition for the reagent ions in APIMS and depletion of the ions may result in differing response factors as a function of sample composition. It is important therefore to understand more about the experimental conditions under which depletion and competition may arise and how to avoid this situation.

The following paragraphs briefly review the basic ionization principles and the potential for quantitation in several common ionization processes which are used in mass spectrometry and which share certain similarities to API. This review will form a basis for comparison when API processes are later considered.

Chemical Ionization. In chemical ionization (CI) mass spectrometry sample ionization takes place along any of the three major reaction pathways: proton transfer, charge transfer, and cluster formation. API is a special case of chemical ionization, where ionization occurs at atmospheric pressure (760 Torr) rather than at the reduced pressures typical in CI (0.01-1 Torr). For this reason API is sometimes termed atmospheric pressure chemical ionization APCI (for instance by Sciex Corporation, manufacturers of a commercial APIMS system). Proton transfer reactions in CI occur at reduced pressures, where the choice of an ionization agent allows the degree of fragmentation to be controlled as a function of the exothermicity of the ionization reaction. Potential ionization reagents include hydrogen, methane, isobutane or ammonia. The most typical approach to

quantitative analysis using a chemical ionization source involves the creation of a three point (minimum) calibration curve. The standard for the calibration is ideally the same as the analyte to be measured, presented in the same sample matrix as the unknown. Unfortunately, environmental samples may contain as many as 50-100 components, and there are a limited number of certified standards available for these compounds (Facchetti, 1989). The ability to perform quantitative analysis is thus dependent on the availability of reliable standards from either commercial sources or laboratory synthesis.

Fast Atom Bombardment. Fast atom bombardment (FAB) has become an important technique in the analysis of polar and nonvolatile compounds. There are at present two views on the mechanism of ionization in FAB, the precursor model (Cooks and Busch, 1983) and the gas collision model (Sunner, Ikonomou, and Kebarle, 1988b). Analyte sensitivities in FAB are generally thought to relate to the analytes' proton affinity (PA), as well as to the surface activity of the compound relative to the sample matrix. Proton affinities are defined as the negative enthalpy of reaction for the reaction $B + H^+ \rightarrow BH^+$. Since gas-phase basicities are defined as the negative of the free energy for the same reaction, we can relate proton affinity and gas-phase basicities by the expression: $GB = PA + T\Delta S$. Kebarle has defined the preference factor in FAB as the ratio of ion intensities for an analyte and its matrix (Sunner, Kulatunga, and Kebarle, 1986). In this study Kebarle found that increasing the analyte concentration by 2 orders of magnitude had (within a factor of 2) no effect on the preference factor. The influence of surface activity and gas-phase basicity difference (GB) between analytes has also been examined (Lacey and Keough, 1989). In this study several pairs of

compounds were selected for their similarities in surface activity or gas phase basicity or both. When a GB difference of 12.5 kcal/mol between analytes sharing similar surface activities were compared, the response of the lower GB compound was suppressed by a factor of 2.5. When the surface activities were different, this same GB difference results in a suppression factor of 29 (Lacey and Keough, 1989). The nonlinearity of FAB response and the dependence on GB and surface activity make quantitation in FAB difficult.

Ion Mobility Mass Spectrometry. Ionization processes in ion mobility mass spectrometry (IMMS) share certain similarities with APIMS. In IMMS, analyte molecules are generally ionized by a radioactive Nickel-63 foil at atmospheric pressure and then admitted to chamber where their mobility in an electric field is measured against a counter flow of a neutral gas. Corona discharges have been compared to Nickel-63 sources as ionization sources for APIMS and found to be equivalent (Dzidic et al., 1976). Eiceman (Vandiver, Leasure, and Eiceman, 1985) has evaluated the response of several polycyclic aromatic hydrocarbons (PAH) alone, and in binary and tertiary mixtures, as a function of analyte proton affinities. The response curves for these compounds show linear behavior at lower concentrations where the levels of hydronium are presumably much larger than the analyte. At higher concentrations the sensitivity was found to diminish as the reagent hydronium ions are consumed. Eiceman found that small differences in proton affinity (PA) have large effects on the response factors in mixtures. In a binary mixture of naphthalene and pyrene, equal signal intensities were not obtained until the naphthalene concentration was nearly 10^5 greater than that of pyrene (Vandiver, Leasure, and Eiceman, 1985). Naphthalene and pyrene differ in

their proton affinities by only 12 kcal/mol ($PA_{\text{NAPHTHALENE}}=196.3$, $PA_{\text{PYRENE}}=208.5$ kcal/mol (Lias, Liebman, and Levin, 1984)).

Quantitation in API

Corona Discharges. Some aspects of quantitative analysis using APIMS have been evaluated in the past. Eiceman et. al. (1988) examined the use of corona discharge in a Sciex TAGA 6000 APIMS, evaluating the experimental conditions under which the discharge was stable and reproducible. In addition to measuring the effects of source parameters such as needle current and alignment, response curves were obtained for triethylamine, ethyl acetate and dimethylmethylphosphonate. The response curves for the individual compounds were linear at low concentrations and showed a negative deviation at high concentrations. The relative responses of the three pure compounds were qualitatively proportional to their gas-phase basicity, the higher GB compound giving a larger ion intensity for a given concentration. Binary mixtures of the compounds were also evaluated. When there are not sufficient numbers of reagent ions, relative to the concentration of analytes, depletion of the reagents can occur. In such a case, the presence of a high GB compound suppresses the response of lower GB analytes in a manner similar to FAB ionization described earlier. Experimental conditions resulting in depletion may be apparent in the signal at the detector with the rapid falloff of the primary charge carriers (hydronium ions and their hydrates) (Eiceman et al., 1988).

Oxidation Studies. The use of API to semi-quantitatively examine oxidation products produced in a smog chamber has also been reported using a Sciex TAGA

6000 APIMS (Dumdei et al., 1988). In this study, experimental ion intensities for the oxidation products were corrected based on three calibration compounds which had functionalities generally similar to the oxidation products themselves. These compounds, butanal, 2,4-hexadienal, and 4-hexen-3-one, had experimental ion intensities that varied by only a factor of 2, from which it was concluded there was an uncertainty in the product yields of a factor of two or less. The GBs of these calibration compounds, calculated using semiempirical calculations described in Chapter V, are 187.3, 196.5 and 196.2 kcal/mole respectively. The GBs of the reported products (Dumdei et al., 1988) cover a much wider span than this (ca. 160-230 kcal/mol). Depletion of reagent ions is possible if the sum of all analytes exceeds the concentration of hydronium ions and their hydrates.

Analysis of toluene's oxidation products has been carried out in our own lab using API source reactions, which identified analytes in a mixture where the components had a range of GBs similar to Dumdei et al. (1988). The use of source reactions was discussed in Chapter III. In these experiments there was no apparent reduction in the levels of reagent ions, which were in large excess over the analytes in the mass spectra. Figure 13 plots the experimental ion intensities for some of the oxidation products of toluene as a function of their GB. While these data show considerable scatter, they clearly do not agree with the response observed by Sunner (Sunner, Nicol, and Kebarle, 1988) where a compound with GB of 165 kcal/mol was found to have a sensitivity four orders of magnitude less than a compound having a GB of 200 kcal/mol. Although the yields of the various toluene oxidation products are unknown, it is extremely unlikely that they are

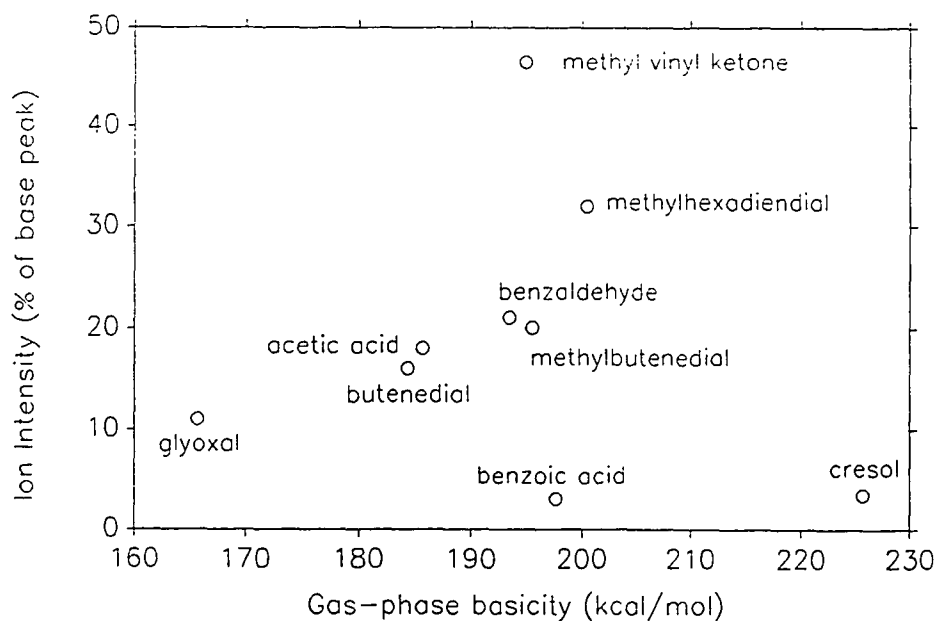


Figure 13. Experimental ion intensities for toluene oxidation products by analyte gas-phase basicity. Ion signals expressed as a percentage of the largest peak in the spectrum. GBs from Lias, Liebman, and Levin (1984) when available or calculated using the method of Chapter V. Experimental conditions described in Chapter III.

inversely proportional to GB so that compounds with very low GB will have very high yields and thus produce a relatively flat signal vs. GB.

CHEMICAL MODELING

There are several approaches one can take to examine the theoretical sensitivities of analytes in atmospheric pressure ionization mass spectrometry (APIMS). These approaches are separated here into the analysis of chemical equilibrium and the numerical integration of reaction rate equations.

Equilibrium Expressions

A fundamental attribute among the many advantages attributed to positive ion APIMS is that protonated analytes can reach chemical and thermal equilibrium as a result of collisions occurring at the elevated pressure in the ion source (Mitchum and Korfmacher, 1983). After the formation of hydronium ions (H_3O^+) by ionization processes in the source (Good, Durden, and Kebarle, 1970a; Good, Durden, and Kebarle, 1970b), protons are transferred to analytes B by reactions such as R9.



Thermodynamic Equilibrium Method. The first approach to examining APIMS sensitivities might therefore be to apply basic equilibrium theory to Reaction 9 (R9). While the relationships between ion intensities and thermodynamic properties have been introduced (Sunner, Nicol, and Kebarle, 1988), the treatment to follow represents a new effort to understand and predict API response from a theoretical standpoint.

Proton transfer reactions are actually much more complex than R9. Reversible proton transfer reactions occur from not only hydroniums but from the hydrated forms of hydroniums and varying numbers of hydrating water molecules may be transferred with the proton to the analyte. Proton transfer between analytes may occur as well. All these reactions are also presumably at equilibrium and will not change the equilibrium distributions among species in R9, so no loss of generality results from considering only R9. In the discussions to follow, square brackets are used to denote the concentration of the enclosed species. In order to describe analyte response as a fraction of the initial concentration of the compound

detected $[B]_o$, we substitute for $[B]$ the equilibrium analyte concentration: $[B]=[B]_o - [BH^+]$, where $[BH^+]$ is the equilibrium concentration of protonated analyte. The fraction of B detected is thus a function of the equilibrium constant for the reaction and concentrations of hydroniums and water. The equilibrium constant K_{eq} , defined for (R9) in the usual way, is also related to the free energy of reaction by the expression $\Delta G_{rxn}(R9) = -RT \ln(K_{eq}(R9))$,

$$K_{eq}(R9) = [BH^+][H_2O]/[H_3O^+][B] \quad (E7)$$

and to the gas-phase basicities of the analyte and water. The gas-phase basicity

$$[BH^+]/[B]_o = K_{eq}(R9)[H_3O^+]/([H_2O] + K_{eq}[H_3O^+]). \quad (E8)$$

(GB) of a compound is defined as the negative of the free energy change for protonation R15, $\Delta G(R15) = -GB(B)$. This allows the equilibrium constant (E7) to be expressed in terms of the gas-phase basicity of the analyte and water (E9), and analyte response to be defined in terms of water and analyte concentrations (E10a and E10b).



$$K_{eq}(R9) = \exp((GB(B) - GB(H_2O))/RT) \quad (E9)$$

$$\text{Response} \equiv [BH^+]/[B]_o = K_{eq}(R9)[H_3O^+] / ([H_2O] + K_{eq}(R9)[H_3O^+]) \quad (E10a)$$

$$\begin{aligned} \log(\text{Response}) \equiv \log(BH^+/B_o) &= GB(B)/2.3RT - (GB(H_2O))/2.3RT \\ &+ \log([H_3O^+]/[H_2O]) - \log(1 + K_{eq}(R9)[H_3O^+]/[H_2O]) \end{aligned} \quad (E10b)$$

Figure 14 plots the log of analyte response from E10b as a function of analyte GB.

The set of curves shown is based on a range of relative humidities at a constant hydronium ion concentration of 1.25×10^7 molecules cm^{-3} . The highest water concentration, 1.67×10^{17} , corresponds to about 5 Torr or 20% relative humidity.

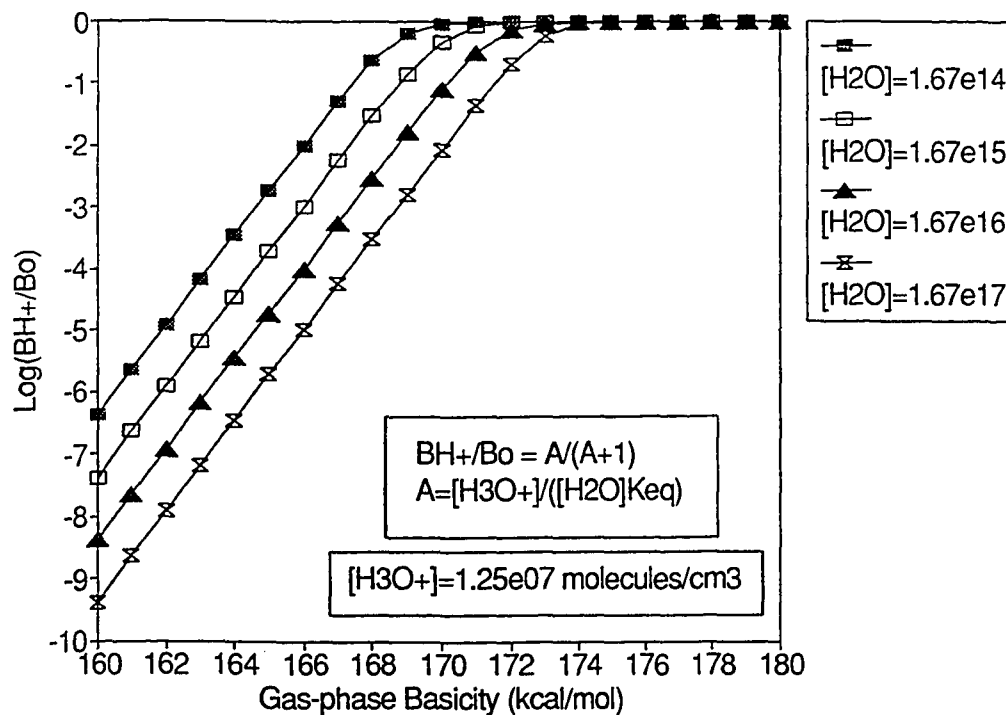


Figure 14. Analyte response as a function of gas-phase basicity and initial water concentration in thermodynamic equilibrium case (R10). Initial $[H_3O^+]=1.25e07$ molecules cm^{-3} .

The initial portions of the response curves in Figure 14 have slopes equal to $(2.3RT)^{-1}$, which arises naturally out of Equation 10 and equates to a 7.3 decade increase in sensitivity for each 10 kcal/mol increase in gas-phase basicity. This value can be compared with the IMMS studies which found a 5 decade response difference between two compounds with a 12 kcal/mol difference in GB (Vandiver, Leasure, and Eiceman, 1985). Cooks and Busch (1983) used a mass-analyzed ion kinetic energy spectrometer (MIKES) to evaluate analyte proton affinities by comparing the dissociation ratios of proton bound dimers. Depending on the analyte series used, these experiments found log responses varying linearly by 2-3 decades per 5 kcal/mol difference in analyte proton affinities. Kebarle observed a 9

kcal/mol difference in GB to result in a factor of 10 difference in analyte response relative (Sunner, Nicol, and Kebarle, 1988b).

TABLE X

COMPARISON OF INITIAL ANALYTE RESPONSE VS. GAS-PHASE BASICITY

Study	Log(Analyte Response)
Thermodynamic Equilibrium Model; (Figure 14.)	7.3 decade per 10 kcal/mol
Vandiver, Leasure, and Eiceman., 1985; (IMMS)	4.2 decade per 10 kcal/mol
Cooks and Busch, 1983; (MIKES)	4-6 decades per 10 kcal/mol
Sunner, Nicol, and Kebarle; (APIMS)	1 decade per 10 kcal/mol

For compounds on the initial sloping portions of the response curves in Figure 14, response is thermodynamically controlled. The response for these compounds results from the proton transfer reactions reaching equilibrium before the reagent ions are consumed or the sample leaves the source region. These reactions are able to reach equilibrium because the extent of proton transfer to these weak bases is minimal. Decreasing the relative humidity at constant hydronium shifts the breakpoint GB for unit response to a lower value, since this results in a shift in the equilibrium toward more complete protonation. Increasing hydronium at constant relative humidity would have the same effect. The breakpoint GB can be defined from E10a as the point at which analyte response = 1/2; then in the denominator of E10a, $[H_2O] = K_{eq}(R9)[H_3O^+]$. Rearranging this expression and solving for the breakpoint in terms of GB(B) gives Equation 11.

$$K_{eq} = [H_2O]/[H_3O^+] = \exp\{(RT)^{-1}[GB(B)-GB(H_2O)]\}$$

$$GB(B)_{\text{BREAKPOINT}} = GB(H_2O) - RT\ln([H_3O^+]/[H_2O]) \quad (R11)$$

Steady State Method. A second equilibrium approach considers the proton transfer reactions, and the subsequent removal of ionic species to the mass spectrometer, to be in steady state, with their overall concentrations not changing with time. This is a more comprehensive approach since it accounts for the removal of the reagent and analyte ions from the API source and the large effect this has on protonation of analytes. We begin by describing the sources and sinks of the protonated analyte (BH^+), which sum to zero under steady state conditions, E12. The term $\delta[BH^+]/\delta t$ is the change in concentration of the protonated species in time, k_f and k_b are the forward and reverse rate constants for R9. k_d is the first-order rate constant for detection, the rapid removal of ionized species by the applied 3kV electric field. Experimentally, the detection rate is determined by the potential gradient between the corona discharge needle and the first orifice. Typically, a 3 kV difference is needed to initiate the corona discharge. For our source, $k_d = 4.35 \times 10^4$ calculated from the 4.6 mm distance from the needle tip to the orifice and an ion velocity of 2×10^4 cm sec⁻¹ based on the potential gradient and distance (McDaniel, 1964).

Kebarle, using a Sciex TAGA 6000 APIMS, has reported relative API sensitivities as a function of analyte GB (Sunner, Nicol, and Kebarle, 1988; Sunner, Ikonomou, and Kebarle, 1988a), in terms of the kinetic and thermodynamic control of proton transfer. Relative analyte sensitivity was defined as the analyte ion counts per second per concentration unit, ratioed to the ion count per second per concentration for pyridine. Figure 15 reproduces Kebarle's figure, which was based on a series of experiments in which each analyte was ionized in the presence of unspecified concentrations of pyridine ($GB_{PYRIDINE}=213$

kcal/mole). Response curves were found to be linear on a log scale at low analyte concentrations with negative deviations at higher concentrations, presumably as the reagent ions are consumed. Compounds with gas-phase basicities greater than a threshold value were generally observed to have uniformly high and equal sensitivities. These compounds had sensitivities that were described as being kinetically controlled. Kinetically controlled compounds have large GBs which shift their proton transfer equilibrium far to the right. In the available residence time in the source they cannot reach proton transfer equilibrium and the extent of protonation is then a function of the residence time in the source. For compounds below this threshold (ca. GB=200 kcal/mol) the observed sensitivities decreased with decreasing analyte GB. The response of these lower GB compounds was termed thermodynamic. Thermodynamically controlled compounds have equilibria which are shifted to the left, allowing them to reach proton transfer equilibrium in the available source residence time. Increasing the distance between the needle and the orifice increases the residence time by decreasing the ion velocity and lengthening the ion path, and would be expected to increase analyte response for kinetically controlled species. This increased response is offset by having a smaller portion of the ionized particles impact the orifice as the distance increases (Sunner, Nicol, and Kebarle, 1988; Eiceman et al., 1988). Rearranging E12 expression, we can relate analyte response ($[BH^+]/[B]_0$) to the equilibrium constant (E9), the concentrations of hydroniums and water, the protonation rate constant k_p , and the detection rate constant, k_d .

$$\delta[BH^+]/\delta t = k_p[H_3O^+][B] - k_b[H_2O][BH^+] - k_d[BH^+] = 0 \quad (E12)$$

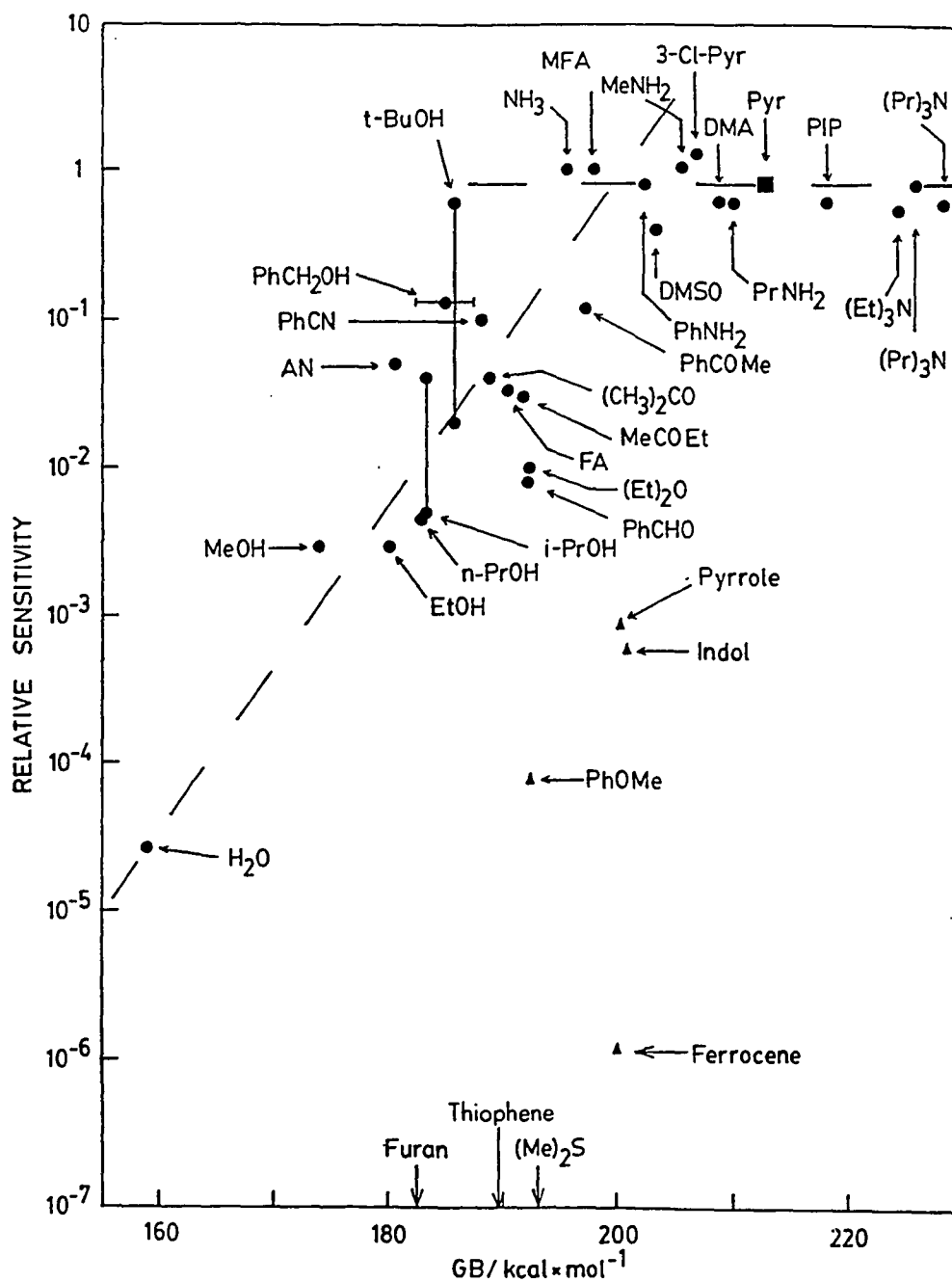


Figure 15. Sensitivity, relative to pyridine, in an API source as a function of analyte GB. Source: Sunner, Nicol, and Kebarle, 1988.

$$\text{Response} \equiv [\text{BH}^+]/[\text{B}]_0 = k_f[\text{H}_3\text{O}^+] / (k_f[\text{H}_3\text{O}^+] + k_b[\text{H}_2\text{O}] + k_d) \quad (\text{E13a})$$

$$= [\text{H}_3\text{O}^+] / ([\text{H}_2\text{O}]/K_{\text{eq}} + [\text{H}_3\text{O}^+] + k_d/k_f) \quad (\text{E13b})$$

The two equivalent forms of Equation 13 are similar to E10 with the exception of the detection term. K_{eq} could be replaced using E9 to relate analyte response directly to analyte GB. Figures 16-19 represent the solutions to E13 as the initial concentrations of reagents and reaction parameters are changed. Equation 13 was solved using a range of analyte GBs, holding all but one of the other parameters constant. Except when it was the parameter being varied: $[\text{H}_3\text{O}^+]=1.25\text{e}07$, $[\text{H}_2\text{O}]=1.67\text{e}17$ each in units of molecules cm^{-3} , $k_f=3.0\text{e}-9$ cm^3 sec molecules^{-1} , and $k_d=8.348\text{e}4$ sec^{-1} . The GB of water is 159 kcal/mol (Lias, Liebman, and Levin (1984)). In order to better isolate the effect of GB in determining analyte response, all forward proton rate constants are assumed to be equal, $3\text{e}-9$ $\text{molecules cm}^{-3} \text{sec}^{-1}$. Actual forward rates vary by a factor of three or less for most compounds (Bohme, Mackay, and Tanner, 1979). The rate of the reverse reaction, $\text{H}_2\text{O} + \text{BH}^+ \rightarrow \text{B} + \text{H}_3\text{O}^+$ is then determined from K_{eq} , ($k_b = k_f/K_{\text{eq}}$).

The fundamental appearance of the curves, which incorporate the detection step, is the same as in Figure 14, which ignored the effects of the 3kV ionization potential. Figures 16-19 have a initial linear response region corresponding to achievement of thermodynamic equilibrium for the low GB compounds. The slope of the initial region is $1/2.3RT$, as in the case of Figure 14. Compounds above a breakpoint GB all reach a response plateau defined by the $k_d[\text{H}_3\text{O}^+]/k_f$ in E13b. We can define the breakpoint in the response curve as occurring when $[\text{BH}^+]/[\text{B}]_0 = \alpha$, where α is a number less than 1. This allows E12 to be rewritten in terms of the breakpoint GB, where α is the fraction of B_0 which is protonated.

$$\text{GB}_\alpha = 2.3RT \log((\alpha[\text{H}_2\text{O}]) / ([\text{H}_3\text{O}^+] - \alpha[\text{H}_3\text{O}^+] - \alpha k_d/k_f)) + \text{GB}(\text{H}_2\text{O}) \quad (\text{E14})$$

Steady State: Hydroniums. Increasing the hydronium ion concentration, Figure 15, increases the response for all analytes equally, but it does not change the breakpoint GB below which analyte response decreases. Experimentally, the reagent ion concentration can be increased by increasing the corona discharge current. The upper usable limit in the current arises from increased likelihood of a breakdown of the corona discharge into an arcing discharge. Unlike Figure 14, the maximum response is no longer unity. As a result of the removal of the ionized species, in particular reagent hydroniums, the analyte does not have the opportunity to fully participate in proton transfer reactions. This forms a kinetic limitation (expressed by the term k_d/k_r in E13b) to the extent of reaction and lowers the ultimate response possible for each set of conditions.

The limiting behavior of the curves in Figure 15 can be explained from Equation 13b. At low GB the equilibrium constant is small and the ratio of $[H_2O]/K_{eq}$ is much larger than either of the other two terms in the denominator. Response is thus linear in GB, as reflected the value of K_{eq} and increasing the hydronium concentration increases the response of all compounds equally. At high GB the ratio of $[H_2O]/K_{eq}$ is smaller than either of the denominator terms and response is no longer a function of GB.

Steady State: Water. Decreasing the water concentration, Figure 16, enhances analyte response by shifting the equilibrium R9 in favor of the species which have not reached maximum response. Compounds well below the breakpoint GB increase in response inversely proportionate to the decrease in water vapor concentration, while compounds with GB just below the breakpoint reach maximum response. This has the effect of shifting the breakpoint GB to

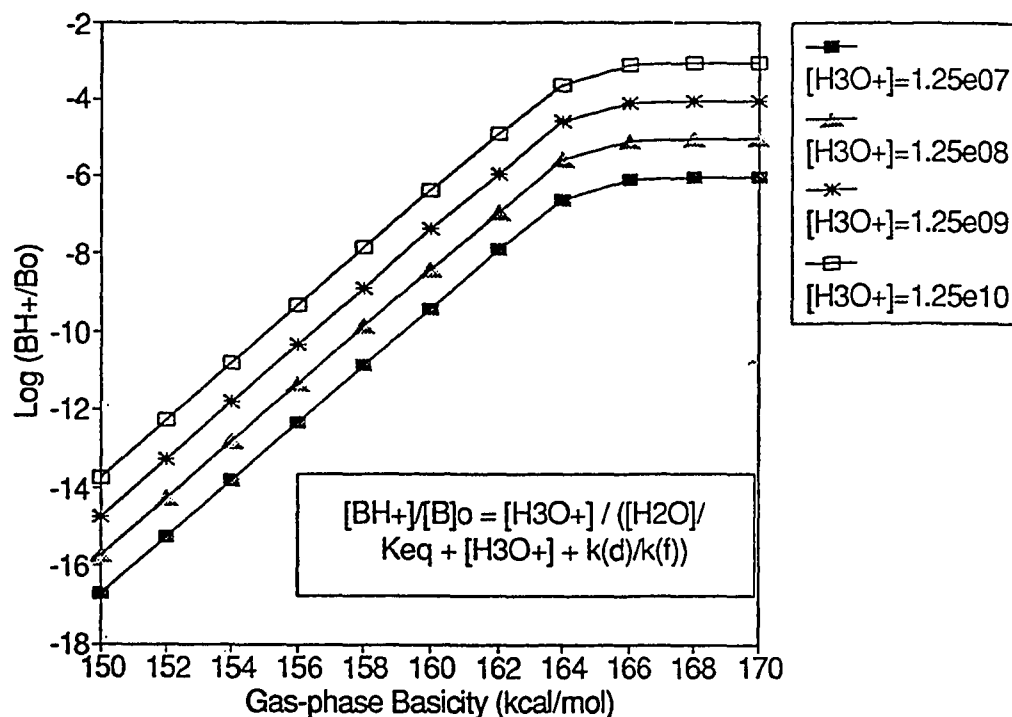


Figure 16. Analyte response in steady state model (R13) as a function of GB and $[H_3O^+]_o$. Initial $[H_2O]=1.67e17$ molecules cm^{-3} , $k_a=4.35e4$ sec^{-1} , and $k_f=3.0e-9$ cm^3 sec molecules $^{-1}$.

lower values. Reducing the humidity of an ambient sample, without removing analyte, presents unique problems. Semi-permeable membranes designed to selectively remove water vapor (Cochran, 1987; Cox and Earp, 1982; Singh and Salas, 1983) are one possibility, although loss of analyte to the membrane surface must be considered.

Water concentration only affects the region of the curves in Figure 17 at low GB, small K_{eq} . As before, at low GB the ratio of $[H_2O]/K_{eq}$ is large compared to the other denominator terms and for a constant $[H_3O^+]$ response will be dependent on the water concentration. At high GB values ratio of $[H_2O]/K_{eq}$ becomes negligible and water is no longer a determining factor.

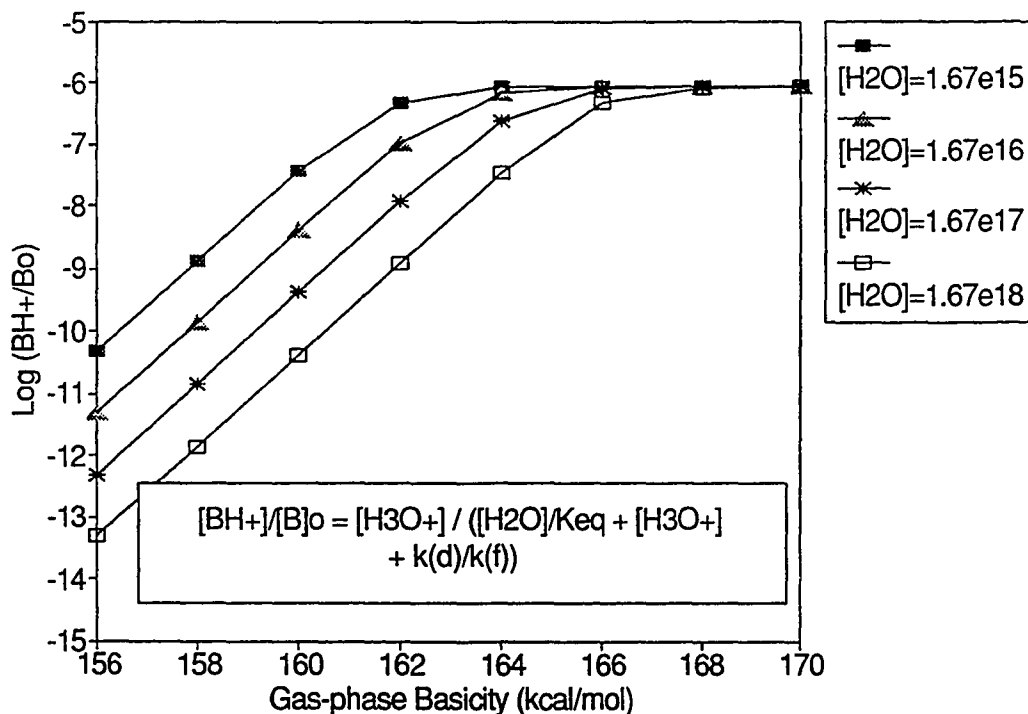


Figure 17. Analyte response in steady state model (R13) as a function of GB and $[H_2O]_0$. Initial $[H_3O^+] = 1.25e07$ molecules cm^{-3} , $k_d = 4.35e4$ sec^{-1} , and $k_f = 3.0e-9$ cm^3 sec $molecules^{-1}$.

Steady State: Detection. The detection rate, as illustrated in Figure 18, has yet a different effect on analyte response. A large k_d relates to the rapid removal of ions from the API source, and results in reduced response. Proton transfer reactions are in direct competition with the removal steps and large detection rates mean that the reagent hydroniums are removed from the reaction mix before quantitative protonation of the analytes can occur. Only at extremely slow proton transfer rates can analyte response become quantitative, equivalent to the results of Figure 14, solved without detection steps, where the response plateau at high GB corresponds to complete analyte protonation. When k_d is varied, the response plateau varies in inverse proportion to k_d , until it reaches near unit response.

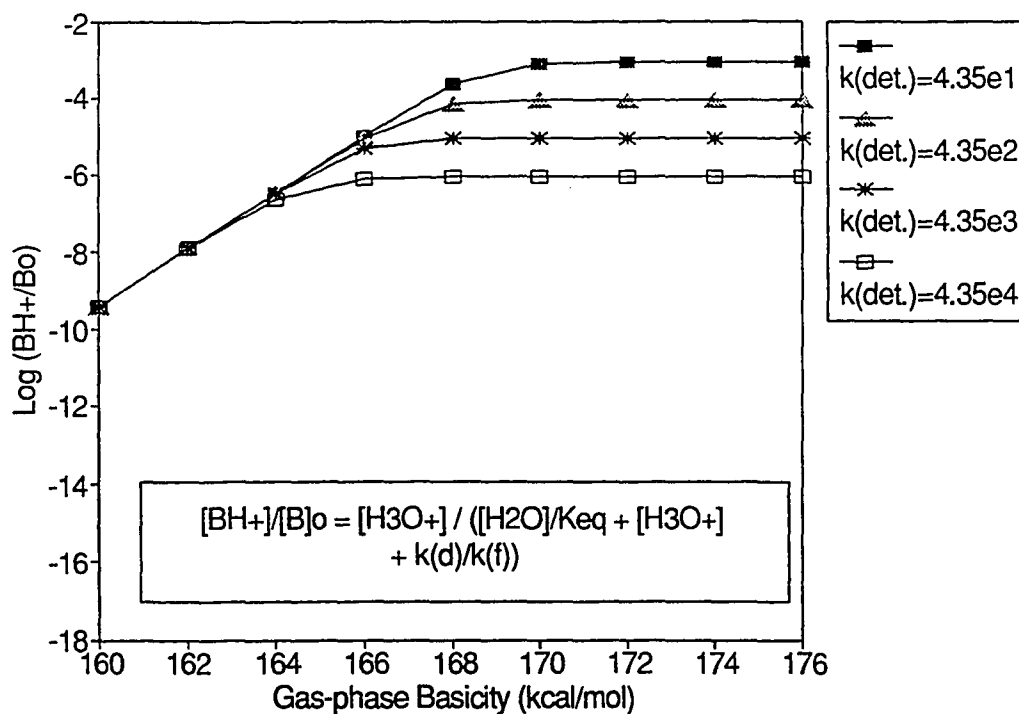


Figure 18. Analyte response in steady state model (R13) as a function of GB and k_d . Initial $[H_3O^+]_0 = 1.25e07$, $[H_2O]=1.67e17$ in units of molecules cm^{-3} , and $k_f = 3.0e-9$ cm^3 sec molecules $^{-1}$.

Analyte response increases with a decrease in the detection rate only for the high GB compounds. For lower GB's the ratio of $[H_2O]/K_{eq}$ continues to predominate. At high GB the ration of k_d/k_f becomes the controlling factor for analyte response. As k_d approaches zero quantitative detection of the analyte becomes possible, assuming adequate reagent ions, $\log(\text{response})=0$.

Steady State: Forward Rates. Figure 19 displays a family of curves where at each GB the value of K_{eq} remains the same, based on the GB from E9, but the forward protonation rate was changed. As in previous cases, at small GBs the ratio of $[H_2O]/K_{eq}$ continues to determine analyte response. At high GBs larger

forward rate can decrease the contribution in the denominator from the ratio of k_d/k_f , allowing analyte response to increase.

Kinetic Modeling-Rate Constants

A still more complete approach to evaluating API response is to use chemical kinetics to model the reaction sequences. This approach does not assume any type of equilibrium, but must reproduce the results and conclusions of the previous methods if the mechanisms are integrated to equilibrium. Computer modeling was conducted with a variety of distinct chemical systems, each designed to examine a particular experimental process or aspect of API analysis. Knowledge of the rates of reaction for all the species is necessary to affect the modeling, yet experimental measurements of such rates are available for only a few species. Before discussing the models themselves we will direct our attention to the origins of the rate constants we will use.

Hydration. The first family of reactions that are of interest are the hydration reactions of water with hydronium ions. Kebarle et al. (Good, Durden, and Kebarle, 1970a; Good, Durden, and Kebarle, 1970b) have reported the rates of hydration for hydronium ions through the formation and dissociation of $H_3O^+(H_2O)_n$ up to $n=4$. Integrating these reactions alone gives the families of hydrated hydroniums (masses 19, 37, 55, 73, ... which dominate the background of spectra in Chapters 2 and 3). The most abundant hydrate species in the family is determined by the total water vapor available. Figure 20 represents the integration of the hydration reactions which are presented in Table XI. Equilibrium is reached very quickly, within 0.1 μ sec, and the dominant hydrate

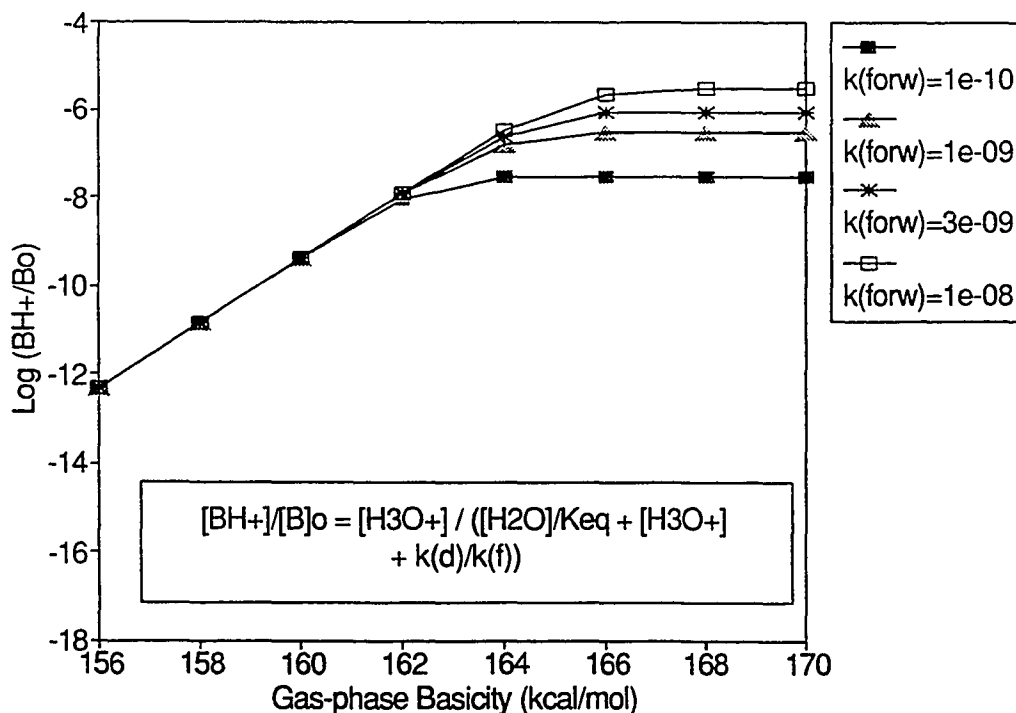


Figure 19. Analyte response in steady state model (R13) as a function of GB and k_f . Initial $[H_3O^+]_0 = 1.25e07$, $[H_2O]=1.67e17$ in units of molecules cm^{-3} , and $k_d=4.35e4 \text{ sec}^{-1}$.

occurs for $n=3$ with a water concentration of 1.6×10^{15} molecules cm^{-3} . Although this water concentration is quite low, it is the water vapor concentration in the CID region at a pressure of about 1/760 atm which controls the cluster formation. Thus 1% water vapor concentration in the API source ($2.5e17$ molecules cm^{-3}) would be reduced to about $2.5e14$ in the CID region, and would be expected to result in peaks in the hydronium clusters of $n=3$ to $n=4$. Conversely, the protonation equilibrium R9 is unaffected by the expansion to lower pressure in the CID region, since this equilibrium is second order in both directions.

The hydration of protonated analytes is another reaction series of interest. The free energies of hydration for a variety of compounds having GBs ranging from

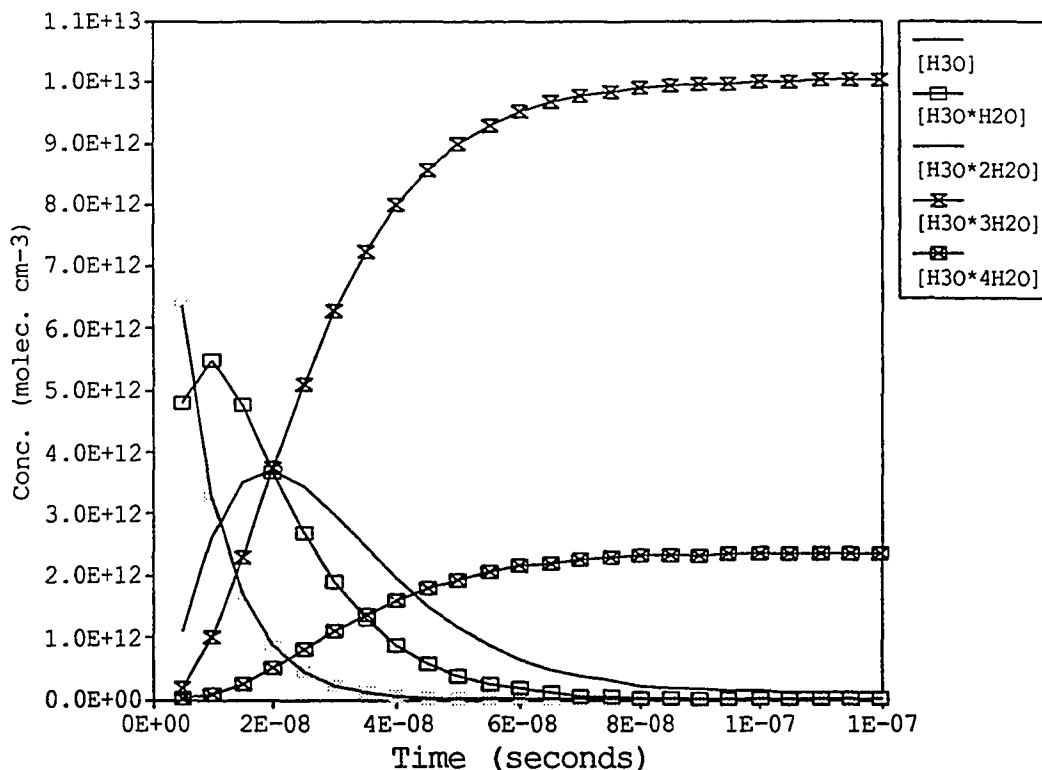


Figure 20. Kinetic modeling of hydration reactions for water with hydronium ions. Reaction rates based on experimental values of Good, Durden, and Kebarle (1970a), mechanism is given in Table XI.

that of water (GB=159 kcal/mol) to that of pyridine (GB=213 kcal/mol) have been measured (Nicol, Sunner, and Kebarle, 1988; Hiraoka, Takimoto, and Morise, 1986; Keesee and Castleman, 1986). In order to evaluate the equilibrium constant and derive deprotonation rates for an analyte as a function of its GB, it would be useful if there was a general relationship between the free energy for hydration and GB. Figure 21 was developed using the GBs (Lias, Liebman, and Levin, 1984) of the compounds for which hydration free energies have been measured. Figure 21 gives a new perspective on the relationship between analyte GB and the negative of the free energy of hydration for R2 where n is the number of hydrating water

TABLE XI

MECHANISM FOR KINETIC MODELING OF HYDRONIUM HYDRATION

H3O	H2O	M	=	H3O1	M	3.4E-27
H3O1	M		=	H3O	M H2O	7E-26
H3O1	H2O	M	=	H3O2	M	2.3E-27
H3O2	M		=	H3O1	H2O M	7E-18
H3O2	H2O	M	=	H3O3	M	2.4E-27
H3O3	M		=	H3O2	H2O M	4E-14
H3O3	H2O	M	=	H3O4	M	9E-28
H3O4	M		=	H3O3	H2O M	6E-12

\$INITIAL CONDITIONS

M	H3O	H2O
2.450E+19	1.250E+13	1.612E+15

Notes: Reaction rates from Bohme, Mackay, and Tanner (1979). Rate constants have units of $\text{cm}^3 \text{molecules}^{-1}$ or $\text{cm}^6 \text{sec}^2 \text{molecules}^{-1}$ as appropriate.

molecules. Each of the curves in Figure 21 represent a second order regression analysis for each value of n. This allows the more generalized expression



of the free energies as a function of GB. The use of the free energy to evaluate the equilibrium constant is described in a later section. As an aside, MOPAC was used to calculate the heat of reaction for the hydration of several compounds (n=1) and found to track the free energies closely. The values derived for ΔH_{rxn} (MOPAC) are the solid squares above the experimental n=1 line. Table XII presents the heats of formation and hydration heat of reaction for compounds with a range of GBs, plotted in Figure 21 as filled squares. The small offset is a result of not accounting for the TΔS term which relates the enthalpies calculated to the free energies which were plotted. Table XIII lists the regression analysis results from

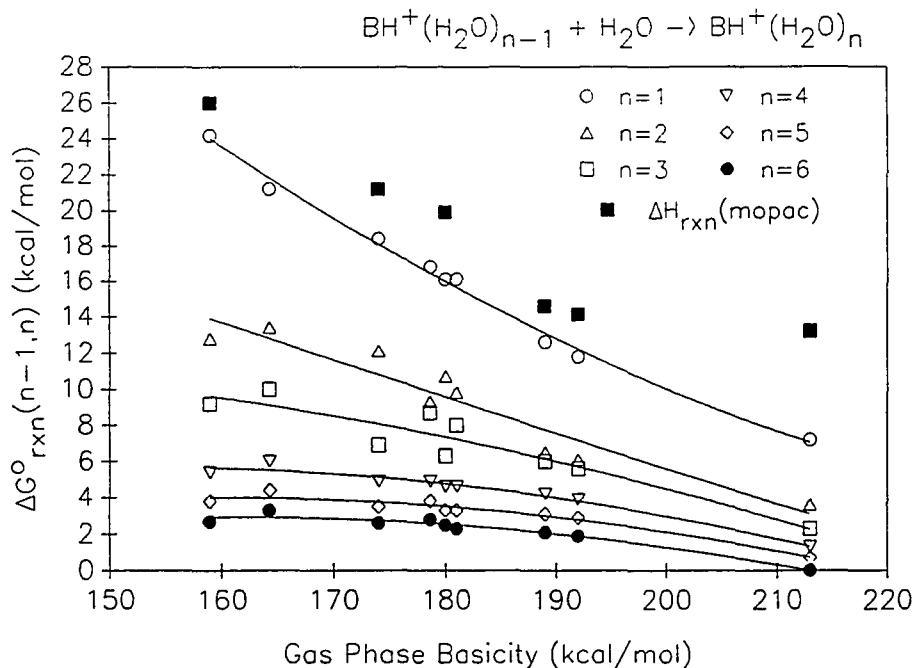


Figure 21. Free energy for the hydration reactions of protonated analytes as a function of GB. Experimental ΔG values from Nicol, Sunner, and Kebarle 1988; Hiraoka, Takimoto, and Morise, 1986; Keese and Castleman, 1986. Enthalpies of the hydration reaction for $n=1$ calculated from MOPAC. Analysis of the curves is given in Table XIII

Figure 21 which are used to evaluate the equilibrium constant and thus the reverse rate as a function of GB.

Forward Protonation Rates. The forward rate constants for proton transfer from the hydronium, and from the first four hydrated hydronium clusters, have been experimentally determined for a variety of compounds by Bohme, Mackay, and Tanner (1979). These rates were found to agree closely with rates predicted with average dipole orientation theory (Su and Bowers, 1979; Su and Su, 1978; Bass et al, 1975). These reactions are of the form shown in R17 where n is the number of

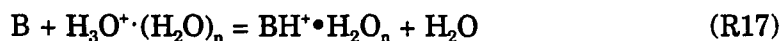
TABLE XII

SEMIEMPIRICAL CALCULATIONS OF HEATS OF REACTION FOR
HYDRATION, $BH^+ + H_2O \leftrightarrow BH^+ \cdot H_2O$

Compound	$\Delta H_f(BH^+)$	$\Delta H_f(BH^+ \cdot H_2O)$	ΔH_{rxn}	GB(B)
water	143.8	58.6	-26.0	159
methanol	138.3	57.9	-21.2	174
ethanol	125.9	46.8	-19.9	180
acetone	125.8	52.0	-14.6	189
diethyl ether	114.2	40.87	-14.1	192
pyridine	202.1	140.5	-2.4	213

Notes: All values are in units of kcal/mol. $\Delta H_f(H_2O) = -59.2$ kcal/mol. Gas phase basicities from Lias, Liebman, and Levin, 1984.

hydrating waters. Reactions which transfer some other fraction of the hydrating water molecules to the analyte B are also possible but were not experimentally



distinguishable (Bohme, Mackay, and Tanner, 1979). Quantitatively, proton transfer rates are close to the collision rate right down to near zero exothermicity ($\Delta G_{\text{proton transfer}} \leq 0$) and do not seem to be functions of GB, as illustrated in Figure 22. All the forward proton transfer rates fall within the range of 1.5 to 3×10^9 cm^3 $\text{molecules}^{-1} \text{sec}^{-1}$, with protonation faster for the smaller hydrates. Unless otherwise noted, the forward rates for protonation from hydrated hydroniums where $n=0-3$ will be modeled at 3.0 , 2.5 , 2.0 and 1.5×10^9 $\text{molecules}^{-1} \text{cm}^3 \text{sec}^{-1}$ respectively.

Reverse Protonation Rates. Reverse rate constants for protonation are not generally available experimentally but can be derived from the equilibrium constants and the forward rates. Consider the protonation of analyte molecules

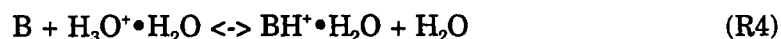
Table XIII

REGRESSION ANALYSIS OF FREE ENERGIES OF HYDRATION AS A
FUNCTION OF ANALYTE GB FOR $\text{BH}^+\cdot\text{H}_2\text{O}_{n-1} + \text{H}_2\text{O} \rightarrow \text{BH}^+\cdot\text{H}_2\text{O}_n$

n-1,n	a0	a1	a2	r
0,1	1.57E2	-1.21	2.4E-3	.998
1,2	3.88E1	-1.31E-1	-1.71E-4	.948
2,3	3.58E1	1.86E-1	-8.29E-4	.958
3,4	-2.77E-1	0.4175	-1.32E-3	.998
4,5	-2.91E1	0.401	-1.23E-3	.994
5,6	-2.91E1	0.386	-1.17E-3	.998

Notes: ΔG of reaction for the hydration of BH^+
based on Figure 21. $\Delta G(n-1,n) = a0 + a1*\text{GB}(\text{B}) +$
 $a2*\text{GB}(\text{B})^2$. GBs in kcal/mol.

from singly hydrated hydronium ions ($\text{H}_3\text{O}^+\cdot\text{H}_2\text{O}$). The free energy for the reaction can be described in terms of: the gas-phase basicities of the analyte and water; the free energies of hydration for water, available from experiments; and the free energy of hydration of the analyte, available from the regression analysis in Table XIII using the analyte GB.



$$\Delta G(\text{R17}) = \Delta G(\text{B} + \text{H}^+ \rightarrow \text{BH}^+) - \Delta G(\text{H}_2\text{O} + \text{H}^+ \rightarrow \text{H}_3\text{O}^+) - \Delta G(\text{H}_3\text{O}^+ + \quad (\text{E15})$$



$$K_{\text{eq}}(\text{R17}) = \exp(-\Delta G(\text{R17})/\text{RT}) = \exp[1/\text{RT}\{-\text{GB}(\text{B}) + \text{GB}(\text{H}_2\text{O}) - \Delta G(\text{H}_3\text{O}^+ \quad (\text{E16})$$



Kinetic Modeling-Batch Mode

The simplest system to model and to understand considers the API source as a well mixed cell where reactants and products flow in and out at fixed rates. While this is not a strictly true representation of the API source it is sufficiently

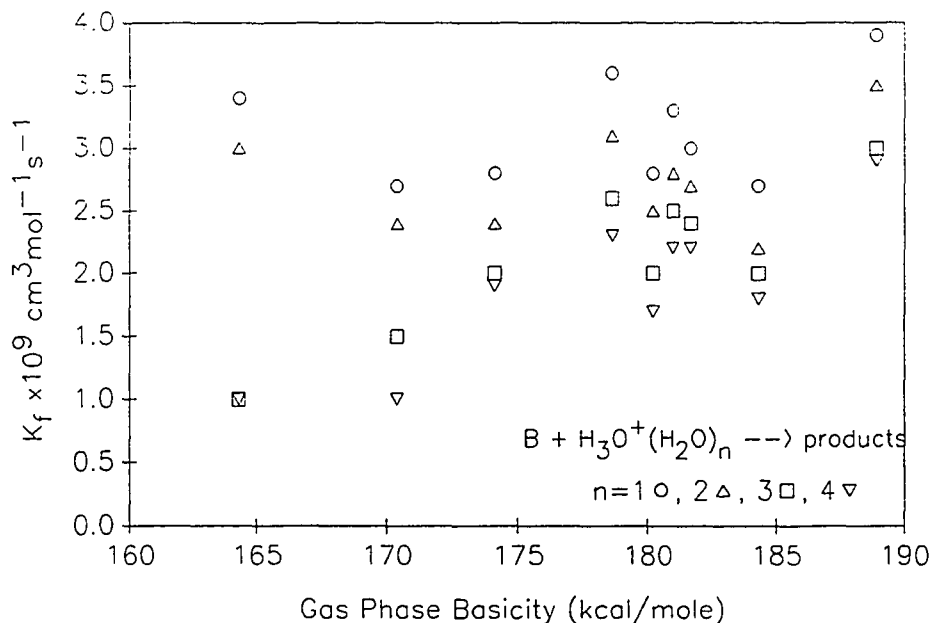


Figure 22. Forward rate constants for protonation as a function of analyte GB. Experimental data from Bohme, Mackay, and Tanner (1979).

close to provide valuable insights into API processes. Reagents flow into such a cell from sources whose concentrations remain fixed. The zero-order rates for these processes are based on the cell volume, the flow rate of the sample gas stream, and the concentration in this gas stream. Reversible proton transfer reactions occur in the cell. The rates for reversible proton transfer are obtained for an analyte of GB=180 kcal/mol using the analysis described above. All species leave the cell in first-order processes determined by their instantaneous concentrations in the cell, the flow rate, and the volume, forming lost species in the mechanism (ie. lh2o). In addition, charged species are removed in the detection steps; the loss rate to detection is based on the 3 kV potential and 4.6 mm needle to orifice gap.

Figure 23 plots the results of two separate integrations of the mechanism in Table XIV. The figure shows the concentrations present in the API source; the amount which reaches the detector of the mass spectrometer is simply k_d times the API ion concentration. For these integrations the initial conditions were $[H_3O^+]=2.45 \times 10^{11}$, $[B]=2.45 \times 10^9$, $[H_2O]=1 \times 10^{16}$ molecules cm^{-3} , and $k_f=3.0e-9$ cm^3 molecules $^{-1}$. The time scale of the x-axis represents the length of time required for the system to reach the steady-state conditions discussed in the previous section. The first integration, filled symbols, is based upon a detection rate of 4.35×10^4 sec^{-1} , representative of our API source. The steady state concentration of reagent hydroniums, filled squares, is small relative to the analyte concentration, filled triangles. The rapid detection step has removed the hydroniums before proton transfer reactions can occur; quantitative protonation cannot occur under conditions where the analyte is in excess over the reagent in the API source.

The second integration in Figure 23 is based upon a detection rate of zero, representing the limit of improved analyte response possible. In this second integration the hydronium ions are in large excess over both the analyte and the protonated analyte. This case illustrates quantitative protonation of the analyte. The conditions under which analyte response can be improved are discussed in the summary, Chapter VII.

It is possible to have linear API response for analyte without having quantitative protonation. To illustrate this with the batch-mode model the mechanism in Table XIV was integrated at a range of initial analyte concentrations, keeping all other conditions the same as above for each integration. Analyte response is linear in the early portion of the plot when the hydronium ion

TABLE XIV

BATCH MODE MODEL OF API RESPONSE

\$SOURCES		
SH3O	= H3O	0.641
SH2O	= WATR	0.641
SB	= B	0.641
\$REACTIONS		
H3O	B = BH	WATR 3E-9
WATR	BH = B	H3O 1.5E-24
\$LOSSES		
B	= LB	0.641
H3O	= LH3O	0.641
WATR	= LH2O	0.641
BH	= LBH	0.641
\$DETECTION LOSSES		
H3O	= DH3O	4.35E4
BH	= DBH	4.35E4
\$INITIAL CONDITIONS		
SH3O	SB	SH2O
2.45E11	2.45E09	1E16
\$CONSTANTS		
SH3O SH2O SB		

Notes: Source and loss rates for linear flow (0.641) are based on API source volume and inlet flow rate of 20 cm³ min⁻¹. Forward protonation rate assumed, k_b derived based on $GB(b)=180$ kcal/mol.

concentration is in excess over the protonated analyte. Once the concentration of the protonated analyte in the source reaches that of the hydroniums the equilibrium becomes less favorable and the response decreases. The range of linear response can be estimated from this approach. The lower limit is based upon the sensitivity of the mass spectrometer and the background signal at the m/z where the analyte is detected, the upper limit based on Figure 24 is near 100 ppb. This general appearance, slope and upper detection limit agree well with those found experimentally (Sunner, Nicol, and Kebarle, 1988; Grange, 1988). A

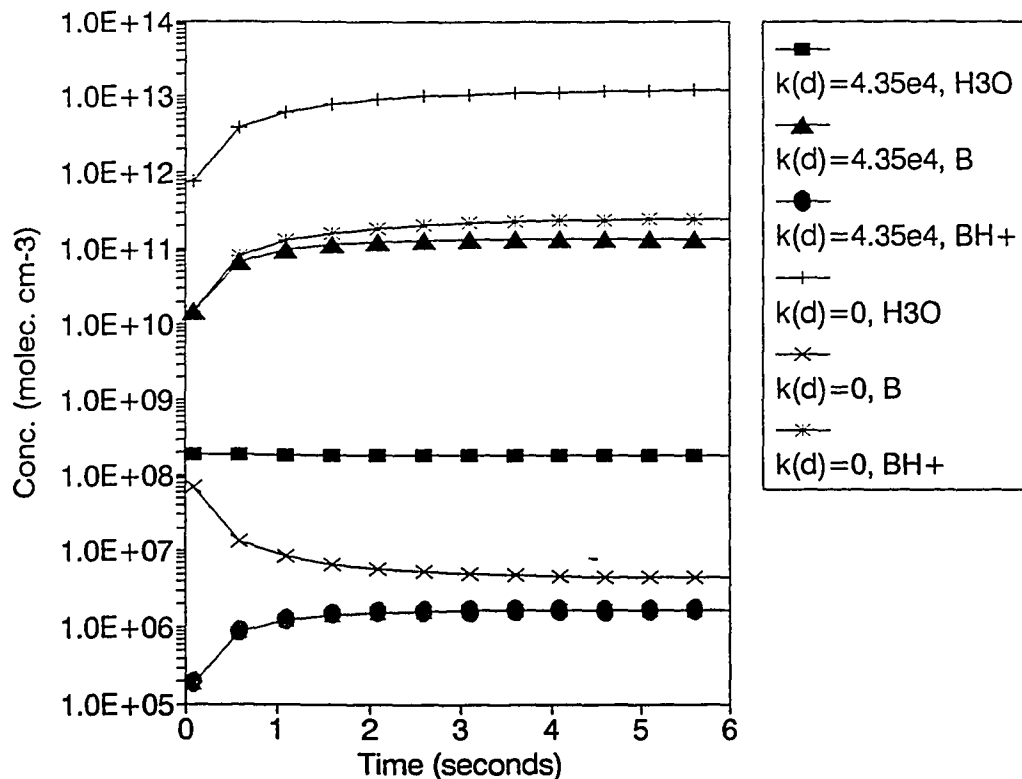


Figure 23. Batch-mode modeling of API source reactions at two detection rates. Reaction mechanism is given in Table XIV. Filled symbols are based on a detection rate of 4.35×10^4 , other points for $k_d=0$. Initial $[H_3O^+]_0 = 2.45 \times 10^{11}$, $[H_2O]_0 = 1 \times 10^{16}$, $[B]_0 = 2.45 \times 10^9$.

response curve based on the TAGA system is shown in Figure 25 the triangles represent the pyridine response curve, the circles the results for acetone (Sunner, Nicol, and Kebarle 1988).

API analysis is generally carried out with complex mixtures where the analyte may be present with other compounds of interest and/or in a matrix of compounds whose identities and concentrations are not of concern. These other components may compete for the available charge carriers in the API source, affecting analyte response and linearity. To the mechanism of Table XIV a second compound was added whose equivalent GB=177 kcal/mole. This second analyte,

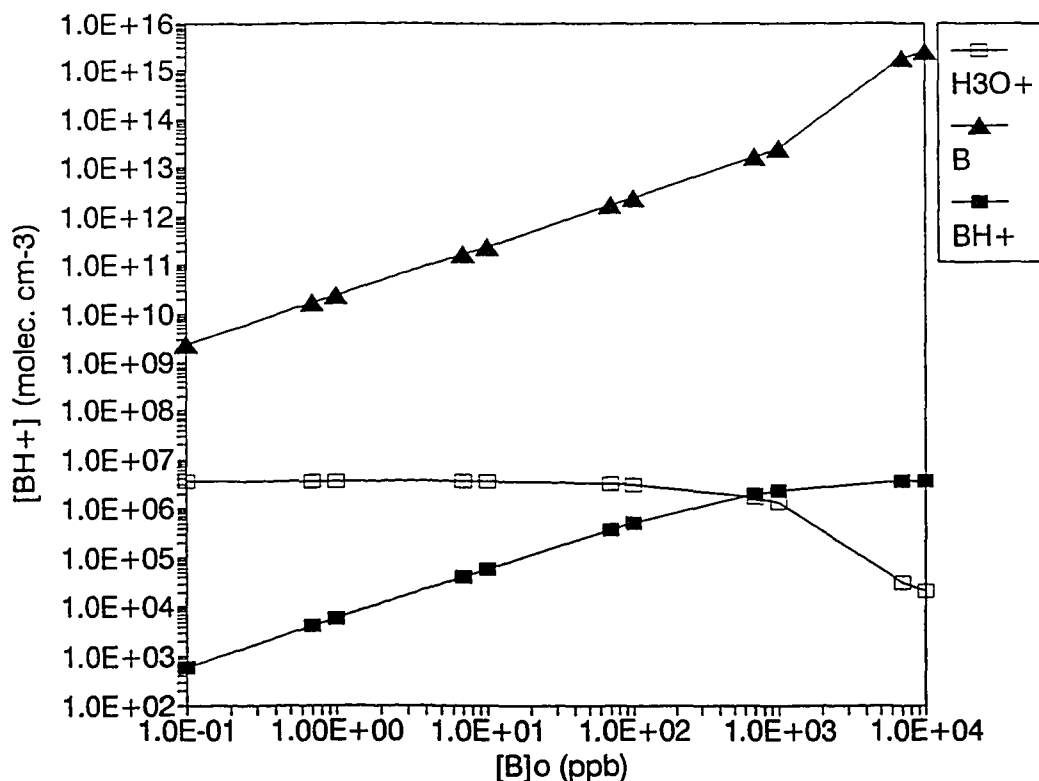


Figure 24. Batch-mode modeling of analyte response as a function of initial analyte concentration. Initial $[H_3O^+]_0 = 2.45e11$, $[H_2O]=1e16$. Response levels off as reagent hydroniums are consumed.

identified as 'C', was increased in initial concentration from 0.1 to 10,000 ppb while the concentration of the other analyte, 'A' (GB=180), was held constant at 0.1 ppb. The results of this integration are presented in Figure 26. The protonated concentrations in the API source are identified with filled symbols, hydronium ion is identified with an asterisk. API log response for analyte C is linear at concentrations up to about 100 ppb, similar with published experimental findings, and the response of analyte A is unperturbed by the presence of C until consumption of the reagent hydroniums begins.

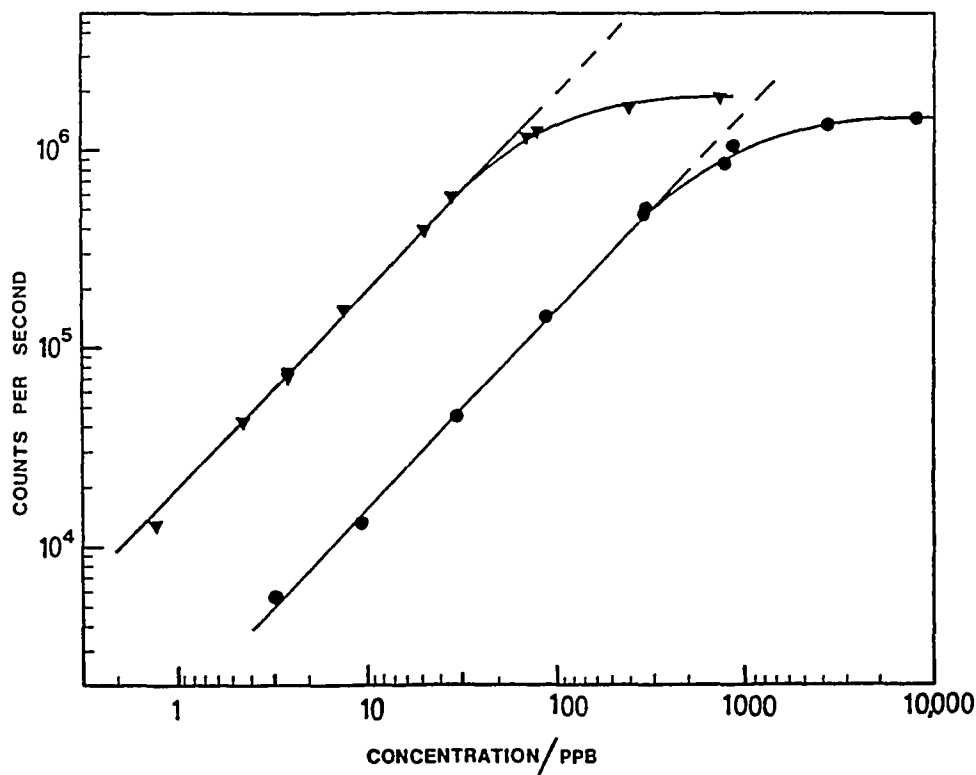


Figure 25. Experimental analyte response using TAGA APIMS as a function of analyte concentration. Filled triangles based on pyridine response, filled circles represent acetone response. Source: Sunner, Nicol, and Kebarle (1988).

The ion signal which will be seen at the detector is given by k_d times the ion concentration in the source times the cell volume (V); for hydroniums this would be $k_d[\text{H}_3\text{O}^+]V$. The presence of a large signal at the mass spectrometer of the mass spectrometer is significantly different than the concentration present in the API source, due to the extraction of ions by the electric field. In the case of Figure 26, for example, little of the initial analyte has been converted to protonated analyte and yet the concentration of hydroniums in the source is at least four orders of magnitude less than the initial concentration. The "missing" hydroniums were drawn out of the API source by the electric field and detected. This will result in a

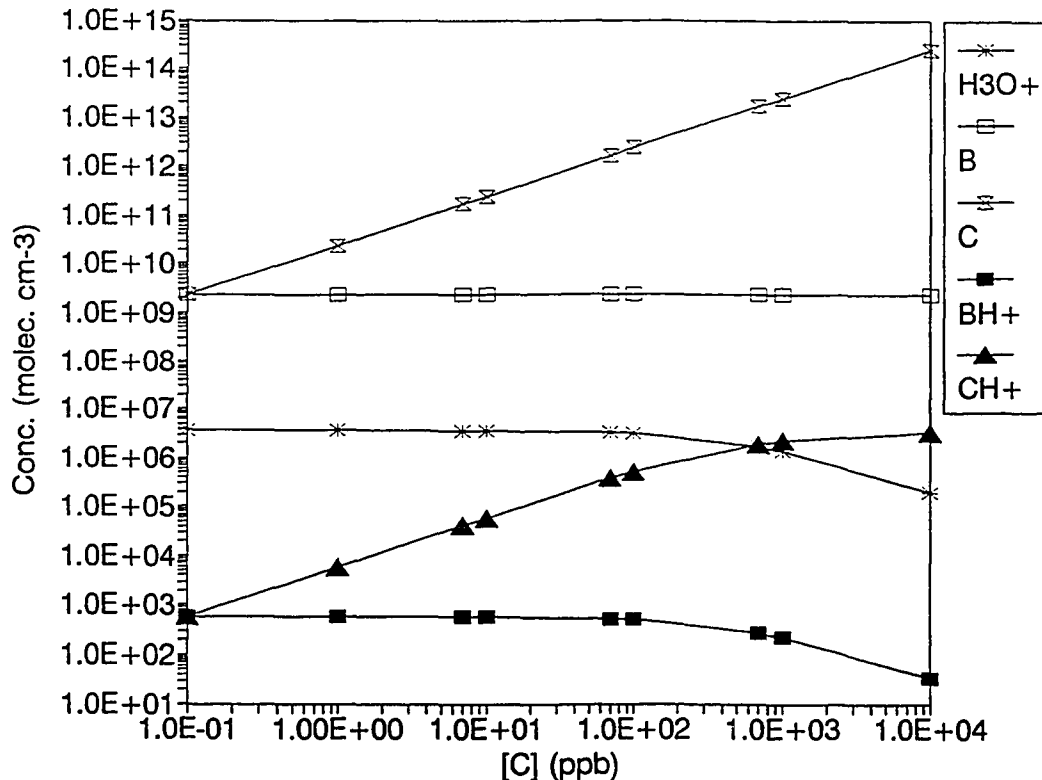


Figure 26. Batch-mode modeling of analyte response for mixtures. Analyte gas phase basicities: $GB(B)=180$, $GB(C)=177$ each kcal/mol. Concentration of B is held constant while [C] is varied.

very large ion signal at the detector for reagent ions, while actually in the source their relative concentrations are much lower.

CONCLUSIONS

As mentioned earlier in the chapter, a prerequisite to quantitative analysis is that all analytes have equal responses, which are linear in analyte concentration. Another alternative is for analyte response to be calibrated, provided that response for one analyte is not perturbed by the presence of other analytes or the sample matrix. Quantitative protonation is the optimal situation

and the most direct to evaluate, since all analytes will have a response which is proportional to their concentration. It is clear that this situation can be obtained using API only when the actual hydronium concentration is in large excess over the analytes' in the API source. This is illustrated in Figure 24 and is most nearly approached when using a slow detection step. It is necessary to specify "actual" concentration since the removal by the electric field depletes the concentration in the source while providing a large signal at the detector.

Linear response is possible in the API source even in if quantitation is not. This is illustrated in Figures 24 and 26 where the response for analytes, both singly and together, is linear up until the point of consumption of the reagents. The linear range based on this modeling is in agreement with the experimental results from Figure 25.

Conclusions relating the kinetic and thermodynamic control of proton transfer to API response may be questionable in that they relate high reagent signal in the spectra to high reagent concentrations in the source. The determinant factor in establishing the upper limits to response is apparently the rate of the detection step, and small differences in the forward rate constants for analytes determine how close to the upper limit the analyte response will be. Kinetic and equilibrium modeling presented here suggest that the API response, in the presence of sufficient reagents, should be uniformly high for all analytes. Our initial experiments under conditions where reagent ions are almost certainly consumed (Chapters III-IV) seem to bear this out, as do the API responses reported by others (Dumdei et al., 1988). Future experiments will stress minimizing the consumption of reagent ions to give direct quantitative assessment of yields.

CHAPTER VII

CONCLUSIONS AND APPLICATIONS

"Many things about chemistry that were once thought to be science fiction now actually are." (Davis, 1969)

PART I: HRKAPIMS

In Chapters II-IV we described the development and applications of a new approach to the study of atmospheric oxidation processes based on the existing technique of atmospheric pressure ionization mass spectrometry. Fundamental to this new approach was the utilization of source-produced hydroxyl radicals, which can initiate the oxidation of compounds present in the source, to mimic atmospheric oxidation processes. When API is to be used to sample ambient air or closed reaction vessels, we have demonstrated how the use of carbon monoxide can eliminate interferences from HO chemistry. HRKAPIMS offers many advantages over other experimental techniques in its ability to evaluate both the stable oxidation products of a compound and the free radical intermediates, and to assign empirical formulas through the accurate mass assignments. The short residence time offers the opportunity to evaluate reaction kinetics and mechanisms by changing the concentrations of reagents.

Oxidation of Small Hydrocarbons

The development of HRKAPIMS has been discussed in earlier chapters in the context of evaluating toluene oxidation mechanisms. Toluene oxidation is perhaps one of the most complicated mechanisms which might be undertaken for such a study. Future work might first focus on the products and free radical intermediates from simpler hydrocarbons to better understand the nature of the oxidation reactions and the API source reactions in general. Following such fundamental studies, the oxidation of such important NMHCs as isoprene and the larger terpene compounds could be undertaken. The following paragraphs outline and evaluate the oxidation mechanisms of several simple hydrocarbons and may serve to guide future work.

Tables XV-XVIII summarize the oxidation mechanisms for four simple hydrocarbons that would be likely candidates for a fundamental study using APIMS. These are partial mechanisms in that they do not follow the oxidation pathways all the way to the formation of carbon dioxide and water. The reactions in each of the four tables fall into two categories: atmospheric oxidation processes and protonation reactions. In the oxidation reactions the free radical intermediates are identified by a dot symbolizing the unpaired electron. Stable, closed-shell oxidation products are printed in italics. In the protonation reactions, the underlined atom was the lowest energy site for protonation. Heats of formation for the unprotonated and protonated species are listed in the first two columns. The enthalpies for these compounds are not available based on experimental measurements in Lias, Liebman, and Kebarle (1984), and are not corrected using the linear regression analysis given in an earlier chapter. The GBs are based upon

the slope corrected values of the enthalpies and are themselves adjusted using the method described in this Chapter V. The final column provides the accurate mass for each protonated compound in Daltons.

Methane. Atmospheric oxidations are initiated by reactions with the hydroxyl radical (HO). In alkanes such as methane, HO abstracts a hydrogen from the compound. Methane oxidation, Table XV generates only two products with gas phase basicities greater than that of water. Any analyte with a GB less than water will have little desire to accept a proton from a hydronium ion.

TABLE XV
PARTIAL METHANE PHOTOOXIDATION MECHANISM

	$\Delta H_f(B)$	$\Delta H_f(BH^+)$	GB	Mass
$CH_4 + H^* \rightarrow \underline{C}H_5^*$	-8.8	226.3	114.7	17.039
$CH_4 + HO^* \rightarrow CH_3^*$				
$CH_3^* + H^* \rightarrow \underline{C}H_4^*$	30.0	265.2	110.6	16.031
$CH_3^* + O_2 \rightarrow CH_3O_2^*$				
$CH_3O_2^* + H^* \rightarrow CH_3O\underline{O}H^*$	-9.1	198.0	148.8	48.021
$2CH_3O_2^* \rightarrow 2CH_3O^* + O_2$				
$CH_3O_2^* + NO \rightarrow CH_3O^* + NO$				
$CH_3O^* + H^* \rightarrow CH_3\underline{O}H^*$	-9.2	185.9	162.9	32.026
$CH_3O^* + O_2 \rightarrow CH_2O + HO_2^*$				
$CH_2O + H^* \rightarrow CH_2\underline{O}H^*$	-31.3	161.4	168.1	31.018
$CH_2O + HO^* \rightarrow CHO^* + H_2O$				
$CHO^* + H^* \rightarrow CH\underline{O}H^*$	-2.0	206.9	145.9	30.011
$CHO^* + O_2 \rightarrow CO + HO_2^*$				
$CO + H^* \rightarrow C\underline{O}H^*$	-5.7	229.5	115.3	29.003

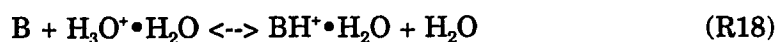
Notes: Heats of Formation for unprotonated $\Delta H_f(B)$ and protonated $\Delta H_f(BH^+)$ are based on semi-empirical calculations using the program MOPAC. Gas-phase Basicities (GB) are derived from corrected Heats of Formation using the methodology of Chapter V. Enthalpies and GB are in kcal/mol. Accurate masses for the protonated species are in Daltons. The underlined atoms represent the site of protonation. Italics denote stable products.

Since the relative humidity is generally high in most ambient API analyses, we would not expect APIMS analysis to detect these compounds. Formaldehyde is the major oxidation product of methane oxidation, with a GB of only 168 kcal/mol. As discussed in the previous chapter API response is determined by several factors acting singly and together. Increasing the hydronium ion concentration in the source will increase analyte response. This can be accomplished through the use of higher discharge currents and/or increased source residence time. Decreasing the water concentration increases response by shifting equilibrium toward the protonated form.

Protonation is also more favorable for reactions of the smaller hydrated hydroniums. The discussions in Chapter VI are focused on Reaction 9.

Protonation from hydrated hydroniums takes the form of R18, which is written for the monohydrate species. The equilibrium constant is then a function of analyte and water GB as well as the free energies for hydration. Hydration free energies can be evaluated from Figure 21 in Chapter VI as a function of analyte GB.

Protonation reactions and equilibrium constants for the other hydrated species is written similarly. The effect of the additional terms in E16 is to reduce the extent of proton transfer reaction for compounds with low GBs.



$$K_{eq}(R18) = \exp[RT^{-1}(GB(B)-GB(H_2O)+\Delta G(BH^+ + H_2O \rightarrow BH^+ \cdot H_2O) - \Delta G(H_3O^+ + H_2O \rightarrow H_3O^+ \cdot H_2O))] \quad (E16)$$

Ethene. In the oxidation of alkenes, HO can either abstract a hydrogen or break the double bond in an addition reaction, with the latter pathway dominant for the smaller alkanes. The products of ethene oxidation, Table XVI, do not have

TABLE XVI
PARTIAL ETHENE PHOTOOXIDATION MECHANISM

	$\Delta H_f(B)$	$\Delta H_f(BH^+)$	GB	Mass
$CH_2=CH_2 + H^* \rightarrow CH_2=\underline{C}H_2^*$	16.6	216.9	153.4	29.039
$CH_2=CH_2 + HO^* \rightarrow CH_2OH-CH_2^*$				
$CH_2OH-CH_2^* + H^* \rightarrow CH_2OH-\underline{C}H_2^*$	-28.6	161.7	170.2	46.042
$CH_2OH-CH_2^* + O_2 \rightarrow CH_2OH-CH_2O_2^*$				
$CH_2OH-CH_2O_2^* + H^* \rightarrow CH_2OH-CH_2O_2H^*$	-59.6	139.6	162.9	78.032
$CH_2OH-CH_2O_2^* + NO \rightarrow CH_2OH-CH_2O^* + NO_2$				
$2CH_2OH-CH_2O_2^* \rightarrow 2 CH_2OH-CH_2O^* + O_2$				
$CH_2OH-CH_2O^* + H^* \rightarrow CH_2OH-CH_2OH^*$	-61.0	114.9	191.0	62.037
$CH_2OH-CH_2O^* + O_2 \rightarrow CH_2OH-CHO + HO_2^*$				
$CH_2OH-CHO + H^* \rightarrow CH_2OH-CHOH^*$	-85.7	108.3	172.2	61.029
$CH_2OH-CH_2O^* \rightarrow HCHO + HOCH_2^*$				
$HCHO + H^* \rightarrow HCHOH^*$	-31.3	161.4	168.1	43.018
$HOCH_2^* + H^* \rightarrow HO\underline{C}H_2^*$	-27.7	179.2	150.2	44.026
$HOCH_2^* + O_2 \rightarrow HCHO + HO_2^*$				

Note: Heats of Formation for unprotonated $\Delta H_f(B)$ and protonated $\Delta H_f(BH^+)$ based on semi-empirical calculations using the program MOPAC. Gas-phase Basicities (GB) derived from corrected Heats of Formation using the methodology of Chapter V. Enthalpies and GB in kcal/mol, accurate masses for the protonated species in Daltons.

GBs much higher than those of methane's oxidation products. The major products formaldehyde and hydroxyethanal have GBs of 168 and 172 kcal/mol respectively. One of the free radical intermediates, $CH_2OH-CH_2O^*$, has a GB of 191 and might be detected using API.

Propene. With propene, HO addition can occur at the terminal or central carbon. These two oxidation pathways result in the same final products but the free radical intermediates will differ. Such information may provide insights into the lowest energy pathway to the formation of those products. While the isomeric structures and GBs of the intermediates may differ, their accurate masses are the

TABLE XVII
PARTIAL PROPENE PHOTOOXIDATION MECHANISM

	$\Delta H_f(B)$	$\Delta H_f(BH^+)$	GB	Mass
$CH_3CH=CH_2 + H^* \rightarrow CH_3CH=CH_2^*$	7.0	192	172.4	43.055
$CH_3CH=CH_2 + HO^* \rightarrow CH_3CHOH-CH_2^*$				
$CH_3CHOH-CH_2^* + H^* \rightarrow CH_3CH(OH_2)-CH_2^*$	-33.5	152.2	175.8	60.057
$CH_3CHOH-CH_2^* + O_2 \rightarrow CH_3CHOH-CH_2O_2^*$				
$CH_3CHOH-CH_2O_2^* + H^* \rightarrow CH_3CH(OH_2)-CH_2OO^*$	-65.5	124.4	174.5	92.047
$CH_3CHOH-CH_2O_2^* + NO \rightarrow CH_3CHOH-CH_2O^* + NO_2$				
$2CH_3CHOH-CH_2O_2^* \rightarrow 2CH_3CHOH-CH_2O^* + O_2$				
$CH_3CHOH-CH_2O^* + H^* \rightarrow CH_3CHOH-CH_2OH^*$	-67.5	100.5	201.0	76.052
$CH_3CHOH-CH_2O^* + NO_2 \rightarrow CH_3CH(OH_2)-CH_2ONO_2$				
$CH_3CHOH-CH_2ONO_2 + H^* \rightarrow CH_3CH(OH_2)-CH_2ONO_2$	-86.6	103.6	176.3	122.049
$CH_3CHOH-CH_2O^* + O_2 \rightarrow CH_3CHOHCH(OH)^*$				
$CH_3CHOHCHO + H^* \rightarrow CH_3CHOHCH(OH)^*$	-60.2	101.2	208.0	75.045
$CH_3CHOH-CH_2O^* \rightarrow HCHO + CH_3CHOH^*$				
$HCHO + H^* \rightarrow HCHOH^*$	-31.3	161.4	168.1	31.018
$CH_3CHOH^* + O_2 \rightarrow CH_3CHO + HO_2^*$				
$CH_3CHO + H^* \rightarrow CH_3CHOH^*$	-41.3	141.8	180.4	45.034
$CH_3CH=CH_2 + HO^* \rightarrow CH_3CH(\cdot)CH_2OH$				
$CH_3CH(\cdot)CH_2OH + H^* \rightarrow CH_3CH(\cdot)CH_2OH_2^*$	-40.7	145.5	176.3	60.057
$CH_3CH(\cdot)CH_2OH + O_2 \rightarrow CH_3CH(O_2\cdot)CH_2OH$				
$CH_3CH(O_2\cdot)CH_2OH + H^* \rightarrow CH_3CH(O_2\cdot)CH_2OH_2^*$	-67.9	123.9	172.5	92.047
$CH_3CH(O_2\cdot)CH_2OH + NO \rightarrow CH_3CH(O\cdot)CH_2OH + NO_2$				
$2CH_3CH(O_2\cdot)CH_2OH \rightarrow 2CH_3CH(O\cdot)CH_2OH + O_2$				
$CH_3CH(O\cdot)CH_2OH + H^* \rightarrow CH_3CH(OH\cdot)CH_2OH^*$	-67.1	100.0	202.0	76.052
$CH_3CH(O\cdot)CH_2OH + NO_2 \rightarrow CH_3CH(ONO_2)CH_2OH$				
$CH_3CH(ONO_2)CH_2OH + H^* \rightarrow CH_3CH(ONO_2)CH_2OH_2^*$	-86.5	102.4	177.9	122.049
$CH_3CH(O\cdot)CH_2OH + O_2 \rightarrow CH_3C(O)CH_2OH$				
$CH_3C(O)CH_2OH + H^* \rightarrow CH_3C(OH)CH_2OH$	-93.5	85.1	191.2	75.045
$CH_3CH(O\cdot)CH_2OH \rightarrow CH_3CHO + CH_2OH^*$				
$CH_2OH^* + O_2 \rightarrow HCHO + HO_2^*$				

Note: Heats of Formation for unprotonated $\Delta H_f(B)$ and protonated $\Delta H_f(BH^+)$ based on semi-empirical calculations using the program MOPAC. Gas-phase Basicities (GB) derived from corrected Heats of Formation using the methodology of Chapter V. Enthalpies and GB in kcal/mol, accurate masses for the protonated species in Daltons.

same and the isomers are indistinguishable using mass spectrometry. With propene's oxidation, Table XVI, both the number of products and the GB of the products increases dramatically over the first two examples. The GBs of the products and intermediates range from 168 to 208 kcal/mol. Depending on analyte concentration and experimental conditions propene should be an excellent candidate for analysis using APIMS.

Butane. The oxidation of butane is more complex because of the multiple sites for hydroxyl radical attack. A complete discussion of the butane oxidation mechanism was undertaken by Baldwin et al. (1977). Hydroxyl abstraction of a hydrogen can occur at a terminal carbon where there are six equivalent hydrogens, or at an internal carbon where there are 4 equivalent sites. To simplify the interpretation of Table XVIII, the reactions have been categorized into reaction types. Within each type, i.e. ROO• representing the various peroxy radical species, the oxidation process is listed along with the protonation of the product or free radical intermediate. Alkanes have generally lower GBs than unsaturated or heteroatom containing compounds, and the GBs of butane oxidation products range from 144.6 to 194.5 kcal/mol.

An early effort using API to identify the products of butane oxidation found many of these products. While the conditions were not suitable for quantitative assessment of the product yields, the presence of most of the products and many intermediates in the spectra is an important finding. Figure 27 shows two mass spectra from the oxidation of butane. Part (a) is the background scan with a relative humidity approximately 20% and the corona discharge operated at 2.0 μ A. The peaks at m/z 19, 37, 55, 73, 91, ... represent hydronium ion-water clusters.

Part (b) is after the addition of butane vapor directly into API source. While there were background peaks due to hydroniums at m/z 73 and 91, the relative sizes of these peaks has increased dramatically due to the formation of butane oxidation products. Methyl ethyl ketone is the major butane oxidation product with a large ion intensity in part (b). Other prominent species include acetaldehyde at 45 daltons and two of the ROOR species at 91 and 147 daltons. Asterisks in Table XVIII identify products or intermediates which were present in the analysis of butane oxidation in Figure 27. Butane chemistry is very interesting from a mechanistic standpoint and its reactions are well understood from studies using other methods (Baldwin et al., 1977). Butane should be a good candidate for further HRKAPIMS work, offering the potential to further verify the ability of the method to evaluate reaction kinetics and free radical intermediates of atmospheric oxidations.

PART II: ANALYTE GB AND API RESPONSE

Gas-phase Basicities

Gas-phase basicity is an important thermodynamic property which reflects a compounds potential response in API analysis, its willingness to participate in proton transfer and hydration reactions, and the equilibrium constant for these reactions. However, GBs are not available for many compounds of environmental significance. Of special interest to us are the atmospheric oxidation products for a wide range of organic compounds including nitrates, nitrites, nitro compounds, aldehydes, dialdehydes, ketones, di- and tri-ketones and a variety of multifunctional compounds. We have demonstrated the ability to evaluate a

TABLE XVIII
PARTIAL BUTANE PHOTOOXIDATION MECHANISM

	$\Delta H_f(B)$	$\Delta H_f(BH^*)$	GB	Mass
$RH + HO^* \rightarrow R^* + H_2O$				
$CH_3CH_2CH_2CH_3 + HO^* \rightarrow CH_3CH_2CH_2CH_2^* + H_2O$				
$CH_3CH_2CH_2CH_3 + HO^* \rightarrow CH_3CH_2CH(\bullet)CH_3 + H_2O$				
$CH_3CH_2CH_2CH_2^* + H^* \rightarrow CH_3CH_2CH_2\dot{C}H_3^*$	1.9	211	144.6	*58.078
$CH_3CH_2CH(\bullet)CH_3 + H^* \rightarrow CH_3CH_2\dot{C}H(H^*)CH_3^*$	-3.1	210.6	139.9	58.078
$R^* + O_2 \rightarrow ROO^*$				
$CH_3CH_2CH_2CH_2^* + O_2 \rightarrow CH_3CH_2CH_2CH_2O_2^*$				
$CH_3CH_2CH(\bullet)CH_3 + O_2 \rightarrow CH_3CH_2CH(OO^*)CH_3$				
$CH_3CH_2CH_2CH_2O_2^* + H^* \rightarrow CH_3CH_2CH_2CH_2O\dot{O}H^*$	-29.0	166.9	164.1	90.068
$CH_3CH_2CH(OO^*)CH_3 + H^* \rightarrow CH_3CH_2CH(O\dot{O}H^*)CH_3^*$	-27.0	166.5	166.7	90.068
$ROO^* + NO \rightarrow RO^* + NO_2$				
$CH_3CH_2CH_2CH_2O_2^* + NO \rightarrow CH_3CH_2CH_2CH_2O^* + NO_2$				
$CH_3CH_2CH(OO^*)CH_3 + NO \rightarrow CH_3CH_2CH(O^*)CH_3 + NO_2$				
$ROO^* + R'OO^* \rightarrow RO^* + R'O^* + O_2$				
$2CH_3CH_2CH_2CH_2O_2^* \rightarrow 2CH_3CH_2CH_2CH_2O^* + O_2$				
$2CH_3CH_2CH(OO^*)CH_3 \rightarrow 2CH_3CH_2CH(O^*)CH_3 + O_2$				
$CH_3CH_2CH_2CH_2O_2^* + H^* \rightarrow CH_3CH_2CH_2CH_2O\dot{H}^*$	-29.3	155.8	176.8	74.073
$CH_3CH_2CH(O^*)CH_3 + H^* \rightarrow CH_3CH_2CH(O\dot{H}^*)CH_3^*$	-25.9	147.8	189.9	*74.073
$RO^* + O_2 \rightarrow R=O + HO_2^*$				
$CH_3CH_2CH_2CH_2O^* + O_2 \rightarrow CH_3CH_2CH_2CHO + HO_2^*$				
$CH_3CH_2CH(O^*)CH_3 + O_2 \rightarrow CH_3CH_2CH(O)CH_3 + HO_2^*$				
$CH_3CH_2CH_2CHO + H^* \rightarrow CH_3CH_2CH_2CH\dot{O}H^*$	-54.5	126.4	184.4	73.065
$CH_3CH_2CH(O)CH_3 + H^* \rightarrow CH_3CH_2CH(O\dot{H}^*)CH_3^*$	-53.6	118.3	194.9	*73.065
$CH_3CH_2CH(O^*)CH_3 \rightarrow CH_3CHO + CH_3CH_2^*$				
$CH_3CH_2^* + O_2 \rightarrow CH_3CH_2OO^*$				
$CH_3CH_2OO^* + H^* \rightarrow CH_3CH_2O\dot{O}H_2^*$	-16.1	181.9	160.1	62.037
$CH_3CH_2OO^* + NO \rightarrow CH_3CH_2O^* + NO_2$				
$2CH_3CH_2OO^* \rightarrow 2CH_3CH_2O^* + O_2$				
$CH_3CH_2O^* + H^* \rightarrow CH_3CH_2O\dot{H}^*$	-15.9	173.4	170.5	*46.042
$CH_3CH_2O^* + O_2 \rightarrow CH_3CHO + HO_2^*$				
$CH_3CHO + H^* \rightarrow CH_3C\dot{H}O^*$	-41.3	141.8	180.4	*45.034

TABLE XVIII
 PARTIAL BUTANE PHOTOOXIDATION MECHANISM
 (continued)

	$\Delta H_f(B)$	$\Delta H_f(BH^+)$	GB	Mass
$ROO\cdot + R'OO\cdot \rightarrow ROOR' + O_2$				
$2CH_3CH_2CH_2CH_2OO\cdot \rightarrow CH_3CH_2CH_2CH_2OOCH_2CH_2CH_2CH_3 + O_2$				
$2CH_3CH_2OO\cdot \rightarrow CH_3CH_2OOCH_2CH_3 + O_2$				
$CH_3CH_2CH_2CH_2OO\cdot + CH_3CH_2OO\cdot \rightarrow CH_3CH_2CH_2CH_2OOCH_2CH_3$				
$CH_3CH_2CH_2CH_2OOCH_2CH_2CH_2CH_3 + H\cdot \rightarrow CH_3CH_2CH_2CH_2OO(H)CH_2CH_2CH_2CH_3^*$	-65.5	124.1	173.3	*147.139
$CH_3CH_2OOCH_2CH_3 + H\cdot \rightarrow CH_3CH_2OO(H)CH_2CH_3^*$	-38.4	152.3	171.2	*91.076
$CH_3CH_2CH_2CH_2OOCH_2CH_3 + H\cdot \rightarrow CH_3CH_2CH_2CH_2OO(H)CH_2CH_3$	-51.9	138.2	175.3	119.107
$ROO\cdot + HO_2\cdot \rightarrow ROOH + O_2$				
$CH_3CH_2CH_2CH_2OO\cdot + HO_2\cdot \rightarrow CH_3CH_2CH_2CH_2OOH + O_2$				
$CH_3CH_2OO\cdot + HO_2\cdot \rightarrow CH_3CH_2OOH + O_2$				
$CH_3CH_2CH_2CH_2OOH + H\cdot \rightarrow CH_3CH_2CH_2CH_2OOH_2^*$	-50.7	159.2	150.3	90.068
$CH_3CH_2OOH + H\cdot \rightarrow CH_3CH_2OH_2^*$	-37.1	160.8	154.9	62.037

Note: Heats of Formation for unprotonated $\Delta H_f(B)$ and protonated $\Delta H_f(BH^+)$ based on semi-empirical calculations using the program MOPAC. Gas-phase Basicities (GB) derived from corrected Heats of Formation using the methodology of Chapter V. Enthalpies and GB in kcal/mol, accurate masses for the protonated species in Daltons. Asterisks denote compounds with strong signals in the mass spectrum, Figure 27

compounds' GB through the use of semi-empirical calculations, based on the heats of formation for the protonated and unprotonated forms. Clearly the next application of semiempirical calculations is to real environmental problems, in particular to evaluate the GB of many of toluene's actual oxidation products which we have analyzed using HRKAPIMS.

Table XIX lists the calculated GBs for 57 compounds based on semiempirical calculations of enthalpies of formation. None of these compounds

TABLE XIX
GAS-PHASE BASICITIES BASED ON SEMI-EMPIRICAL
HEATS OF FORMATION

Compound	ΔH_f		Protonated Atom
	GB	(B) (BH ⁺)	
benzyl alcohol	181.8	-30.8	149.8 ortho carbon
			152.2 hydroxyl oxygen
benzyl-NO ₂	176.0	17.3	199.4 terminal O in NO ₂
butenedial	184.4	-44.6	135.8 carbonyl oxygen
			155.7 carbonyl carbon; H ₂ loss
			165.3 carbon 2
CH ₃ -ONO ₂	159.9	-31.0	169.0 terminal O in NO ₂
			169.0 nitrogen; H shift to O
			150.5 inner O; NO ₂ loss
CH ₃ -OONO ₂	154.0	-3.0	199.5 terminal O in NO ₂
			203.6 nitrogen; H shift to O
			173.9 outer O; NO ₂ loss
CH ₃ -C(O)-ONO ₂	167.3	-40.1	216.3 inner O; NO ₂ loss
			154.0 carbonyl O
			161.6 outer O in NO ₂
			166.0 nitrogen; H shift to O
dinitrotoluene o- p-	171.5	27.0	130.3 outer O; NO ₂ loss
			148.4 inner O; HNO ₄ loss
			212.0 ortho NO ₂ oxygen
dioxohexenal	207.4	-77.5	218.9 para NO ₂ oxygen
			86.3 end carbonyl oxygen
			103.4 center carbonyl oxygen
ethyl-ONO ₂	164.8	-37.8	98.1 end carbonyl oxygen
			158.6 terminal O
			158.6 nitrogen; shifts to O
ethyl-OONO ₂	157.1	-9.1	142.6 inner O; NO ₂ loss
			191.3 terminal O in NO ₂
			195.2 nitrogen; H shift to O
ethyl-C(O)-NO ₂	171.3	-46.3	167.3 inner O; NO ₂ loss
			145.0 carbonyl oxygen
			154.5 terminal O in NO ₂
			158.7 nitrogen; H shift to O
furfural	194.6	-24.5	123.9 outer O; NO ₂ loss
			139.5 inner O; HNO ₄ loss
			145.1 carbonyl oxygen
glyoxyl	165.7	-58.2	162.4 ring carbon 1
			139.3 oxygen
			137.7 carbon; dissociates

TABLE XIX

GAS-PHASE BASICITIES BASED ON SEMI-EMPIRICAL
HEATS OF FORMATION
(continued)

Compound	ΔH_f		Protonated Atom
	GB	(B) (BH ⁺)	
H-C(O)-OONO ₂	153.7	-33.8	171.7 terminal O in NO ₂ 168.8 carbonyl O; loss of NO ₂
hexadienal	195.8	-.5	166.0 carbonyl oxygen
hexadiendial	197.7	-32.8	135.3 carbonyl oxygen 154.4 vinyl carbon
hydroxydioxohexenal	194.1	-124.3	54.6 center carbonyl oxygen 55.0 end carbonyl oxygen 57.7 carbonyl O by hydroxyl
hydroxyhexadienal	216.3	-59.1	95.2 carbonyl oxygen
hydroxyoxohexenal	205.9	-104.6	62.5 terminal carbonyl oxygen 78.0 carbonyl oxygen
indole	213.7	60.3	206.2 nitrogen 251.5 carbon 1
isobutanol	180.8	-74.0	111.3 oxygen
maleic acid	206.2	-156.2	15.2 carbonyl oxygen
m-hydroxybenzaldehyde	197.6	-51.6	117.9 carbonyl oxygen
methylglyoxyl	179.3	-66.4	119.9 carbonyl oxygen 1 119.9 carbon 1; H shifts to O 145.9 carbon 2; H ₂ loss 128.4 carbonyl oxygen 2
nitropentane	180.6	-37.1	145.9 oxygen
o-cresol	225.7	-29.1	114.1 meta carbon 162.3 ortho carbon 163.0 hydroxy oxygen
o-hydroxybenzaldehyde	211.1	-49.3	108.5 carbonyl oxygen
o-hydroxy-m-cresol	177.7	-72.7	115.1 hydroxy oxygen
o-nitrotoluene	176.4	19.5	201.0 oxygen 222.3 nitrogen
o-nitrophenol	183.7	-15.2	163.2 oxygen
pentadienal	197.3	-.2	165.0 carbonyl oxygen
phenyl-CH ₂ -ONO ₂	160.8	-2.8	193.6 nitrogen 178.3 center O; loss of HNO ₃
phenyl-CH ₂ -OONO ₂	156.8	26.4	223.9 terminal O in NO ₂ 200.6 outer O; no ₂ loss 210.2 inner O; HNO ₄ loss
phenyl-C(O)-ONO ₂	201.8	-29.4	134.5 oxygen in NO ₂ ; NO loss 143.1 loss of HNO ₃

TABLE XIX
 GAS-PHASE BASICITIES BASED ON SEMI-EMPIRICAL
 HEATS OF FORMATION
 (continued)

Compound	ΔH_f		Protonated Atom
	GB	(B) (BH ⁺)	
phenyl-C(O)-OONO ₂	175.5	-4.4	179.6 carbonyl oxygen
			197.0 terminal O in NO ₂
			196.9 nitrogen; H shift to O
			163.9 outer O; NO ₂ loss
			175.2 inner O; HNO ₄ loss
phenyl-ONO	159.4	10.9	207.6 terminal O in NO ₂
			186.3 inner O; NO ₂ loss
p-hydroxybenzaldehyde	203.5	-53.3	111.3 carbonyl oxygen
p-nitrobenzaldehyde	181.8	.9	179.5 oxygen on NO ₂
			182.5 carbonyl oxygen
propyl-ONO ₂	156.8	-44.7	159.1 terminal O in NO ₂
propyl-OONO ₂	156.7	-15.8	185.6 terminal O; in NO ₂
			155.1 nitrogen; HNO ₂ loss
			160.3 outer O; NO ₂ loss
			197.5 inner O; NO ₂ loss
pyruvic acid	181.8-125.5		63.5 acid carbonyl oxygen
			64.7 carbonyl oxygen
tripropylamine	229.1	-34.0	107.2 nitrogen
1-butyne	172.4	22.4	206.3 carbon 1
1-methylbutenedial	195.5	-53.7	117.7 carbonyl oxygen 1
			155.2 carbon 1; H shifts to C4
			155.2 carbon 2
			156.3 carbon 3
			126.1 carbonyl 4
1-methylhexadienedial	200.4	-41.8	124.4 carbonyl oxygen 2
			129.3 carbonyl oxygen 6
2-HO-1-methylbutenedial	203.9	-97.0	71.1 carbonyl oxygen 4
			80.5 carbonyl oxygen 1
2-HO-1-Mehexadienedial	209.4	-82.3	79.9 carbonyl oxygen 6
			88.8 carbonyl oxygen 1
2-hydroxybutenedial	182.1	-95.5	90.6 carbon 4
			95.3 carbonyl oxygen 1
			128.3 carbon 2
			102.8 carbon 4
			92.4 carbonyl oxygen 4
			120.1 hydroxyl oxygen

TABLE XIX
GAS-PHASE BASICITIES BASED ON SEMI-EMPIRICAL
HEATS OF FORMATION
(continued)

Compound	ΔH_f		Protonated Atom
	GB	(B) (BH ⁺)	
2-hydroxy 3-butyl-ONO2	176.1	-89.7 101.0	hydroxy oxygen 104.7 terminal -ONO2 oxygen 90.8 center oxygen; NO2 lost
2-hydroxy-3-oxo-butanal	189.5-120.4	62.0	carbonyl oxygen 3 69.3 carbonyl oxygen 1
2-hydroxypropanedial	153.9-113.5	98.1	hydroxy alcohol 92.1 carbonyl oxygen; splits
2,6-dioxaheptane	186.1-106.3	78.1	oxygen
3-HO-2-oxy-3,5-hexadiene	201.8	-50.6 115.2	carbonyl oxygen
3-nitro-2-hydroxycresol	194.1	-22.3 147.9	terminal O in NO2
4-hydroxy-2-butenal	197.7	-69.7 101.3	carbonyl oxygen 134.9 carbon 3
4-hydroxy-2,4-pentadienal	197.1	-46.2 123.2	carbonyl oxygen
5-oxo-1,3-hexadiene	201.3	-10.5 152.2	carbonyl oxygen

Notes: Heats of formation for unprotonated ($\Delta H_f(B)$) and protonated ($\Delta H_f(BH^+)$) species are uncorrected values from MOPAC using keywords: AM1 bonds precise and charge=1 as appropriate. Gas-phase basicities (GB) are based on the lowest energy protonation site and derived from the corrected heats of formation, adjusted using the linear regression analysis methodology of Chapter V. All values are in kcal/mol. Protonation sites are identified by the functionality of the protonated atom or the carbon number for alkyl chains.

were reported in Lias, Liebman, and Levin. (1984). The heats of formation in Table XIX are uncorrected values directly from MOPAC. In many cases there is more than one likely protonation site and little prior evidence for which site will have the lowest energy. The last column in Table XIX lists the protonated atom when more than one location was evaluated. The lowest energy site which did not lead to dissociation of the molecule was used to calculate the GB. This information

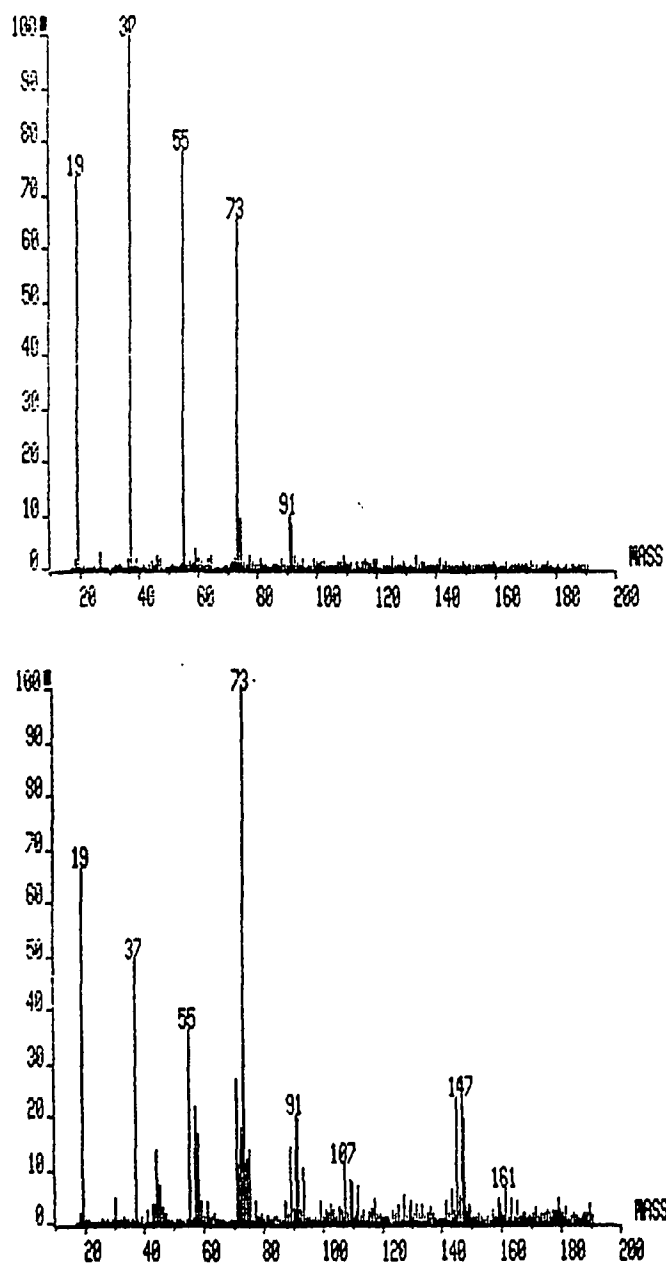


Figure 27. Low resolution mass spectra from APIMS analysis of butane. (a) Background spectrum, predominant peaks from hydrated hydroniums. (b) Spectrum after addition of butane. Oxidation products identified in Table XIX.

is valuable in assessing the potential API response for a compound (as described in Part I), for gaining insights into the stability of proposed oxidation products and

evaluating the estimated product yields to be expected along alternate oxidation pathways.

The atmospheric oxidation mechanism of toluene is very complex, as has already been discussed. One portion of the toluene oxidation mechanism is illustrated in Figure 28. Hydroxyl radicals abstract a hydrogen from the methyl carbon, or add across an unsaturated bond in the aromatic ring. Figure 28 emphasizes the free radical intermediates, some of which were detected and identified in experiments described in Chapter IV. Using the method of Chapter V, gas phase basicities have been calculated for each of the species in Figure 28 and the results summarized in Table XX. The GBs of these products range from a low of 154 to a maximum of near 229 kcal/mol. Very few compounds reported by Lias, Liebman, and Levin (1984) were free radical species, none were included in the analysis of Chapter V, and none as were large and complex as these for toluene. While there may be some error in the GBs for the radical species estimated here, this type of analysis can give valuable insights into potential analyte response. This information is also vital in order to calibrate API spectra for use in quantitative analysis.

Analyte Response in API

The simplest approach to evaluating API response is the steady state model from the previous chapter. More sophisticated models can be developed to describe API response, yet the limiting equilibrium cases ultimately reduce to the simple steady state model of E13.

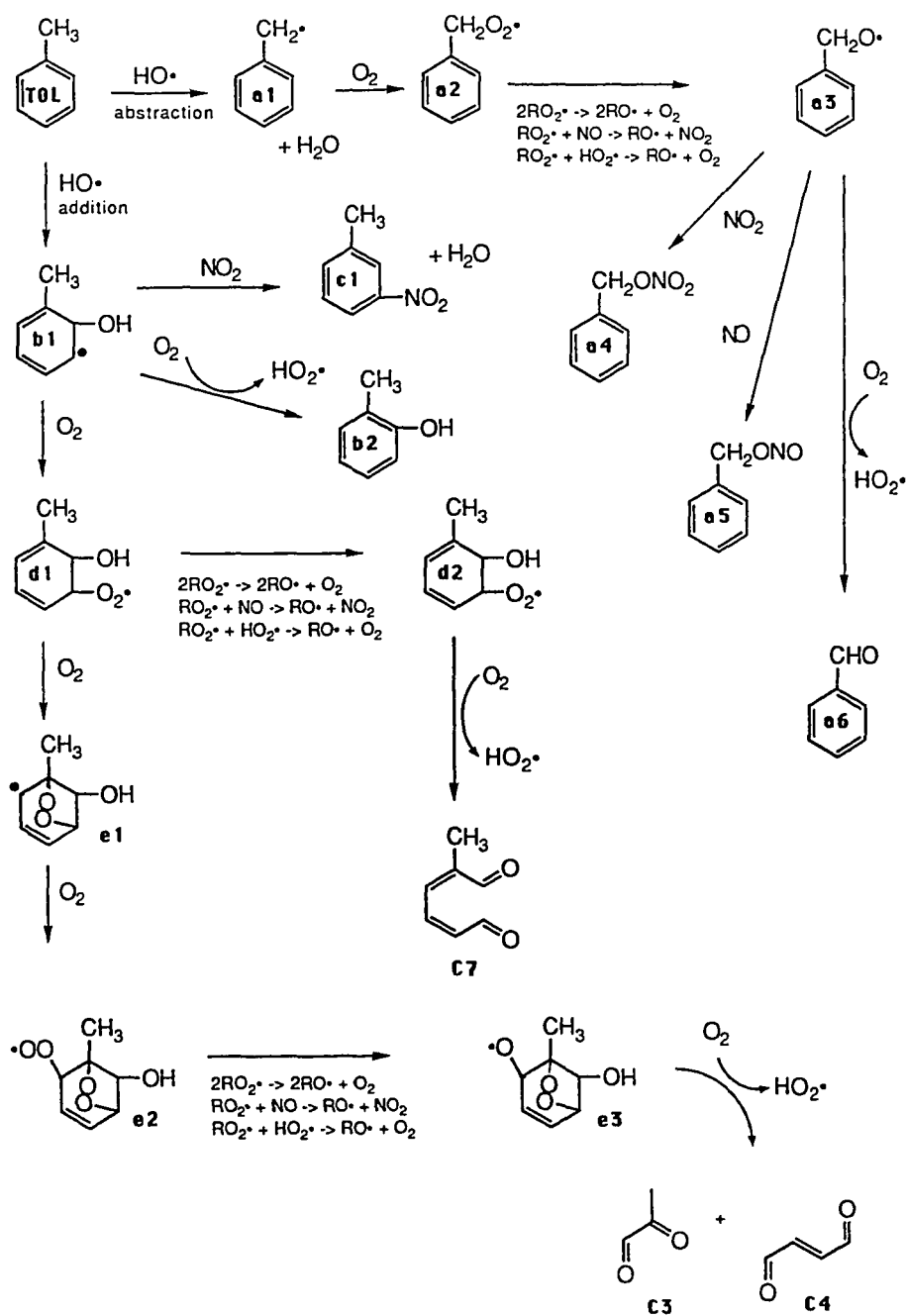


Figure 28. Partial toluene photooxidation mechanism showing formation of major ring opened products and free radical intermediates. GBs of each species in Table XX.

TABLE XX

GAS PHASE BASICITY CALCULATIONS FOR TOLUENE
FREE RADICAL INTERMEDIATES AND PRODUCTS

Compound	$\Delta H_f(B)$	$\Delta H_f(BH^+)$	GB(B)
a1	38.9	216.2	178.2
a2	13.4	199.8	176.3
a3	17.6	173.9	206.0
a4	-3.1	188.6	166.3
a5	-8.3	176.7	174.8
a6	-8.3	161.6	192.6
b1	-18.4	148.7	196.5
b2	-28.6	163.6	167.9
c1	18.2	194.6	182.2
d1	-25.4	144.5	194.4
d2	-28.2	115.4	225.7
e1	-20.1	183.5	153.6
e2	-8.6	165.2	153.6
e3	-9.9	118.1	242.2
c7	-41.8	124.4	200.4
c5	-53.7	117.7	195.5

Notes: The structures for each product or intermediate are given the the mechanism of Figure 28. Heats of formation for the unprotonated and protonated forms are based on semiempirical calculations and are not corrected for systematic errors. Gas-phase basicities are calculated from the heats of formation using the method described in Chapter V. All values are in kcal/mol.

The key observation obtained in the modeling of the previous chapter is the effective depletion of the reagent hydronium ions in the API source due to the extraction by the electric field. Corona discharges are now the more common ion source for atmospheric pressure work due to their greater dynamic range of available currents. They also afford the opportunity to adjust analyte residence time through adjusting the needle alignment. There is a tradeoff, however, in terms of the "actual" hydronium concentration, since an increase in discharge

current results from increasing the potential applied to the needle. This increased potential has the effect of increasing the ion velocity and decreasing the residence time for ions in the source. As an alternative to a corona discharge, radioactive Ni-63 foil can provide the same ionization processes without the large potential gradient. While radioactive foil sources do not have as large an absolute ionization rate, it may be that the enhancement in analyte response resulting from a longer residence time when using Ni-63 would offset the lower ionization currents.

SUMMARY

The previous chapters have described the development and application of a new approach to the study of atmospheric oxidation processes. The use of APIMS using ambient sampling techniques and in the analysis of "smog chamber" experiments can suffer from interferences due to hydroxyl radical reactions. Chapter II described one method to avoid the consumption of the sample due to HO reactions through the addition of about 1% CO to the sample. A new alternative approach to studying atmospheric oxidation processes is described in Chapter III which uses the HO reactions themselves to simulate the oxidation reactions present in the atmosphere. The effectiveness of this in-situ approach is demonstrated in a study of toluene oxidation. Toluene is a common organic compound used as a solvent and a major component in fuels; its presence in polluted urban atmospheres is primarily a result anthropogenic activity. High resolution spectra of toluene oxidation provide accurate mass assignments allowing the identification of the oxidation products through their empirical formulas. Chapter IV described the valuable insights into reaction mechanisms and reaction

kinetics that can be obtained from experiments which vary the experimental conditions. This approach, well matched to the short residence time of the API source, also provided insights into the free radical intermediates of toluene oxidation and their relative yields as experimental conditions were varied. This approach to the study of atmospheric oxidation processes using API source reactions, varied experimental conditions and accurate mass assignments we have termed High Resolution Kinetic Atmospheric Pressure Ionization Mass Spectrometry (HRKAPIMS).

Analyte response in HRKAPIMS is integrally linked to the gas-phase basicity of the analyte through the equilibrium constant for the proton transfer equilibrium. The gas-phase basicities of many compounds have been measured experimentally and are available in tabulated form. However many of the compounds are of interest to the environmental chemist have not yet been evaluated, particularly atmospheric oxidation products. Chapter V described the use of semiempirical calculations to estimate the GB of a large number of compounds, and to evaluate the error when these estimates are compared to experimental values. In the earlier portions of the present chapter these same semiempirical calculations were applied to compounds for which no experimental values are available, including toluene oxidation products, and the stable products and free radical intermediates for a variety of compounds. This information is useful in evaluating product yields and in guiding future experimental work.

Finally, in Chapter VI the theoretical basis for API and HRKAPIMS sensitivity was addressed. Three different approaches were used to evaluate analyte response as a function of analyte GB: thermodynamic equilibrium; steady

state equilibrium; and a integration of the reactions for a batch-mode reaction cell. Based on this study, insights into the experimental conditions necessary for linear response and for quantitative analysis were found which will form the basis for the future experiments.

HRKAPIMS is an important new technique for the analysis of atmospheric oxidation processes. It is hoped that through this study HRKAPIMS will find wide application in atmospheric chemistry, providing new insights and information into the important oxidation processes which dominate the lower atmosphere.

REFERENCES

- Arnts, R. and Meeks, S. *Atmos. Environ.* 1981, *15*, 1643-1651.
- Atkinson, R. *Chem. Rev.* 1986, *86*, 69-201.
- Atkinson, R. *Atmos. Environ.* 1990, *24A*, 1-41.
- Atkinson, R. "Kinetics and mechanisms of the gas-phase reactions of the hydroxyl radical with organic compounds. *J. Phys Chem. Ref. Data* (in press).
- Atkinson, R.; Aschmann, S.M.; Arey, J.; Carter, W.P.L. *Int. J. Chem. Kinet.* 1989, *21*, 801-827.
- Atkinson, R.; Bull, D.C.; Shuff, P.J. *Combust. Flame* 1980, *39*, 287.
- Atkinson, R.; Carter, W.P.L.; Darnall, K.R.; Winer, A.M.; Pitts, J.N., Jr. *Int. J. Chem. Kinet.* 1980, *12*, 779-836.
- Atkinson, R.; Carter, W.P.L.; Winer, A.M. *J. Phys. Chem.* 1983, *87*, 1605-1610.
- Atkinson, R.; Darnall, K.R.; Lloyd, A.C.; Winer, A.M.; Pitts, J.N., Jr. In *Advances in Photochemistry*; Pitts, J.N., Jr.; Hammond, G.S.; Gollnick, K., Eds.; Grosjean, D., Assoc. Ed.; John Wiley & Sons: New York, 1979; Vol. 11.
- Atkinson, R. and Lloyd, A.C. *J. Phys. Chem. Ref. Data* 1984, *13*, 315-444.
- Bailey, W.F. and Monahan, A.S. *J. Chem. Ed.* 1978, *55*, 489-493.
- Baldwin, A.C.; Barker, J.R.; Golden, D.M.; Hendry, D.G. *J. Phys. Chem* 1977, *81*, 2483-2492.
- Bandow, H.; Washida, N.; Akimoto, H. *Bull. Chem. Soc. Jpn.* 1985, *58*, 2531-2540.
- Bass, L.; Su, T.; Chesnavich, W.J.; Bowers, M.T. *Chem. Phys. Letters* 1975, *34*, 119-122.
- Besemer, A.C. *Atmos. Environ.* 1982, *16*, 1599-1602.
- Bishop, D.M. and Laidler, K.J. *J. Chem. Phys.* 1965, *42*, 1688.

- Black, F.M.; High L.E.; Lang, J.M. *J. Air Pollut. Control Assoc.* 1980, *30*, 1216-1221.
- Bohme, D.K.; Mackay, G.I.; Tanner, S.D. *J. Am. Chem. Soc.* 1979, *101*, 3724-3730.
- Carroll, D.I.; Dzidic, I.; Horning, E.C.; Stillwell, R.N. *Appl. Spectrosc. Rev.* 1981, *17*, 337-406.
- Carter, W.P.L. *Atmos. Environ.* 1990, *24A*, 481-518.
- Chameides, W.L.; Lindsay, R.W.; Richardson, J.; Kiang, C.S. *Science* 1988, *241*, 1473.
- Chase, M.W., Jr.; Curnutt, J.L.; Downey, J.R., Jr.; McDonald, R.A.; Syverud, A.N.; Valenzuela, E.A. *J. Phys. Chem. Ref. Data* 1982, *11*, 695-940.
- Cochran, J.W.H. *High Res. Chrom. and Chrom. Comm.* 1987, *10*, 573-575.
- Cooks, R.G. and Busch, K.L. *Int. J. Mass Spectrom. Ion Phys.* 1983, *53*, 111.
- Cox, R.D. and Earp, R.F. *Anal. Chem.* 1982, *54*, 2265-2270.
- Davis, C. *Catholic School Journal* 1969, *December*, 16-17.
- Dewar, M.J.S.; Zoebisch, E.G.; Healy, E.F.; Stewart, J.J.P. *J. Am. Chem. Soc.* 1985, *107*, 3902-3909.
- Dumdei, B.E.; Kenny, D.V.; Shepson, P.B.; Kleindienst, T.E.; Nero, C.M.; Cupitt, L.T.; Claxton, L.D. *Environ. Sci. Technol.* 1988, *22*, 1493-1498.
- Dumdei, B.E. and O'Brien, R.J. *Nature* 1984, *311*, 248-250.
- Dzidic, I.; Carroll, D.I.; Stillwell, R.N.; Horning, E.C. *Anal. Chem.* 1976, *48*, 1763-1768.
- Eiceman, G.A.; Kremer, J.H.; Snyder, A.P.; Tofferi, J.K. *Intern. J. Environ. Anal. Chem.* 1988, *33*, 161-183.
- Facchetti, S. In *Advances in Mass Spectrometry*; Longevialle, P., Ed.; Heyden & Son: London, 1989; Vol. 11B, pp 1542-1579.
- Finlayson-Pitts, B.J.; Pitts, J.N., Jr. In *Atmospheric Chemistry: Fundamentals and Experimental Techniques*; John Wiley & Sons: New York, 1986.
- Fund, K. and Grosjean, D. *Anal. Chem.* 1981, *53*, 168-171.

- Gery, M.W.; Fox, D.L.; Jeffries, H.E.; Stockburger, L.; Weathers, W.S. *Int. J. Chem. Kinet.* 1985, *17*, 931-955.
- Good, A.; Durden, D.A.; Kebarle, P. *J. Chem. Phys.* 1970a, *52*, 212-221.
- Good, A.; Durden, D.A.; Kebarle, P. *J. Chem. Phys.* 1970b, *52*, 222-229.
- Graedel, T.E. and Crutzen, P.J. *Sci. Am.* 1989, *September*, p 58-68.
- Grange, A.H. Ph.D. Dissertation, Oregon Graduate Center, February 1988.
- Grange, A.H.; O'Brien, R.J.; Barofsky, D.F. *Rapid Comm. in Mass Spec.* 1988a, *2*, 163-166.
- Grange, A.H.; O'Brien, R.J.; Barofsky, D.F. *Rev. Sci. Instrum.* 1988b, *59*, 573-579.
- Grange, A.H.; O'Brien, R.J.; Barofsky, D.F. *Rev. Sci. Instrum.* 1988c, *59*, 656-658.
- Grosjean, D. *The Science of the Total Environment* 1991 *100*, 367-414.
- Halim, H.; Heinrich, N.; Koch, W.; Schmidt, J.; Frenking J. *Comput. Chem.* 1986, *7*, 93-104.
- Hiraoka, K.; Takimoto, H.; Morise, K. *J. Am. Chem. Soc.* 1986, *108*, 5683-5689.
- Horning, E.C.; Horning, M.G.; Carroll, D.I.; Dzidic, I.; Stillwell, R.N. *Anal. Chem.* 1973, *45*, 936-943.
- Houriet, R.; Schwarz, H.; Schleyer, P.v.R. *Nouv. J. Chim.* 1981, *5*, 505.
- Kambara, H. and Kanomata, I. *Int. J. Mass Spectrom. Ion Phys.* 1977, *25*, 129-136.
- Kass, S.R. *J. Comput. Chem.* 1990, *11*, 94-104.
- Keesee, R.G. and Castleman, A.W., Jr. *J. Phys. Chem. Ref. Data* 1986, *15*, 1011-1061.
- Kenley, R.A.; Davenport, J.E.; Hendry, D.G. *J. Phys. Chem.* 1981, *85*, 2740-2746.
- Killus, J.; Witten, G. *Environ. Sci. Technol.* 1984, *18*, 142-148.
- Lacey, M.P. and Keough, T.; *Rapid Comm. Mass Spec.* 1989, *3*, 46-50.
- Lamb, B.; Westberg, H.H.; Allwire, G. *J. Geophys. Res.* 1985, *90*, 2380-2390.
- Leighton, P.A. In *Photochemistry of Air Pollution*; Academic Press: New York, 1961.

- Leone, J.A.; Flagan, R.C.; Grosjean, D.; Seinfeld, J.H. *Int. J. Chem. Kinet.* 1985, *17*, 177-216.
- Lias, S.G.; Liebman, J.F.; Levin, R.D. *J. Phys. Chem. Ref. Data* 1984, *13*, 695-808.
- Mahle, N.H.; Cooks, R.G.; Korzeniowski, R.W. *Anal. Chem.* 1983, *55*, 2272-2275.
- McDaniel, E.W. In *Collision Phenomena in Ionized Gases*; John Wiley: New York, 1964, Chapter 9.
- Mitchum, R.K. and Korfmacher, W.A. *Anal. Chem.* 1983, *55*, 1485-1499.
- Moylan, C.R. and Brauman, J.I. *Ann. Rev. Phys. Chem.* 1983, *34*, 187-215.
- Nicol, G.; Sunner, J.; Kebarle, P. *Int. J. Mass Spectrom. Ion Processes* 1988, *84*, 135-155.
- Niki H. and Maker P.D. In *Advances in Photochemistry*; Volman, D.H.; Hammond, G.S.; Gollnick, K., Eds.; John Wiley & Sons: New York, 1990, 69-137.
- O'Brien, R.J.; Dumdei, B.E.; Hummel, S.V.; Yost, R.A. *Anal. Chem.* 1984, *56*, 1329-1335.
- O'Brien, R.J.; Green, P.J.; Doty, R.A.; Vanderzanden, J.W.; Easton, R.R.; Irwin, R.P. In *Chemical and Biological Implications of Nitrogenous Air Pollutants*; Grosjean, D. Ed.; Ann Arbor Science: Ann Arbor, MI, 1979; pp 189-210.
- O'Brien, R.J.; Green, P.J.; Nguyen, N.-L.; Doty, R.A.; Dumdei, B.E. *Environ. Sci. Technol.* 1983, *17*, 183-186.
- O'Brien, R.J. and Hightower, J.C. In *The Alkylbenzenes*; National Academy of Science: Washington, DC, 1981, Chapter I.
- Perry, R.A.; Atkinson, R.; Pitts, J.N., Jr. *J. Phys. Chem.* 1977, *81*, 296-304.
- Pierotti, D.; Wofsy, S.C.; Jacob, D.; Rasmussen, R.A. *J. Geophys. Res.* 1990, *95*, 1871-1881.
- Plum, C.N.; Sanhueza, E.; Atkinson, R.; Carter, W.P.L.; Pitts, J.N., Jr. *Environ. Sci. And Technol.* 1983, *17*, 479-484.
- Proctor, C.J. and Todd, F.J.J. *Org. Mass Spectrom.* 1983, *18*, 509-516.
- Rasmussen, R. *J. Air Polut. Control Assoc.* 1972, *22*, 537-543.
- Rasmussen, R.; Khalil, A. *Geophys. Res.* 1988, *93*, 1417-1421.

- Rasmussen, R.; Went, F.W. *Proc. Natl. Acad. Sci.*, 1965, 53, 215-220.
- Reid, N.M.; Buckley, J.A.; French, J.B.; Poon, C.C. *Adv. Mass Spectrom.* 1979, 8B, 1843.
- Reid, N.M.; French, J.B.; Buckley, J.A.; Lane, D.A.; Lovett, A.M.; Rosenblatt, G. *Proceedings, 4th Joint Conference on Sensing Environmental Pollutants*, ACS: Washington, D.C. 1978.
- Roboz, J. In *Introduction to Mass Spectrometry: Instrumentation and Techniques*; Interscience: New York, 1968; Chapter 10.
- Sakairi, M. and Kambara, H. *Anal. Chem.* 1988, 60, 774-780.
- Seinfeld, J.H. In *Atmospheric Chemistry and Physics of Air Pollution*; Wiley Interscience Publication: John Wiley and Sons, New York, 1986.
- Seinfeld, J.H. *Science* 1989, 243, 745-752.
- Shah, J.J. and Singh, H.B. *Environ. Sci. Technol.* 1988, 22, 1381-1388.
- Shepson, P.B.; Edney, E.O.; Corse, E.W. *J. Phys. Chem.* 1984, 88, 4122-4126.
- Shepson, P.B.; Kleindienst, T.E.; Edney, E.O.; Namie, G.R.; Pitmann, J.H.; Cupitt, L.T.; Claxton, L.D. *Environ. Sci. Technol.* 1985, 19, 249-255.
- Singh, H.B.; Salas, L.J. *Atmos. Environ.* 1983, 17, 1057-1983.
- Singh, H.B.; Salas, L.J.; Cantrell, B.K.; Redmond, R.M. *Atmos. Environ.* 1985, 19, 1911-1919.
- Sloane, T.M. *Chem. Phys. Lett.* 1978, 54, 269-272.
- Stewart, J. *J. Comput. Chem.* 1989, 10, 221-264.
- Su, T. and Bowers, M.T. In *Gas Phase Ion Chemistry*; Bowers, M.T., Ed.; Academic: New York, 1979, Chapter 3.
- Su, T. and Su, E.C.F. *J. Chem. Phys.* 1978, 69, 2243-2250.
- Sunner, J.; Gordon, N.; Kebarle, P. *Anal. Chem.* 1988, 60, 1300-1307
- Sunner, J.; Ikononou, M.G.; Kebarle, P. *Anal. Chem.* 1988a, 60, 1308-1313.
- Sunner, J.; Ikononou, M.G.; Kebarle, P. *Int. J. Mass Spectrom. Ion Proc.* 1988b, 82, 221-237.

- Sunner, J.; Kulatunga, R.; Kebarle, P. *Anal. Chem.* 1986, *58*, 1312-1316.
- Tingey, D.T.; Manning, M.; Grothouse, C.C.; Burns, W.F. *Physiol. Plant* 1979, *47*, 112-118.
- Tuazon, E.C. and Atkinson, R. *Int. J. Chem. Kinet.* 1990, *22*, 1221-1236.
- Tuazon, E.C.; Atkinson, R.; MacLeod, H.; Biermann, H.W.; Winer, A.M.; Carter, W.P.L.; Pitts, J.N., Jr. *Environ. Sci. Technol.* 1984, *18*, 981-984.
- Tuazon, E.C.; MacLeod, H.; Atkinson, R.; Carter, W.P.L. *Environ. Sci. Technol.* 1986, *20*, 383-387.
- Tully, F.P.; Ravishankara, A.R.; Thompson, R.L.; Nicovich, J.M.; Shah, R.C.; Dreutter, N.M.; Wine, P.H. *J. Phys. Chem.* 1981, *85*, 2262-2269.
- Vandiver, V.J. Ph.D. Dissertation, New Mexico State University, Las Cruces, NM, May 1987.
- Vandiver, V.J.; Leasure, C.S.; Eiceman, G.A. *Int. J. Mass Spectrom. Ion Proc.* 1985, *66*, 223-238.
- Voets, R.; Francois, J.-P.; Martin, J.M.L.; Mullens, J.; Yperman, J.; Van Poucke, L.C. *J. Comput. Chem.* 1989, *10*, 449-467.
- Washburn, H.W.; Wiley, H.F.; Rock, S.M. *Ind. Eng. Chem. Anal. Ed.* 1943, *15*, 541.
- Washburn, H.W.; Wiley, H.F.; Rock, S.M. *Ind. Eng. Chem. Anal. Ed.* 1945, *17*, 74.
- Weinstock, B. *Science* 1969, *166*, 224-225.
- Went, F.W. *Proc. Natl. Acad. Sci. USA* 1960, *46*, 212-221.
- Zellner, R.; Fritz, B.; Preidel, M. *Chem. Phys. Letters* 1985, *121*, 412-416.
- Zimmerman, P.R. *Rep. EPA 904/9-77-028*, Environ. Prot. Agency, Research Triangle Park, N.C., 1979.
- Zimmerman, P.R.; Chatfield, R.B.; Fishman, J.; Crutzen, P.J.; Hanst, P.L. *Geophys. Res. Lett.* 1978, *5*, 679-682.
- Zimmerman, P.R.; Greenberg, J.P.; Westberg, C.E. *J. Geophys. Res.* 1988, *93*, 1407-1416.